A general setting for halo theory

Walter Tape and Günther P. Können

We describe a general framework for systematically treating halos that are due to refraction in preferentially oriented ice wedges, and we construct an atlas of such halos. Initially we are constrained neither by the interfacial angles nor the orientations of real ice crystals. Instead we consider "all possible" refraction halos. We therefore make no assumption regarding the wedge angle, and only a weak assumption regarding the allowable wedge orientations. The atlas is thus a very general collection of refraction halos that includes known halos as a small fraction. Each halo in the atlas is characterized by three parameters: the wedge angle, the zenith angle of the spin vector, and the spin vector expressed in the wedge frame. Together with the sun elevation, the three parameter values for a halo not only permit calculation of the halo shape, they also give much information about the halo without extensive calculation, so that often a crude estimate of the halo's appearance is possible merely from inspection of its parameters. As a result, the theory reveals order in what seems initially to be a staggering variety of halo shapes, and in particular it explains why halos look the way they do. Having constructed and studied the atlas, we then see where real or conceivable refraction halos, arising in specific crystal shapes and crystal orientations, fit into the atlas. Although our main goal is to understand halos arising in pyramidal crystals, the results also clarify and unify the classical halos arising in hexagonal prismatic crystals. © 1999 Optical Society of America

OCIS code: 010.1290.

1. An Atlas of Halos

A. Introduction

In this article we present a unified conceptual approach to the theory of halos. The article is motivated by a desire to understand the many exotic halos that might arise in preferentially oriented pyramidal crystals. Although the approach of the article can be extended to halos involving both reflection and refraction, the discussion here is restricted to refraction halos—those halos that are due to refraction only. The approach permits the parameterization and hence the classification of all refraction halos arising in preferentially oriented crystals, with only three parameters necessary to determine a halo. Together with the sun elevation, the three parameter values not only permit calculation of the halo shape, but they also give qualitative information about the halo shape, without calculation. The parameters themselves are easily calculated, thus making possible a systematic treatment of all (refraction) halos.

This article is divided into three major sections. In Section 1 we construct an atlas (Appendix A) of all possible halos, making no assumptions about real crystal shapes and only a weak assumption about real crystal orientations. In Section 2 we discover patterns and structure in the atlas, and we show why the halos in the atlas look the way they do. In Section 3 we show how real halos, or at least plausible halos, with their specific crystal shapes and orientations, fit into the atlas.

We make a number of idealizations that qualify our results. For example, we make no intensity calculations; we treat all rays as being of equal intensity, and we neglect the effects of shielding of one crystal face by another. So our approach is not meant to compete in realism with the highly successful Monte Carlo simulations of halos originated by Pattloch and Tränkle.[1] Rather it complements the Monte Carlo simulations by giving conceptual insights that the simulations alone cannot provide.

Those who are familiar with the classical halos but who have not thought about halos arising in pyramidal crystals may question the need for another treatment of halo theory. One of the outcomes of this

W. Tape is with the Department of Mathematical Sciences, University of Alaska Fairbanks, 101 Chapman Building, P.O. Box 756660, Fairbanks, Alaska 99775-6660; e-mail address is ffwrt@aurora.alaska.edu. G. Können is with the Royal Netherlands Meteorological Institute, P.O. Box 201, 3730 AE De Bilt, The Netherlands.

Received 18 May 1998; revised manuscript received 6 August 1998.
0003-6935/99/091552-74$15.00/0

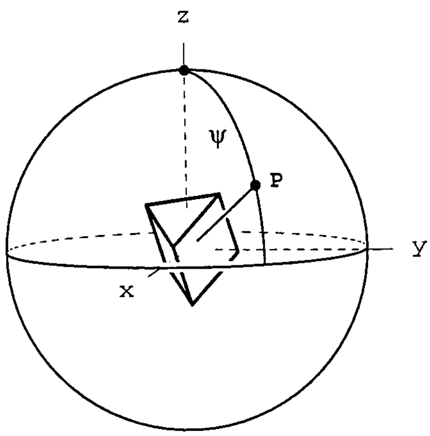

Fig. 1. Wedge and spin vector **P**. The vector **P** is fixed in the wedge and has constant zenith angle ψ. The wedge is otherwise unconstrained; it is free to rotate about **P**, and **P** is free to rotate about the vertical.

study is that the classical halos are relatively simple—simple, in fact, to the point of being misleading. A casual comparison of Fig. 55, which is for the classical 22° arcs in hexagonal prismatic crystals, with Fig. 57, which is for 24° arcs in pyramidal crystals, will make the point.

Perhaps the closest precursor of this paper is the one by Tricker,[2] who calculated a number of halos arising in preferentially oriented pyramidal crystals.

B. Spin Vector Assumption

We study refraction halos in their most rudimentary form. Each halo arises in an idealized ice wedge bounded by two half-planes. To calculate the halo, we follow light rays from the sun through the wedge as the wedge assumes various prescribed orientations. We then plot the points on the celestial sphere that are in the direction opposite to the outgoing rays.

Later when the halo atlas is constructed, the set of wedge orientations for each halo in the atlas will be assumed to satisfy the *Spin Vector Assumption*:

There is a unit vector **P** that is fixed in the wedge and has constant zenith angle ψ (Fig. 1). Therefore, with $\mathbf{k} = (0, 0, 1)$,

$$\mathbf{P} \cdot \mathbf{k} = \cos \psi = \text{constant}. \tag{1}$$

The wedge is otherwise unconstrained. The vector **P** is the *spin vector*.

Equivalently, there is a spin axis fixed in the wedge, with the wedge free to rotate about the spin axis, and the spin axis free to rotate about the vertical.

The Spin Vector Assumption may seem narrow and contrived, but it is satisfied approximately by all known halos arising in preferentially oriented crystals. Examples are given in Section 3. As suggested by the examples, known halos require only **P** vertical ($\psi = 0$ or 180) or **P** horizontal ($\psi = 90$), and we restrict our illustrations to halos in these two categories. We refer to them as *point halos* and *great circle halos*, respectively, for reasons that will become clear in Section 2. (All angles are in degrees.)

The following informal description suggests how the Spin Vector Assumption will lead to natural parameters for halos and then to the halo atlas.

The spin vector for a halo can be modeled by a nail driven into a wooden wedge. The placement of the nail in the wedge determines the wedge orientations responsible for the halo. For a point halo, for example, the orientations are obtained by first tipping the wedge so that the nail points directly up, and then by giving the wedge all possible rotations about the vertical.

To describe the placement of the nail, we put the wedge in a preassigned standard orientation and then record the direction of the nail (spin vector). The direction corresponds to a point on the (unit) sphere. This point is the "pole" of the halo. The pole determines the nail placement, and the nail placement determines the wedge orientations. Together with the wedge angle, the orientations determine the halo.

In this way every point halo is given by a wedge angle and a point of the sphere. A similar conclusion holds for great circle halos. In either case the appearance of the halo at any given moment depends also on the sun elevation. The halo atlas will be a depiction of point halos and great circle halos for representative sun elevations, wedge angles, and points on the sphere.

We have introduced the Spin Vector Assumption here at the beginning because it will be the key to the construction of the halo atlas. The assumption plays no role, however, until later in the section, and we do not invoke it at the present time. At the moment we make no assumption about the set of crystal orientations responsible for a halo.

C. Snell's Law is Parallel Projection

To find halo shapes, whether computationally or conceptually, we need to study the passage of light through a wedge.

For positive numbers n_1 and n_2 and for vectors **S** and **N** of lengths n_1 and 1, we define

$$\mathbf{pr}(\mathbf{S}, \mathbf{N}, n_2) = \mathbf{S} + \lambda \mathbf{N}, \tag{2}$$

where

$$\lambda(\mathbf{S}, \mathbf{N}, n_2) = [(\mathbf{S} \cdot \mathbf{N})^2 + n_2{}^2 - n_1{}^2]^{1/2} - \mathbf{S} \cdot \mathbf{N}. \tag{3}$$

Then $\mathbf{pr}(\mathbf{S}, \mathbf{N}, n_2)$ is the parallel projection of **S** to the sphere of radius n_2, with the direction of the projection parallel to **N**; we call it the **N**-*projection* of **S** to the sphere of radius n_2.

To express Snell's law in the above terms, let incident and refracted rays **I** and **J** have lengths equal to the refractive indices n_1 and n_2 of their respective mediums, and let **N** be the unit normal to the bound-

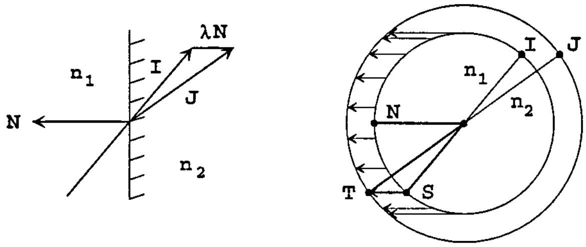

Fig. 2. Left, light ray proceeding from left to right, from medium with refractive index n_1 to medium with refractive index n_2. The vector **I**, with length n_1, is the incident ray, and **J**, with length n_2, is the refracted ray. The vector **N** is the unit normal vector. Right, same but with the addition of the light points $\mathbf{S} = -\mathbf{I}$ and $\mathbf{T} = -\mathbf{J}$, which give the directions from which the rays **I** and **J** appear to be coming. The point **T** is the **N**-projection of **S** to the sphere of radius n_2. The relation between **S** and **T**, like that between **I** and **J**, is parallel projection between concentric spheres of radii n_1 and n_2.

ary between the mediums and in the direction from the second medium to the first (Fig. 2). Then

$$\mathbf{J} = \mathbf{pr}(\mathbf{I}, -\mathbf{N}, n_2). \tag{4}$$

Rather than a ray itself, we are almost always interested in its negative, which gives the point of light on the celestial sphere apparently lit by the ray, and which we therefore call the *light point* of the ray. Thus if $\mathbf{S} = -\mathbf{I}$ and $\mathbf{T} = -\mathbf{J}$ are the light points of **I** and **J**, then

$$\mathbf{T} = \mathbf{pr}(\mathbf{S}, \mathbf{N}, n_2), \tag{5}$$

with **S** and **T** having lengths n_1 and n_2. In words, **T** is the **N**-projection of **S** to the sphere of radius n_2. The point **T** will be defined if $\mathbf{S} \cdot \mathbf{N} \geq 0$, which ensures that the incoming ray is indeed incident on the boundary in the required direction, and if λ in Eq. (3) is real, which ensures that there is a transmitted ray.

Now if a ray $\mathbf{I} = -\mathbf{S}$ is incident on a wedge with outward normal **N** at the entry face and inward normal **X** at the exit face ("**N**" for "eNtry", "**X**" for "eXit"), and with index of refraction n, then, as above but with $n_1 = 1$ and $n_2 = n$, the light point **T** for the ray within the wedge is

$$\mathbf{T} = \mathbf{pr}(\mathbf{S}, \mathbf{N}, n). \tag{6}$$

And the light point **H** for the outgoing ray from the wedge is

$$\mathbf{H} = \mathbf{F}(\mathbf{N}, \mathbf{X}, \mathbf{S}) = \mathbf{pr}(\mathbf{T}, \mathbf{X}, 1) = \mathbf{pr}[\mathbf{pr}(\mathbf{S}, \mathbf{N}, n), \mathbf{X}, 1]. \tag{7}$$

If **S** is the sun, then **H** is the *halo point*. According to Eq. (7), the relation between **S** and **H** is just a composite of successive projections, as in Fig. 3. The figure will be crucial in Section 2 to understanding why halos look the way they do.

In Eq. (7) the halo point **H** obviously depends on the index of refraction n as well as **N**, **X**, and **S**. However, we always take $n = 1.31$, which is the value for ice.

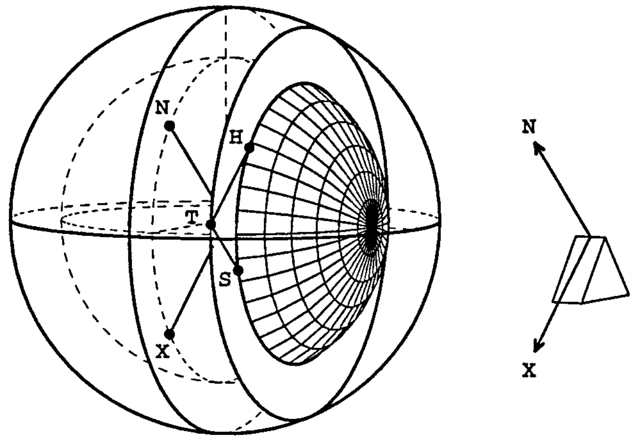

Fig. 3. Sun **S** and corresponding halo point **H**, both on the inner sphere. The halo point is the apparent position of the sun when one looks at the sun through the wedge. To find it geometrically, one **N**-projects point **S** to the outer sphere, getting point **T**, and then **X**-projects back to the inner sphere, getting **H**. The vectors **N** and **X** are the entry and exit face normals of the wedge. The two spheres are concentric and have radii 1 and n, the refractive indices outside and inside the wedge. The outer sphere is cut away completely, leaving only a skeleton, and the inner sphere is cut away at the left to reveal **N** and **X**. The wedge should be thought of as at the center of the spheres, as in Fig. 10.

D. Wedge Frame and Wedge Orientations

As before let **N** be the outward unit normal to the entry face of the wedge and **X** the inward unit normal to the exit face. We now define the *wedge frame* to consist of the orthonormal vectors

$$\begin{aligned} \mathbf{A} &= (\mathbf{N} + \mathbf{X})/\|\mathbf{N} + \mathbf{X}\|, \\ \mathbf{B} &= (\mathbf{N} \times \mathbf{X})/\|\mathbf{N} \times \mathbf{X}\|, \\ \mathbf{C} &= (\mathbf{N} - \mathbf{X})/\|\mathbf{N} - \mathbf{X}\|, \end{aligned} \tag{8}$$

which are fixed in the wedge (Fig. 4). The vector **B** is in the direction of the refracting edge of the wedge. (The refracting edge is the intersection of the entry and exit faces.) The vector **C** is normal to the refracting edge and bisects the angle formed by the entry and exit faces. The vector **A** completes the (right-handed) frame.

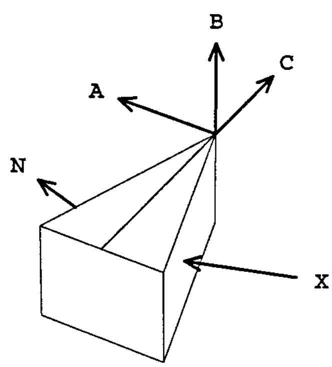

Fig. 4. Wedge frame vectors **A**, **B**, **C** and entry and exit normal vectors **N** and **X**. Note that the light ray (not shown) proceeds approximately opposite to the directions of **N** and **X**.

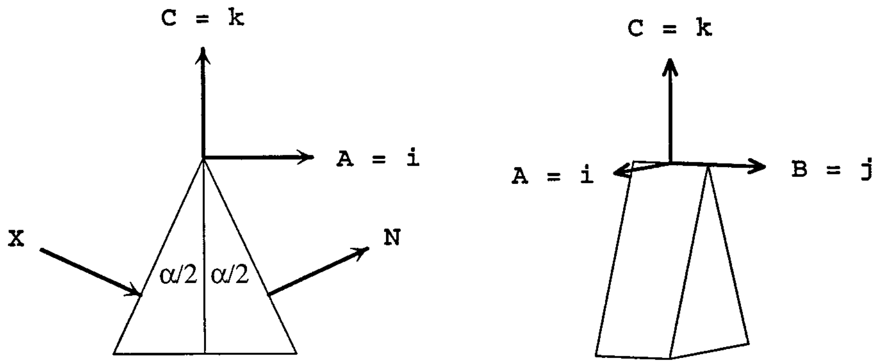

Fig. 5. Wedge in standard orientation. In standard orientation the wedge frame vectors **A**, **B**, **C** coincide with the standard Cartesian coordinate vectors **i**, **j**, **k**. The left-hand diagram, with the vector $\mathbf{B} = \mathbf{j}$ pointing into the paper, also shows the entry and exit normals **N** and **X** as well as the wedge angle α. The right-hand diagram is the more conventional view used in this paper, with the x-axis pointing more or less toward the reader.

The wedge frame depends on the entry and exit faces. The entry and exit faces are designated in advance, and light is permitted to enter the wedge only at the designated entry face.

Define the wedge to be in *standard orientation* when **A**, **B**, **C** coincide with the standard coordinate vectors **i**, **j**, **k**, as in Fig. 5. Some other orientation is given by specifying an *orientation* (or *rotation*) *matrix* u, that is, an orthogonal matrix with determinant 1; such a transformation preserves inner products and handedness. We regard u as starting with the wedge in standard orientation and then giving it the desired orientation. Then $u\mathbf{i} = \mathbf{A}$, $u\mathbf{j} = \mathbf{B}$, and $u\mathbf{k} = \mathbf{C}$, and the columns of the matrix u are **A**, **B**, and **C**, so that u can be thought of as the wedge frame itself.

Each halo is associated with a set U of wedge orientations that give rise to the halo. Each wedge orientation is an orientation matrix u as above. The wedge is in standard orientation when u is the identity matrix e. Note, however, that e need not be in U.

E. Halo Point and Halos

Recall that the halo point **H** is the light point for the outgoing ray from the wedge. It is the point on the celestial sphere apparently lit by the outgoing ray. In making a halo simulation, we therefore express **H** as a function of wedge orientation u and then plot **H** on the celestial sphere as u varies. Continuing from Eq. (7), we have

$$\mathbf{H} = \mathbf{F}(\mathbf{N}, \mathbf{X}, \mathbf{S}) = \mathbf{F}(u\mathbf{N}_0, u\mathbf{X}_0, \mathbf{S}), \tag{9}$$

where $\mathbf{N}_0$ and $\mathbf{X}_0$ are the entry and exit normals for the wedge in standard orientation. From Fig. 5 they are

$$\mathbf{N}_0 = \mathbf{N}_0(\alpha) = [\cos(\alpha/2), 0, \sin(\alpha/2)],$$
$$\mathbf{X}_0 = \mathbf{X}_0(\alpha) = [\cos(-\alpha/2), 0, \sin(-\alpha/2)], \tag{10}$$

where the *wedge angle* α is the angle between the entry and exit faces of the wedge. Thus the halo point can be regarded as a function of u, α, and **S**:

$$\mathbf{H}(u, \alpha, \mathbf{S}) = \mathbf{F}(u\mathbf{N}_0, u\mathbf{X}_0, \mathbf{S}). \tag{11}$$

In most contexts, α or **S** is fixed and we then abbreviate $\mathbf{H}(u, \alpha, \mathbf{S})$ to $\mathbf{H}(u, \mathbf{S})$, $\mathbf{H}(u, \alpha)$, or $\mathbf{H}(u)$, as appropriate.

It is convenient to extend the definition of **H** so that it is defined for all orientations u. We therefore define $\mathbf{H}(u, \alpha, \mathbf{S})$ to be the nonsense symbol "no ray" in case the right-hand side of Eq. (11) is undefined, that is, in case the ray cannot pass through the wedge in the specified direction.

And although u has been assumed to be an orientation, that is, an orthogonal matrix with determinant 1, it will be useful in Sections 2 and 3 to be able to replace u in Eq. (11) with an arbitrary orthogonal matrix w. The equation still makes sense—w is used to give **N** and **X**, that is all. Then it is easy to see, either formally from Eqs. (2), (3), and (7), or intuitively, that for any orthogonal matrix w,

$$\mathbf{F}(w\mathbf{N}, w\mathbf{X}, w\mathbf{S}) = w\mathbf{F}(\mathbf{N}, \mathbf{X}, \mathbf{S}), \tag{12}$$

and then from Eq. (11)

$$\mathbf{H}(wu, \alpha, w\mathbf{S}) = w\mathbf{H}(u, \alpha, \mathbf{S}). \tag{13}$$

For an orientation u and an orthogonal transformation w, we define the orientation $w'(u)$ by

$$w'(u) = \begin{cases} w\,u & \text{if } \det w = 1, \quad (14) \\ w\,u\,\text{yref} & \text{if } \det w = -1, \quad (15) \end{cases}$$

where the transformation yref is reflection in the plane $y = 0$. If u is the orientation of the wedge having entry and exit normals **N** and **X**, then $w'(u)$ is the orientation of the wedge having entry and exit normals $w\mathbf{N}$ and $w\mathbf{X}$, by Eq. (8). Since yref $\mathbf{N}_0 = \mathbf{N}_0$ and yref $\mathbf{X}_0 = \mathbf{X}_0$ then by Eqs. (11) and (13)

$$\mathbf{H}[w'(u), \alpha, w\mathbf{S}] = \mathbf{H}(wu, \alpha, w\mathbf{S}), \tag{16}$$

$$\mathbf{H}[w'(u), \alpha, w\mathbf{S}] = w\mathbf{H}(u, \alpha, \mathbf{S}). \tag{17}$$

What is a halo?

At times we need to be clear about what we mean by a halo. In the common idiom, which we follow, a halo has an existence independent of any one sun

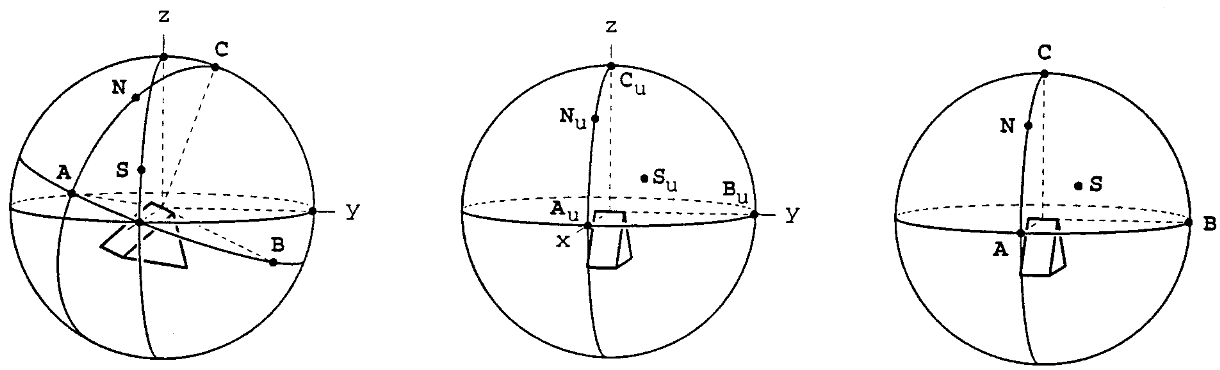

Fig. 6. Left, wedge together with the wedge frame vectors **A**, **B**, **C**, outward normal **N** to the entry face, and sun vector **S**, all shown for a particular wedge orientation u. This is the view from space. Middle, corresponding wedge coordinate vectors $\mathbf{A}_u$, $\mathbf{B}_u$, $\mathbf{C}_u$, $\mathbf{N}_u$, and $\mathbf{S}_u$. This is therefore the view from the wedge. The wedge is shown here in standard orientation in order to emphasize the geometric meaning of the subscripted vectors. The rotation u takes the wedge here to the wedge in the left-hand diagram, and it takes the vectors $\mathbf{A}_u = \mathbf{i}$, $\mathbf{B}_u = \mathbf{j}$, $\mathbf{C}_u = \mathbf{k}$, $\mathbf{N}_u$, $\mathbf{S}_u$ to **A**, **B**, **C**, **N**, **S** [Eq. (23)]. Right, vectors **A**, **B**, **C**, **N**, and **S** as seen from the wedge.

position. The circumzenith arc is the circumzenith arc, no matter where the sun happens to be. In this sense a halo is determined by its set U of wedge orientations and its wedge angle α. Formally, then, the halo is the function

$$\mathbf{S} \rightarrow \mathbf{H}(U, \alpha, \mathbf{S}), \tag{18}$$

where **S** ranges over the celestial sphere, and where

$$\mathbf{H}(U, \alpha, \mathbf{S}) = \{\mathbf{H}(u, \alpha, \mathbf{S}) : u \in U, \quad \mathbf{H}(u, \alpha, \mathbf{S}) \neq \text{“no ray”}\}. \tag{19}$$

On the other hand, $\mathbf{H}(U, \alpha, \mathbf{S})$ is the halo when the sun is at **S**. It is a subset of the celestial sphere—what one sees in the sky.

Thus there are two senses of “halo”. In the first and more fundamental sense [Eq. (18)] a halo is given by U and α alone, whereas in the second [Eq. (19)] it is given by U, α, and **S**. In the first sense a halo is a function, whereas in the second it is a value of the function. Sometimes we speak of the shape or appearance of a halo to distinguish the second sense from the first, but more often than not we use “halo” indiscriminately to apply in either sense, and we trust the meaning will be clear from the context. But our official answer to “What is a halo?” is given by Eq. (18), and it is important to think of halos in this way when comparing and classifying them.

If U is the group $SO(3)$ of all orientations, then $\mathbf{H}(U, \alpha, \mathbf{S})$ is a circular halo with center at **S** and with radius that depends on α. If $\alpha = 60$, for example, then the halo is the common 22° circular halo, and if $\alpha = 90$ the halo is the 46° circular halo.

A halo $\mathbf{H}(U, \alpha, \mathbf{S})$ will be empty if, as the wedge assumes the orientations in U, no sunlight can enter the entry face and exit the exit face.

F. Wedge Frame Versus Space Frame

Let **A**, **B**, **C** be the wedge frame as before. Then for any vector **V**,

$$\mathbf{V} = (\mathbf{V} \cdot \mathbf{A})\mathbf{A} + (\mathbf{V} \cdot \mathbf{B})\mathbf{B} + (\mathbf{V} \cdot \mathbf{C})\mathbf{C}. \tag{20}$$

Thus $\mathbf{V} \cdot \mathbf{A}$, $\mathbf{V} \cdot \mathbf{B}$, $\mathbf{V} \cdot \mathbf{C}$ are the wedge coordinates of **V**. The *wedge coordinate vector* of **V**, which gives the appearance of **V** as seen from the wedge frame, is

$$\mathbf{V}_u = (\mathbf{V} \cdot \mathbf{A}, \mathbf{V} \cdot \mathbf{B}, \mathbf{V} \cdot \mathbf{C}) \tag{21}$$

$$= (\mathbf{V} \cdot \mathbf{A})\mathbf{i} + (\mathbf{V} \cdot \mathbf{B})\mathbf{j} + (\mathbf{V} \cdot \mathbf{C})\mathbf{k}. \tag{22}$$

Since $u\mathbf{i} = \mathbf{A}$, $u\mathbf{j} = \mathbf{B}$, and $u\mathbf{k} = \mathbf{C}$, then from Eqs. (20) and (22)

$$\mathbf{V} = u\mathbf{V}_u. \tag{23}$$

We distinguish *space vectors*, which are fixed in space, from *wedge vectors*, which are fixed in the wedge. The vectors **i**, **j**, **k**, and **S** are space vectors, whereas **A**, **B**, **C**, **N**, **X**, and **P** are wedge vectors. If **V** is a wedge vector, then $\mathbf{V}_u$ is constant, whereas **V** depends on u. In fact, although we do not always do so, we should really write **V** as $\mathbf{V}(u)$. Then Eq. (23) becomes $\mathbf{V}(u) = u\mathbf{V}_u$, and if **V** is a wedge vector, then with e the identity matrix, we have $\mathbf{V}(e) = \mathbf{V}_e = \mathbf{V}_u$, so that

$$\mathbf{V}(e) = \mathbf{V}_u \quad (\text{if } \mathbf{V} \text{ is a wedge vector}). \tag{24}$$

Thus $\mathbf{V}_u$ is the value of **V** when the wedge is in standard orientation.

The preceding equations are clear, but their interpretation can be tricky. We regard xyz-space as our fundamental space, with $\mathbf{i} = (1, 0, 0)$, $\mathbf{j} = (0, 1, 0)$, $\mathbf{k} = (0, 0, 1)$. Vectors are represented as triples of numbers and are normally plotted in xyz-space, regardless of the geometric meaning of the numbers. If in a space with xyz-axes we draw unsubscripted vectors, such as **S** or **N** (left diagram, Fig. 6), then the result shows the world as seen from the space frame; the vector **S**, showing the position of the sun as seen from space, is constant, whereas the vector **N**, showing the entry normal to the wedge, depends on the wedge orientation u. If we draw subscripted vectors, such as $\mathbf{S}_u$ or $\mathbf{N}_u$, also in xyz-space (middle diagram), then the result shows the world as seen from the wedge frame; the vector $\mathbf{N}_u$ is constant, whereas $\mathbf{S}_u$ depends on u. When it is not important to con-

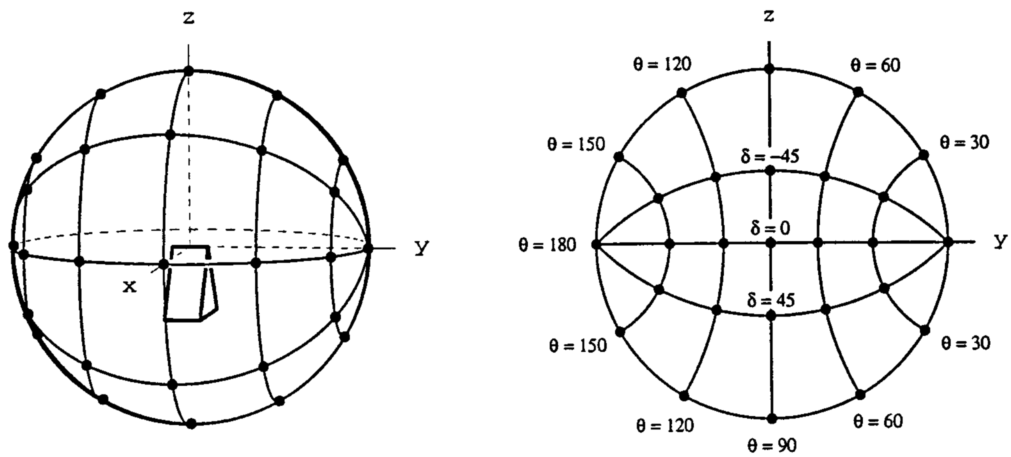

Fig. 7. Left, Bravais coordinate grid. Bravais coordinates (θ, δ) are spherical coordinates centered at (0, 1, 0). The solid dots, all of which are on the front hemisphere ($x \geq 0$), mark the location of poles of halos shown in Appendix A. [Figure 37 of Appendix A also shows halos with poles on the rear hemisphere ($x \leq 0$).] Right, same, but shown in stereographic projection from (−1, 0, 0). This is the layout used in Appendix A.

trast the wedge view and space view, we often draw a diagram with no *xyz*-axes but with the wedge frame vectors **A**, **B**, **C** indicated (right diagram). This diagram contains the same information as the previous one, but it does so with less cumbersome notation. It also gives us a more active feeling of riding with the wedge (Section 2), rather than just a passive logging of coordinate triples. But the diagram should not be misconstrued as implying that the wedge is in standard orientation; we just happen to be viewing the wedge from an unconventional angle.

Note that $\mathbf{N}_u = \mathbf{N}_0$. We could do without the notation "$\mathbf{N}_0$" and use "$\mathbf{N}_u$" instead, but we prefer "$\mathbf{N}_0$" in Eq. (11) as a reminder that $\mathbf{N}_0$ is independent of u. Equations (10) stand alone; the vector $\mathbf{N}_0$ depends only on α. Similar remarks apply to $\mathbf{X}_0$.

G. Pole P_u

We now impose the Spin Vector Assumption [Eq. (1)]. It allows the set U of wedge orientations for a halo to be specified by only two parameters—the zenith angle ψ of the spin vector, and the constant vector $\mathbf{P}_u$, which is the spin vector $\mathbf{P}$ expressed in the wedge frame. Informally the specification of U was described in Subsection 1.B, using a nail and a wooden wedge. Formally the reasoning is simply that, according to Eq. (1), an orientation u is in U if and only if $\mathbf{P} \cdot \mathbf{k} = \cos \psi$, or from Eq. (23)

$$u\mathbf{P}_u \cdot \mathbf{k} = \cos \psi. \tag{25}$$

Therefore U is determined by ψ and $\mathbf{P}_u$. We call $\mathbf{P}_u$ the *pole* of the halo.

The pole $\mathbf{P}_u$ is a point on the unit sphere. For example, it is at (0, ±1, 0) if $\mathbf{P}$ is parallel to the refracting edge of the wedge. It is on the great circle $y = 0$ if $\mathbf{P}$ is perpendicular to the refracting edge.

The pole is a fundamental halo parameter. Since a halo is determined by the set U of responsible wedge orientations and by the wedge angle α, and since U is determined by ψ and $\mathbf{P}_u$, then a halo is determined by ψ, $\mathbf{P}_u$, and α. Thus when ψ and α are fixed, a halo is determined by a choice of pole $\mathbf{P}_u$, that is, by a choice of a point on the (unit) sphere; all halos with fixed ψ and α are represented by points on the sphere. In Appendix A we display some halo simulations to illustrate how halos vary depending on the location of their poles on the sphere. (The simulations also illustrate the dependence of halo shapes on ψ, α, and sun elevation Σ, although in the case of ψ we consider only two values, namely, ψ = 0 and ψ = 90.) In Section 3 we compute the poles for known halos and plausible halos; once the location of the pole on the sphere is known (together with ψ, α, and Σ), the appearance of the halo is determined.

H. Bravais Coordinates

In the figures of Appendix A each halo simulation is located at its pole $\mathbf{P}_u$ on a Bravais coordinate grid. Numbers (θ, δ) are *Bravais coordinates* for the unit vector $\mathbf{Y} = B(\theta, \delta)$, where

$$B(\theta, \delta) = (\sin \theta \cos \delta, \cos \theta, -\sin \theta \sin \delta). \tag{26}$$

Bravais coordinates are like ordinary spherical coordinates but centered at (0, 1, 0) rather than at (0, 0, 1). The angles θ and δ are the *Bravais colatitude* and *longitude* of **Y**. The $\theta = \theta_0$ curves are the *Bravais circles*, and the $\delta = \delta_0$ curves are the *Bravais meridians*; see Fig. 7.

If **V** is a wedge vector and if $\mathbf{V}_u = B(\theta, \delta)$, we also say that (θ, δ) are Bravais coordinates for **V** itself. In this case

$$\begin{aligned}\mathbf{V} &= u\mathbf{V}_u = u\, B(\theta, \delta) \\ &= u(\sin \theta \cos \delta, \cos \theta, -\sin \theta \sin \delta) && (27) \\ &= (\sin \theta \cos \delta)\mathbf{A} + (\cos \theta)\mathbf{B} \\ &\quad - (\sin \theta \sin \delta)\mathbf{C}. && (28)\end{aligned}$$

From this point of view Bravais coordinates move with the wedge; comparison of Eq. (28) with Eq. (26)

shows that they are spherical coordinates centered at the wedge vector $\mathbf{B}$ rather than at (0, 1, 0).

By analogy with coordinates to be defined later, Bravais coordinates are "B-centered"—they are spherical coordinates centered at $\mathbf{B}$ or at $\mathbf{B}_u = (0, 1, 0)$, depending on the point of view.

I. Point Halo Examples

Figure 33 in Appendix A shows point halos ($\psi = 0$) for 27 representative poles $\mathbf{P}_u$ on the front hemisphere ($x \geq 0$). For each halo the wedge angle α is 60 and the sun elevation Σ is zero. For $\Sigma = 0$, halos with poles on the rear hemisphere can be inferred from those on the front using Rule 2 or Rule 4 in Subsection 2.H. If one is willing to interpolate among the halos shown, the figure therefore shows all possible point halos having the given values of α and Σ. A halo that may look familiar is the one at (0, 1, 0)—it is the right 22° parhelion.

Figures 34–36 are similar to Fig. 33 but with different sun elevations. Figures 38–41 are similar to Fig. 34 but with different wedge angles. Figure 37 is similar to Fig. 34, except that the halos have their poles on the rear hemisphere. Point halos with poles on the rear hemisphere, especially the upper part, tend to require negative Σ in order to be nonempty, with halos further up and to the rear requiring ever more negative Σ. Such halos are therefore uncommon in the literature. The Nonempty Halos Theorem, Subsection 2.F, gives a precise condition for determining when a halo is nonempty.

Point halos, or rather their sets of wedge orientations, are always one-dimensional, like those in Figs. 33–41.

J. Great Circle Halo Examples

Figures 42–49 are like Figs. 33–41 but show great circle halos ($\psi = 90$) instead of point halos ($\psi = 0$). The set of wedge orientations is now two-dimensional, and the halos look like folded sheets rather than the curves of the preceding figures. The most familiar halo in these figures is the one at (0, $\pm$1, 0) in Figs. 42–45—it consists of the upper and lower tangent arcs to the common 22° halo.

For great circle halos Eq. (25) shows that the point $\mathbf{P}_u$ and its antipode $-\mathbf{P}_u$ give the same set of wedge orientations and hence the same halo. The front hemisphere therefore suffices to present all great circle halos.

It is impossible in a limited space to collect halo diagrams for a comprehensive range of wedge angles and sun elevations. We nevertheless imagine that this has been done and that the figures in Appendix A are included as a small part of the collection. The result is the halo atlas mentioned in the beginning, containing "all possible halos". In principle, the halo atlas consists of all halos that satisfy the Spin Vector Assumption, with a halo for each choice of ψ, $\mathbf{P}_u$, and α.

2. Riding the Wedge to Analyze the Atlas

A. Zenith Locus and Halo-Making Sets

In Section 1 we used points on the (unit) sphere S^2 to represent halos. At a more fundamental level, the sphere was being used to organize the group $SO(3)$ of orientations, or equivalently, it was being used to depict the world as seen by a rider on the wedge, as we will see.

From Eqs. (21) and (23), the vector $\mathbf{k}_u = u^{-1}\mathbf{k}$ gives the appearance of the zenith point $\mathbf{k}$ as seen from the wedge with orientation u. If U is a set of orientations, then the *zenith locus* of U is the set $K = \{\mathbf{k}_u : u \in U\}$. The zenith locus is the path of the zenith point as seen by the wedge rider while the wedge assumes the orientations in U.

In addition to $\mathbf{k}$, other space vectors also have their corresponding loci as seen from the wedge. The sun locus, for example, is the set $S = \{\mathbf{S}_u : u \in U\}$, the path of the sun as seen by the wedge rider. It too will play a role, but the zenith locus is special, as we will see momentarily.

We do not impose the Spin Vector Assumption [Eq. (1)] at this time but instead make the much weaker and completely plausible assumption that all azimuthal angles are equally likely for a wedge. Therefore, if u is in a set of wedge orientations for a halo, then so is $\mathrm{zrot}(\phi) \cdot u$, where the matrix $\mathrm{zrot}(\phi)$ is rotation through angle ϕ about the z-axis. Formally we define a set U of orientations to be a *halo-making set* if it is *azimuth invariant*:

$$u \in U \text{ implies } \mathrm{zrot}(\phi) \cdot u \in U \text{ for all } \phi. \tag{29}$$

The definition is obviously unrealistic in that it counts too many sets of orientations as halo-making sets, but every set of wedge orientations for a real halo would fit the definition. In particular, if the Spin Vector Assumption is satisfied, then the set of wedge orientations is a halo-making set, according to Eq. (25).

Let Z be the subgroup of $SO(3)$ consisting of rotations $\mathrm{zrot}(\phi)$ about the z-axis. A rotation ζ is in Z if and only if $\zeta\,\mathbf{k} = \mathbf{k}$. In terms of Z, a set U of orientations is a halo-making set if and only if

$$ZU \subseteq U. \tag{30}$$

The *coset* containing an orientation u is the set

$$Zu = \{\zeta u : \zeta \in Z\}. \tag{31}$$

The collection of all cosets is a partition[3] of $SO(3)$, and two orientations u and v are in the same coset if and only if $uv^{-1} \in Z$ or, in words, if and only if u and v differ by a rotation about the z-axis. The halo-making sets are exactly the subsets of $SO(3)$ that are unions of cosets.

The following theorem shows that the halo-making sets are characterized by their zenith loci, which of course are just subsets of the sphere and can be easily visualized.

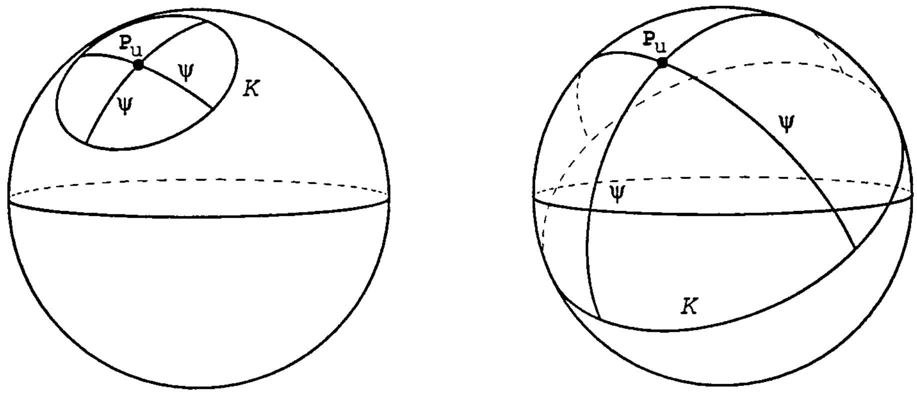

Fig. 8. Left, circle $K = K(\psi, \mathbf{P}_u)$ with radius ψ and center $\mathbf{P}_u$. The circle is the zenith locus of the halo-making set determined by ψ and $\mathbf{P}_u$ according to the Spin Vector Assumption. Here $\psi = 30$. Right, same, but with $\psi = 90$, so that K is a great circle.

Theorem—Characterization of Halo-Making Sets

For each subset K of the sphere, let $U(K) = \{u : \mathbf{k}_u \in K\}$. Then $U(K)$ is a halo-making set, its zenith locus is K, and the mapping $K \to U(K)$ is a 1–1 correspondence between the subsets of the sphere and the halo-making sets. Moreover,

$$U(\cup \{K_\alpha\}) = \cup \{U(K_\alpha)\}, \tag{32}$$

$$U(\cap \{K_\alpha\}) = \cap \{U(K_\alpha)\}, \tag{33}$$

$$U(K_1) \subseteq U(K_2) \text{ if and only if } K_1 \subseteq K_2. \tag{34}$$

Proof

If $\zeta \in Z$, then $\mathbf{k}_{\zeta u} = (\zeta u)^{-1}\,\mathbf{k} = u^{-1}\,\zeta^{-1}\,\mathbf{k} = u^{-1}\,\mathbf{k} = \mathbf{k}_u$, so $U(K)$ is a halo-making set. Define p: $SO(3) \to S^2$ by $p(u) = \mathbf{k}_u$. We will show that

$$p[p^{-1}(K)] = K, \tag{35}$$

$$p^{-1}[p(U)] = U \quad (\text{if } U \text{ is a halo-making set}). \tag{36}$$

From Eqs. (35) and (36) and from the fact that $U(K) = p^{-1}(K)$, it follows that $K \to U(K)$ is indeed a 1–1 correspondence between the subsets of the sphere and the halo-making sets. Equation (35) holds because p is subjective. To show Eq. (36), let $v \in p^{-1}[p(U)]$. Then $p(v) = p(u)$ for some u in U, so $v^{-1}\,\mathbf{k} = u^{-1}\,\mathbf{k}$ and $vu^{-1}\,\mathbf{k} = \mathbf{k}$. Then $vu^{-1} \in Z$, and $v \in Zu \subseteq U$, from Eq. (30). Therefore $p^{-1}[p(U)] \subseteq U$. And $U \subseteq p^{-1}[p(U)]$ for any set U, so Eq. (36) is proved. Since the zenith locus of any set U is $p(U)$, then the zenith locus of $U(K)$ is K, from Eq. (35). Since $U(K) = p^{-1}(K)$ and since for any function f the set function f^{-1} preserves set unions and intersections, then Eqs. (32) and (33) are also proved. Equation (34) can be proved using Eq. (35). This completes the proof.

Summarizing the relation between a halo-making set U and its zenith locus K, we have

$$\begin{aligned} U &= p^{-1}(K) = \{u : \mathbf{k}_u \in K\} \\ &= \{u : u\mathbf{Y} = \mathbf{k} \text{ for some } \mathbf{Y} \text{ in } K\}, \end{aligned} \tag{37}$$

$$\begin{aligned} K &= p(U) = \{\mathbf{k}_u : u \in U\} \\ &= \{\mathbf{Y} : u\mathbf{Y} = \mathbf{k} \text{ for some } u \text{ in } U\}. \end{aligned} \tag{38}$$

The preceding theorem says that subsets K of the sphere correspond in a natural way to halo-making sets U; the set K corresponding to U is the zenith locus of U. Suppose now that U is the set of wedge orientations determined by ψ and $\mathbf{P}_u$ according to the Spin Vector Assumption—then what is the zenith locus of U? According to the next theorem, it is a circle. Of all the subsets of the sphere, each being the zenith locus of a halo-making set, the Spin Vector Assumption rejects all but the circles.

Theorem—Halo-Making Sets when the Spin Vector Assumption is Satisfied

For $0 \le \psi \le 180$ and for $\mathbf{P}_u$ on the sphere, the set of wedge orientations determined by ψ and $\mathbf{P}_u$ according to the Spin Vector Assumption [Eq. (1)] is $U[K(\psi, \mathbf{P}_u)]$, where $K(\psi, \mathbf{P}_u)$ is the circle with angular radius ψ and center $\mathbf{P}_u$, and where the meaning of U is given in the preceding theorem.

In other words, the zenith locus of the halo-making set determined by ψ and $\mathbf{P}_u$ is the circle with radius ψ and center $\mathbf{P}_u$ (Fig. 8). In particular, the zenith locus of a point halo ($\psi = 0$ or 180) is a point, and the zenith locus of a great circle halo ($\psi = 90$) is a great circle.

Proof of the Theorem

An orientation u is in the set of wedge orientations determined by ψ and $\mathbf{P}_u \Leftrightarrow \mathbf{P} \cdot \mathbf{k} = \cos\psi \Leftrightarrow \mathbf{P}_u \cdot \mathbf{k}_u = \cos\psi \Leftrightarrow \mathbf{k}_u \in K(\psi, \mathbf{P}_u) \Leftrightarrow u \in U[K(\psi, \mathbf{P}_u)]$.

The preceding two theorems do not involve wedge angle α; they are statements only about orientations. The first theorem says that a halo-making set of orientations can be given by choosing a subset of the sphere, namely, the zenith locus. The second says that, if the Spin Vector Assumption holds, then the subset will be the circle with radius ψ and center $\mathbf{P}_u$. To get a halo in this case, one therefore chooses a circle, together with α. If α is fixed, one gets a halo by choosing a circle. The circle, rather than ψ or $\mathbf{P}_u$, is often the fundamental thing, whereas ψ and $\mathbf{P}_u$ are simply devices for keeping track of the circle.

If a circle K on the sphere has radius ψ and pole $\mathbf{P}_u$, then it also has radius $180 - \psi$ and pole $-\mathbf{P}_u$. If K is not a great circle, then it has a unique pole with $\psi < 90$. Thus for a point halo we normally choose the pole so that $\psi = 0$ and $\mathbf{P}_u = \mathbf{k}_u$, rather than $\psi = 180$ and $\mathbf{P}_u = -\mathbf{k}_u$. If K is a great circle, however, there is no natural way of choosing between its two poles. Every great circle halo has two poles, both corresponding to the single radius $\psi = 90$. See Figs. 42–49, for example, where diametrically opposite halos on the outer circle ($x = 0$) of each figure have antipodal $\mathbf{P}_u$ and are therefore the same halo.

The cosets are the smallest nonempty halo-making sets; they are the halo-making sets whose zenith loci consist of single points, the zenith locus of Zu being $\{\mathbf{k}_u\}$. The coset Zu is therefore the halo-making set for a point halo with $\mathbf{P}_u = \mathbf{k}_u$. Since every halo-making set is a union of cosets, then every halo is a union of point halos.

Halo Containments, Unions, and Intersections

In keeping with Eq. (18), we regard one halo as a subset of another if

$$\mathbf{H}(U_1, \alpha_1, \mathbf{S}) \subseteq \mathbf{H}(U_2, \alpha_2, \mathbf{S}) \text{ for all } \mathbf{S}, \tag{39}$$

where U_1 and U_2 are the respective sets of wedge orientations, and α_1 and α_2 are the respective wedge angles. Thus the containment is required to hold no matter where the sun happens to be. This may seem like a strong requirement, since both halos are apt to change dramatically as the sun moves. Nevertheless, Eqs. (19) and (34) show that, if $\alpha_1 = \alpha_2$, then halo containments are easily inferred from containment relations between the corresponding zenith loci, which are easy to visualize on the sphere. Similar remarks apply to halo unions and intersections.

Thus, as already mentioned, every halo is a union of point halos. In particular, each great circle halo, whose zenith locus is a great circle on the sphere, is a union of point halos, each corresponding to a point on the great circle. In Fig. 43, for example, the halo with $\mathbf{P}_u = (0, \pm 1, 0)$—the upper and lower tangent arcs—is the union of all the point halos having $\mathbf{P}_u$ on the great circle $y = 0$.

Any two great circle halos contain two point halos in common, since their corresponding great circles intersect in two points (or coincide). Similarly, any two point halos are subsets of some great circle halo.

B. Vectors S and H Revisited

We now reexamine the relation between the light points $\mathbf{S}$ and $\mathbf{H}$ of the incoming and outgoing rays to the wedge. The relation is of course contained in Eq. (7), but we wish to stress the geometric point of view expressed in the fundamental Fig. 3. We emphasize that to get $\mathbf{H}$ from $\mathbf{S}$, we simply project the inner sphere to the outer sphere parallel to the entry face normal $\mathbf{N}$, and then project the outer sphere back to the inner sphere parallel to the exit face normal $\mathbf{X}$.

Not all rays can pass through the wedge in the prescribed way, that is, by entering the entry face and exiting the exit face. For rays that can do so, the light points before entering make up the *entry region* on the sphere, those after exiting make up the *exit region*. These regions can be thought of either as moving with the wedge or as fixed, depending on whether they are viewed from space or from the wedge.

The mapping from $\mathbf{S}$ to $\mathbf{H}$ is a 1–1 correspondence between the entry and exit regions. Classically the mapping was studied by first proving that $\mathbf{H} \cdot \mathbf{B} = \mathbf{S} \cdot \mathbf{B}$, which for us is obvious from Fig. 3, since $\mathbf{B}$ (not shown in Fig. 3) is orthogonal to the brim of the helmet in the figure. The points $\mathbf{S}$ and $\mathbf{H}$ therefore differ by a rotation about point $\mathbf{B}$, as in Fig. 9. The amount of rotation is $d = d(\mathbf{S}) = \delta(\mathbf{H}) - \delta(\mathbf{S})$, which is the (negative of the) deviation between $\mathbf{S}$ and $\mathbf{H}$ but projected onto the normal plane—the plane occupied by the brim of the helmet. Classically[4] the angle d was calculated using Bravais' law and was then used to get $\mathbf{H}$. Bravais' law says that, if the vectors $\mathbf{S}$ and $\mathbf{H}$ are projected to the normal plane, then the projected vectors satisfy Snell's law but with the refractive index n replaced by $(n^2 - \cos^2\theta)^{1/2}/\sin\theta$. This can be seen by constructing the two spheres for which the two dark concentric circles bounding the brim are great circles, by noting that the tips of the vectors $\mathbf{S}$ and $\mathbf{H}$ do not change when they are projected to the normal plane, and by observing that the radii of the two circles are $(n^2 - \cos^2\theta)^{1/2}$ and $\sin\theta$. But for us Bravais' law is of historical interest only.

We get another picture of the relation between $\mathbf{S}$ and $\mathbf{H}$ by considering the deviation $\Delta = \Delta(\mathbf{S})$ between the two, which is given by

$$\cos\Delta = \mathbf{S} \cdot \mathbf{H}. \tag{40}$$

Thus Δ is measured along a great circle, whereas d is measured along a Bravais circle. Figure 9 shows the level curves of Δ, which are in the entry region. Their images are shown as well, in the exit region, each image of a curve being the reflection, in the horizontal plane, of the original curve; this can be easily seen by drawing the $\mathbf{N}$- and $\mathbf{X}$-projections. The mapping from $\mathbf{S}$ to $\mathbf{H}$, however, is not a reflection, but rather takes the lower "half" of one curve to the lower half of the other, and similarly for the upper halves. So from the level curves of Δ together with their images, $\mathbf{H}$ can be located as a function of $\mathbf{S}$, since $\mathbf{H}$ and $\mathbf{S}$ are on the same Bravais circle.

The deviation Δ is known to be minimum exactly when $\mathbf{T} = n\mathbf{A}$. (See Fig. 3 for $\mathbf{T}$ and Fig. 10 for $\mathbf{A}$.) By drawing $\mathbf{S}$, $\mathbf{T}$, and $\mathbf{H}$ appropriately on concentric circles of radius 1 and n, we easily find that the minimum value Δ_m of the deviation is given by

$$\sin[(\alpha + \Delta_m)/2] = n \sin(\alpha/2). \tag{41}$$

The values of $\mathbf{S}$ and $\mathbf{H}$ in this minimum deviation configuration are the *minimum deviation entry* and

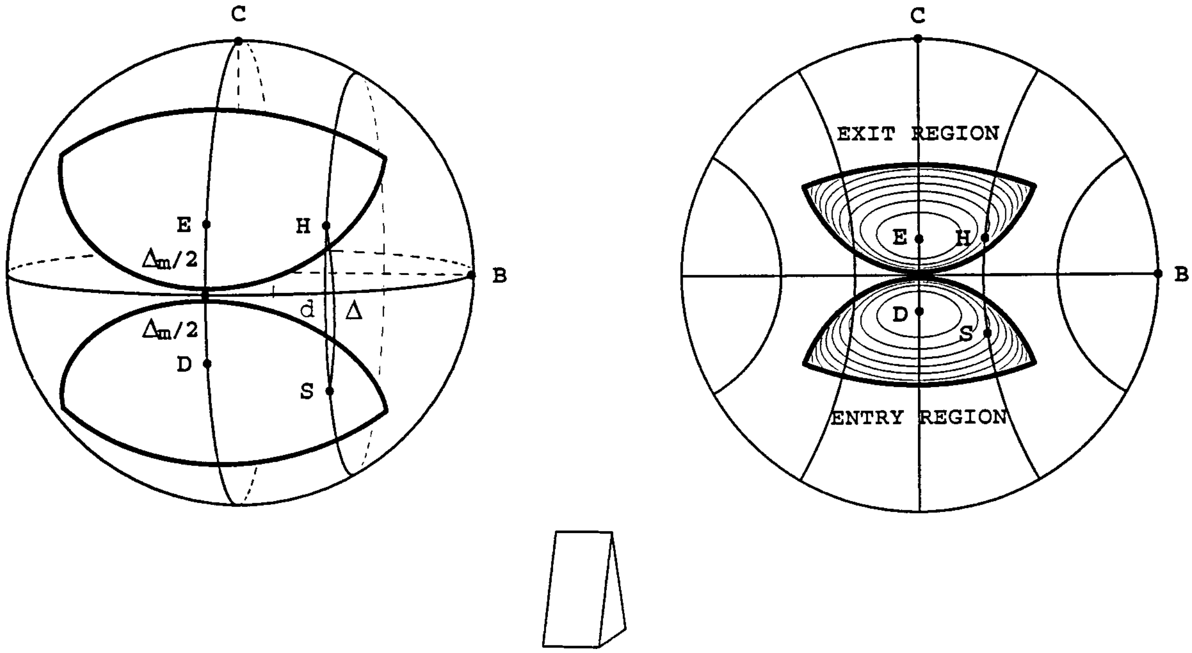

Fig. 9. Above left, entry and exit regions and typical sun point **S** and halo point **H**. The entry region of the sphere is the lower of the two regions enclosed by the heavy curves—it consists of the directions from which light can originate and then pass through the wedge; when **S** lies outside the entry region there is no **H**. The exit region is the upper of the two regions enclosed by the heavy curves—it consists of the directions from which the outgoing light can appear to come; **H** will always be in the exit region. Since from Fig. 3 the points **S** and **H** are on the same Bravais circle, then they differ by a rotation through an angle $d = d(\mathbf{S})$ about **B**. Right, same, but seen in stereographic projection, as in Fig. 7, and with the addition of level curves of the deviation Δ, in the entry region, and their images in the exit region. The vectors **D** and **E** are the minimum deviation entry and exit vectors; Δ is minimum when $\mathbf{S} = \mathbf{D}$ or, equivalently, $\mathbf{H} = \mathbf{E}$. The apparent difference in sizes of the entry regions in the two diagrams is due to the stereographic projection. The wedge at lower center belongs at the center of the sphere. Here $\alpha = 80.2$.

exit vectors **D** and **E**. From their symmetrical placement and from their separation Δ_m,

$$\mathbf{D} = \cos(-\Delta_m/2)\,\mathbf{A} + \sin(-\Delta_m/2)\,\mathbf{C} \tag{42}$$

or

$$\mathbf{D}_u = [\cos(-\Delta_m/2),\, 0,\, \sin(-\Delta_m/2)]. \tag{43}$$

Similarly,

$$\mathbf{E}_u = [\cos(\Delta_m/2),\, 0,\, \sin(\Delta_m/2)]. \tag{44}$$

The ray path for minimum deviation is perpendicular to the refracting edge and has the well-known symmetric form.

We now have several equivalent characterizations of minimum deviation:

$$\begin{aligned} &\Delta(\mathbf{S}) \text{ is minimum} \\ &\text{iff } \Delta(\mathbf{S}) = \Delta_m \\ &\text{iff } \mathbf{S} = \mathbf{D} \\ &\text{iff } \mathbf{T} = n\mathbf{A} \\ &\text{iff } \mathbf{H} = \mathbf{E}. \end{aligned} \tag{45}$$

Figure 10 shows how to find the entry and exit regions. Examination of the figure reveals that the lower boundaries of the regions correspond to grazing entry, and the upper boundaries to grazing exit.

Figure 10 can be used to derive analytic descriptions of the boundaries, which are needed to apply the Nonempty Halos Theorem, Subsection 2.F. To parameterize the upper boundary of the entry region, first parameterize the great circle $\mathbf{X} \cdot \mathbf{H} = 0$ on the inner sphere, which consists of light points **H** of rays that have originated within the wedge and have exited the exit face tangentially. In the lower left diagram of Fig. 10 this is the circle where the lower cylinder is tangent to the inner sphere. It is a union of the two Bravais meridians $\delta = \alpha/2 \pm 90$, and a typical point on it, from Eq. (27), is

$$u\,B(\theta, \alpha/2 - 90), \tag{46}$$

where θ is allowed to range over $0 \le \theta \le 360$. The **X**-projection of the point to the outer sphere is

$$\mathbf{Tx}(\theta) = u\,B(\theta, \alpha/2 - 90) + (n^2 - 1)^{1/2}\,\mathbf{X}, \tag{47}$$

and the upper boundary of the region T in the figure is parameterized by $\mathbf{Tx}(\theta)$, $\theta_0 \le \theta \le 180 - \theta_0$, where θ_0 can be found by requiring $\mathbf{Tx}(\theta)$ to be on the equator:

$$\sin\theta_0 = (n^2 - 1)^{1/2}\tan(\alpha/2). \tag{48}$$

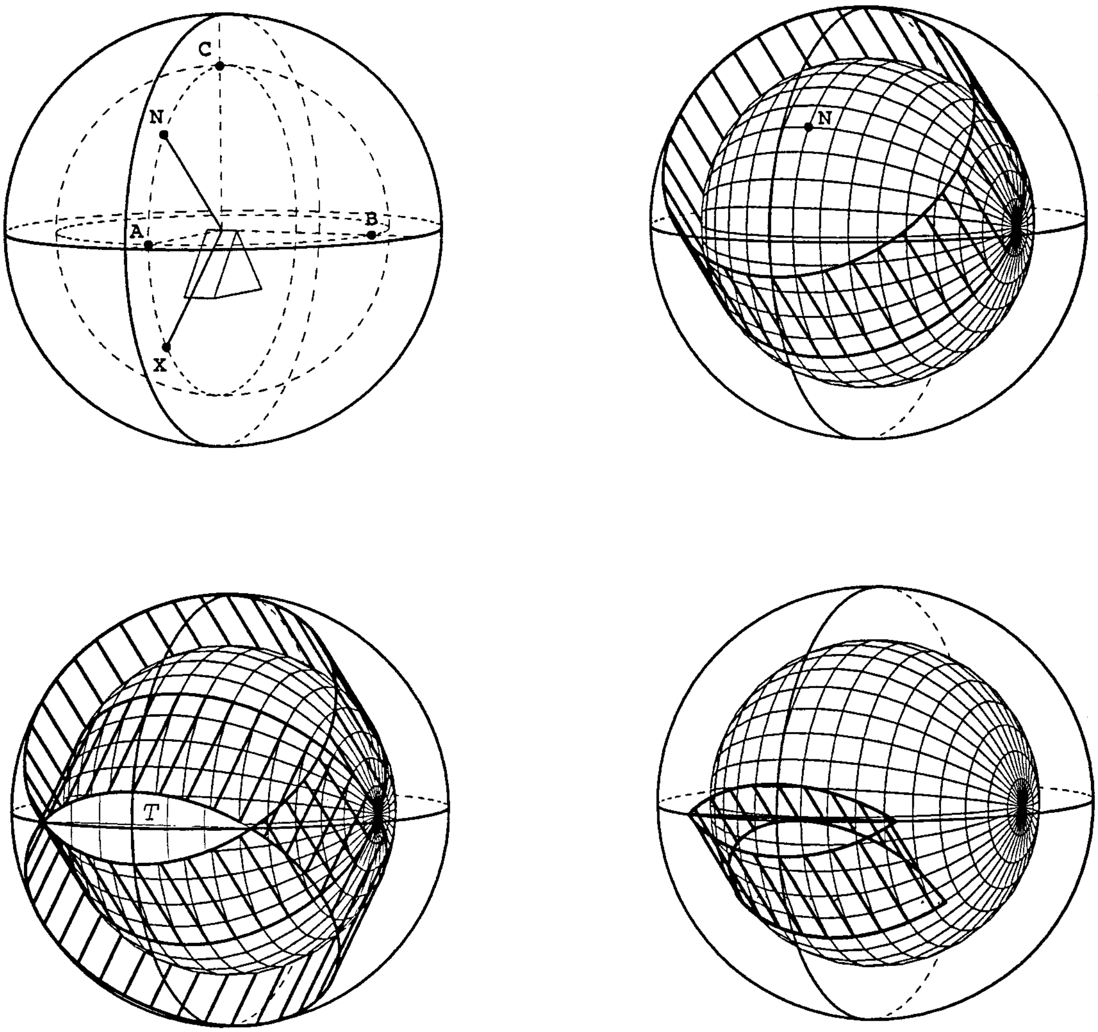

Fig. 10. Finding the entry region. Above left, reference diagram showing concentric spheres of radii 1 and n, with both spheres cut away completely to show the wedge with entry and exit normals **N** and **X**. Compare Fig. 3. Above right, **N**-projection of the inner sphere to the outer. The region of the outer sphere within the cylinder consists of light points of rays that have entered at the entry face. Below left, same, but with **X**-projection of the outer sphere to the inner. The region of the outer sphere within the new cylinder consists of light points of rays that originate within the wedge and that can exit the exit face. The region T on the outer sphere and common to the two cylinders therefore consists of light points of rays within the wedge that have entered the entry face and that can exit the exit face. Below right, the entry region—the result of **N**-projecting T back to the inner sphere. This region consists of light points of rays outside the wedge that can enter the entry face and exit the exit face. Similarly, **X**-projecting T would give the exit region. See also Fig. 9. Here $\alpha = 80.2$.

The upper boundary of the entry region can be found by **N**-projecting back to the inner sphere. A typical point is

$$\mathbf{Sx}(\theta) = \mathbf{pr}(\mathbf{Tx}(\theta), \mathbf{N}, 1), \quad \theta_0 \le \theta \le 180 - \theta_0. \quad (49)$$

The point $\mathbf{Sx}(\theta)$ is the light point of an incoming ray that will pass through the wedge and experience grazing exit.

The lower boundary is part of the Bravais meridian $\delta = -\alpha/2 + 90$. A typical point is

$$\mathbf{Sn}(\theta) = u\, B(\theta, -\alpha/2 + 90), \quad \theta_0 \le \theta \le 180 - \theta_0. \quad (50)$$

The point $\mathbf{Sn}(\theta)$ is the light point of an incoming ray that will pass through the wedge but with grazing entry.

The wedge angle in Figs. 9 and 10 is $\alpha = 80.2$, which is the value for the 35° circular halo, from Eq. (41). Figures 52 and 59 show the entry region for $\alpha = 28$ and $\alpha = 90$, which are the values for the 9° and 46° circular halos. The dramatic dependence on α is easy to understand by considering the region T between the two cylinders in Fig. 10. As α increases, T shrinks, and the entry and exit regions shrink with it.

As α continues to increase, it eventually reaches a value α_{max} at which the entry and exit regions each consist of a single point, **D** and **E**, respectively. Any ray passing through such a wedge will enter from direction **D** and exit from direction **E**. Wedges having larger α cannot pass light at all. The value α_{max} is found from Eq. (48) with $\theta_0 = 90$; for $n = 1.31$ it is $\alpha_{max} = 99.5$.

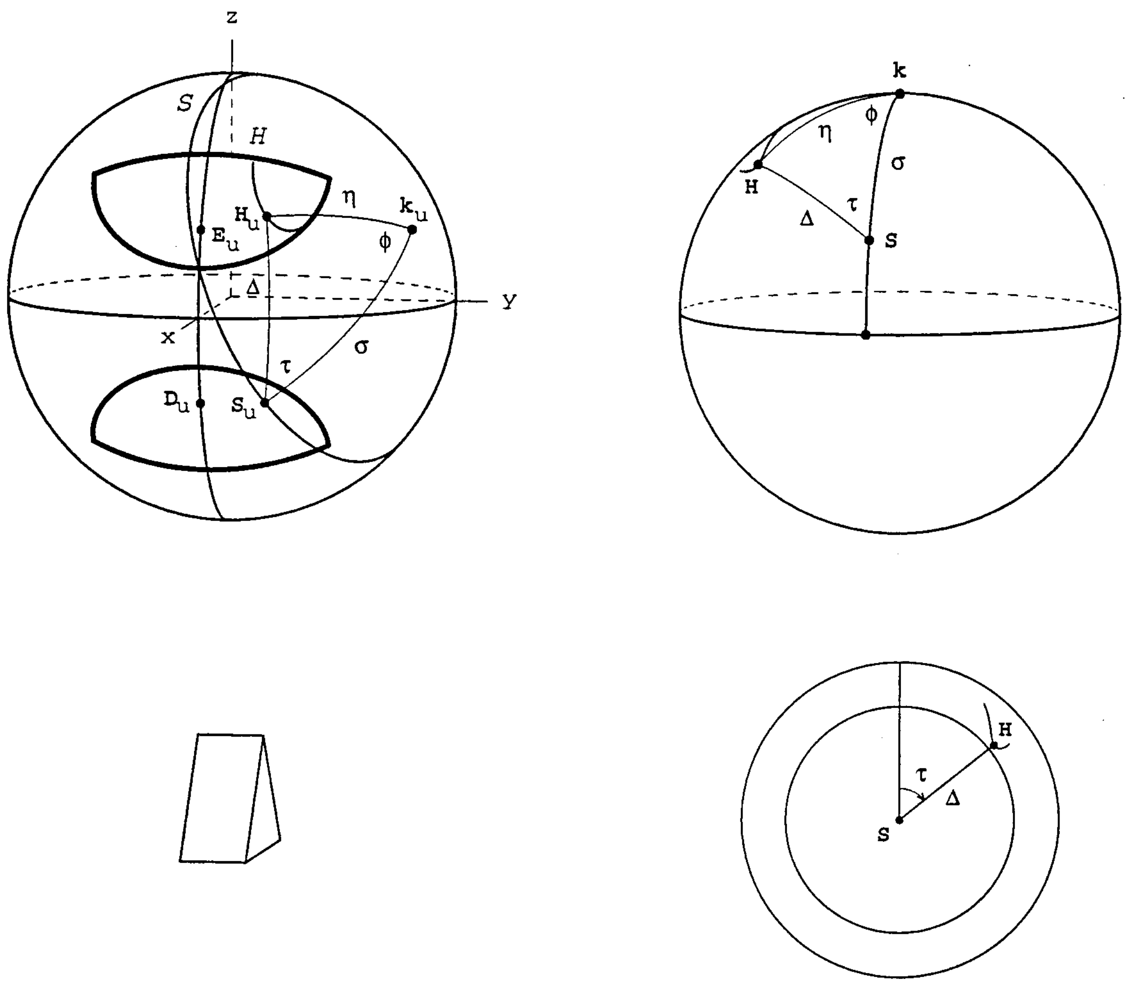

Fig. 11. Creation of a point halo. Above left, view from the wedge. The halo has constant $\mathbf{k}_u$—zenith point as seen from the wedge—as shown. The points $\mathbf{S}_u$ and $\mathbf{H}_u$ are the sun and corresponding halo point as seen from the wedge. The curve S is the sun locus, the path traced out by $\mathbf{S}_u$; it is a circle with center $\mathbf{k}_u$ and radius $\sigma = 90 - \Sigma$, the zenith angle of the sun. The curve H is the halo point locus, the path traced out by $\mathbf{H}_u$. The wedge at lower left belongs at the center of the left-hand sphere. The wedge is shown in standard orientation and is included to emphasize the geometric meaning of the subscripted vectors. Above right, view from space, with the halo at the far upper left of the sphere. Both upper diagrams show the triangle whose vertices are the zenith, the sun, and the halo point; the left diagram is the view from the wedge, the right is the view from space. The meaning of Δ, τ, η, ϕ, σ at left is therefore the same as at the right, namely, Δ, τ, η, ϕ are the deviation, bearing, zenith angle, and azimuth of the halo point, and σ is the zenith angle of the sun. Note that Δ and τ are sufficient to locate $\mathbf{H}$ with respect to $\mathbf{S}$. Below right, same halo but seen from inside the celestial sphere and looking directly toward the sun, as in the halo diagrams of Appendix A. [$\mathbf{k}_u = \mathbf{P}_u = B(30, -45)$, $\alpha = 90$, $\sigma = 65$ (hence $\Sigma = 25$)]

C. Creation of a Halo

We now visualize the creation of a halo, but first from the point of view of a rider on the wedge. It is largely a matter of adding *xyz*-axes appropriately in Fig. 3 and subscripting all vectors with u. The vector $\mathbf{S}_u$ is the direction of the sun as seen from the wedge, and $\mathbf{H}_u$ is similarly the direction of the halo point. To get $\mathbf{H}_u$ from $\mathbf{S}_u$, we project $\mathbf{S}_u$ to the outer sphere parallel to $\mathbf{N}_u$, getting $\mathbf{T}_u$, and then project $\mathbf{T}_u$ back to the inner sphere parallel to $\mathbf{X}_u$, getting $\mathbf{H}_u$. The formal reasoning, from Eqs. (11), (12), and (23), is

$$\begin{aligned}\mathbf{H}_u &= \mathbf{F}(\mathbf{N}, \mathbf{X}, \mathbf{S})_u = u^{-1}\mathbf{F}(\mathbf{N}, \mathbf{X}, \mathbf{S}) \\ &= \mathbf{F}(u^{-1}\mathbf{N}, u^{-1}\mathbf{X}, u^{-1}\mathbf{S}) = \mathbf{F}(\mathbf{N}_u, \mathbf{X}_u, \mathbf{S}_u). \quad (51)\end{aligned}$$

But there is a difference between the space perspective and the wedge perspective. The vectors $\mathbf{N}$ and $\mathbf{X}$, giving the face normals from the space perspective, depend on the wedge orientation u, but $\mathbf{N}_u$ and $\mathbf{X}_u$, giving the wedge perspective, are fixed. Similarly, $\mathbf{S}$ is fixed but $\mathbf{S}_u$ varies. The *sun locus S* is the path traced out by $\mathbf{S}_u$ as the wedge changes its orientation u, and the *halo point locus H* is the path traced out by $\mathbf{H}_u$. If the location of $\mathbf{S}_u$ on the sun locus is known, then $\mathbf{H}_u$ is determined. Where, then, is the sun locus?

Since every halo is a union of point halos, we consider first the case of a point halo. A point halo has constant $\mathbf{k}_u$, the zenith point as seen from the wedge. If $\sigma = 90 - \Sigma$ is the zenith angle of the sun, that is, if $\mathbf{S}$ is at angular distance σ from $\mathbf{k}$, then a rider on the wedge sees $\mathbf{S}_u$ at angular distance σ from $\mathbf{k}_u$; the sun locus S is a circle of radius σ about $\mathbf{k}_u$, as in Fig. 11. When $\mathbf{S}_u$ lies on the part of S outside the entry

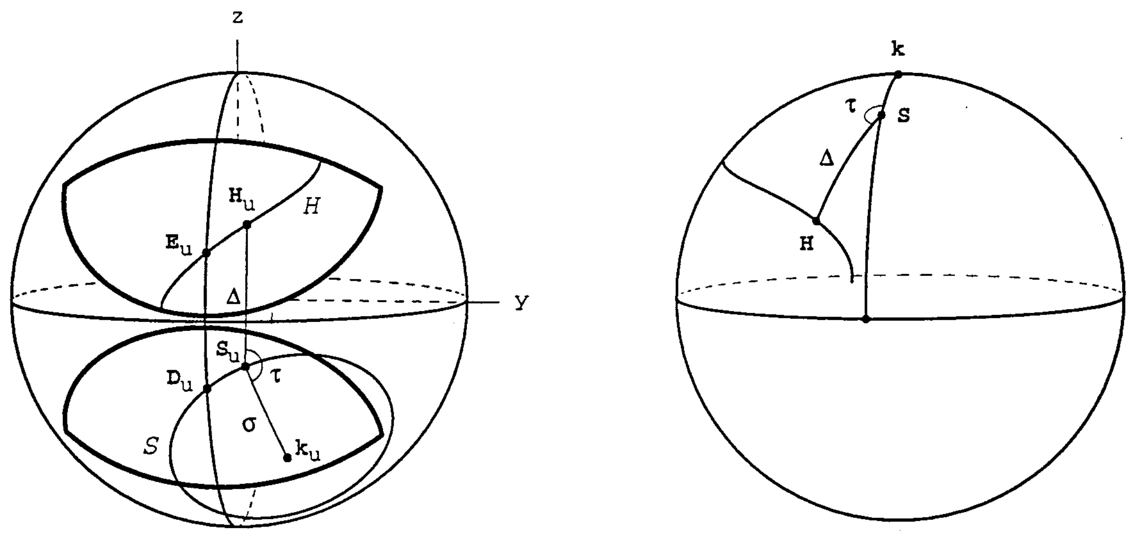

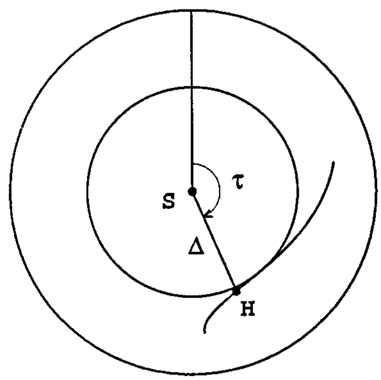

Fig. 12. Creation of another point halo. As in Fig. 11, the point $\mathbf{S}_u$ traverses the sun locus S, and $\mathbf{H}_u$ simultaneously traverses the halo point locus H. In this figure, however, the arc of S within the entry region subtends a much larger angle from $\mathbf{k}_u$, thus producing a wider variation in τ as $\mathbf{S}_u$ varies, so that the halo is no longer confined to a narrow sector but instead extends more than 90° along and just outside the circular halo. [$\mathbf{k}_u = B(71, 41)$, $\alpha = 80.2$, $\sigma = 30$ ($\Sigma = 60$)]

region, the light cannot pass through the wedge and there is no $\mathbf{H}_u$. But as $\mathbf{S}_u$ traces out the part of S within the entry region, then $\mathbf{H}_u$ traces out H in the exit region.

The intelligent wedge rider can also construct the halo itself, as seen from space. The points $\mathbf{k}_u$ and $\mathbf{S}_u$ need only be rotated to $\mathbf{k}$ and $\mathbf{S}$; the same rotation—it is of course u—must take $\mathbf{H}_u$ to $\mathbf{H}$, thus locating $\mathbf{H}$. (The unlikely cases $\sigma = 0$, 180 are slightly different, but easy.) Thus the construction of the halo proceeds point by point; there is no single rotation that takes the curve H to the halo. We next consider the construction in detail and discover that the shape of the halo is predictable without elaborate calculation.

D. Why the Halos Look the Way They Do

It is crucial to recognize that $\mathbf{k}_u$, $\mathbf{S}_u$, and $\mathbf{H}_u$ are indeed the zenith, the sun, and the halo point, just seen from the unconventional perspective of the wedge. In Fig. 11, then, the triangle $\mathbf{k}$ $\mathbf{S}$ $\mathbf{H}$ at the right can be trivially reconstructed from the triangle $\mathbf{k}_u$ $\mathbf{S}_u$ $\mathbf{H}_u$ at the left, thus locating the halo point $\mathbf{H}$ on the celestial sphere. In particular, the angular distance Δ between $\mathbf{S}_u$ and $\mathbf{H}_u$ in the left diagram must be the deviation between $\mathbf{S}$ and $\mathbf{H}$. Similarly, the angular distance η between $\mathbf{k}_u$ and $\mathbf{H}_u$ must be the zenith angle of $\mathbf{H}$. And the angle τ must be the bearing of $\mathbf{H}$ from $\mathbf{S}$, that is, the angle from the vertical arc $\mathbf{S}$ $\mathbf{k}$ to the arc $\mathbf{S}$ $\mathbf{H}$.

Now suppose we wish to start from scratch and recreate the halo, at least qualitatively. We are therefore given $\mathbf{k}_u$, α, and σ. Then S is known from $\mathbf{k}_u$ and σ, and the entry and exit regions are known from α. Because the arc of S that is within the entry region subtends a relatively small angle as seen from $\mathbf{k}_u$, and because $\mathbf{H}_u$ is on the same Bravais circle as $\mathbf{S}_u$, then the angle τ_{var}—the variation in τ as $\mathbf{S}_u$ varies (not shown)—is small. But since τ_{var} is small in the left diagram, then the same is true in the right, and hence the halo is confined to a rather narrow sector having vertex at the sun and having sector angle τ_{var}. By examining the way $\mathbf{S}_u$ cuts across the level curves of Δ shown in Fig. 9, or rather their analogs for the wedge angle under consideration here, we see that Δ varies from a relative maximum where $\mathbf{S}_u$ enters the entry region, down to a minimum in the interior, and then back up to a relative maximum where it exits. So the halo must be a U-shaped curve, with the bottom of the U pointing approximately toward the sun. Finally, as viewed from inside the celestial sphere, the bearing of the halo from the sun must be about the same as the bearing of $\mathbf{k}_u$ from $\mathbf{D}_u$. This halo is the right Parry supralateral arc, which is the point halo with $\alpha = 90$ and $\mathbf{k}_u = B(30, -45)$ [i.e., $\mathbf{k}_u$ has Bravais coordinates $(\theta, \delta) = (30, -45)$]. In the two right-hand diagrams of Fig. 11 the halo is shown with $\Sigma = 25$, and in Fig. 41 with $\Sigma = 20$. (Recall that $\mathbf{P}_u = \mathbf{k}_u$ for point halos.)

Any point halo can be understood by making the drawing comparable with Fig. 11 and by considering the arc of S within the entry region. Figure 11 is typical of point halos with $\mathbf{k}_u$ in a broad and vaguely defined annular region centered at $\mathbf{D}_u$ and approximately 90° away, and with the sun not too far above or below the horizon. The arc of S that is within the entry region subtends a relatively small angle as seen from $\mathbf{k}_u$, and the halo is therefore a more or less U-shaped curve confined to a narrow sector, with the bearing of the halo from the sun being about the same as the bearing of $\mathbf{k}_u$ from $\mathbf{D}_u$. All of the above is more nearly correct when α is large, so that the entry region is small; see Figs. 33–41, especially Figs. 40 and 41.

For comparison, consider the point halo in Fig. 12. The wedge angle is smaller than in Fig. 11, and so the entry region is larger. Also, $\mathbf{k}_u$ is much closer to the entry region (within it, in fact) and σ is much smaller, so that the arc of S within the entry region now subtends a considerable angle as seen from $\mathbf{k}_u$, and τ_{var} is no longer small but rather 90° or more. This same τ_{var} is seen in the halo itself, where the halo extends a little more than 90° along and just outside the circular halo.

For $\mathbf{k}_u$ which, like this one, are within the entry region, sufficiently small σ will give a sun locus S that is entirely in the entry region. Then $\tau_{\text{var}} \geq 360°$ and the halo is a closed loop encircling the sun, as in Fig. 13. There the level curves of Δ indicate that Δ should have two relative minima and two relative maxima on S, and this is borne out by the halo itself. Figure 36 contains four other examples of halos with S entirely in the entry region, but in contrast to Fig. 13, the point $\mathbf{D}_u$ lies outside S, and the level curve picture as well as the halos themselves suggest that there is just one relative maximum and one relative minimum for each.

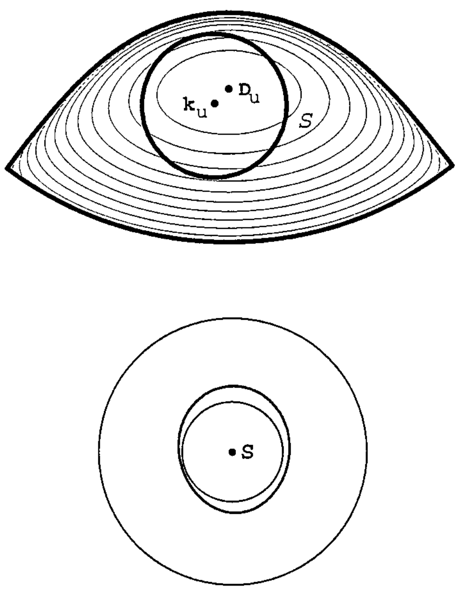

Fig. 13. Creation of another point halo. The upper diagram shows the entry region together with the sun locus S and level curves of the deviation Δ. Tangencies of S with the level curves give relative extrema of Δ, which can then be located on the halo itself, in the lower diagram. Here there are two relative minima and two relative maxima. [$\mathbf{k}_u = B(95, 16)$, $\alpha = 60$, $\sigma = 25$ ($\Sigma = 65$)]

The halos at $\mathbf{P}_u = (1, 0, 0)$ in Figs. 34 and 39 provide one final interesting feature—each is disconnected. This is not surprising if one considers the portion of the sun locus that lies in the entry region, for it too is disconnected.

In either Fig. 11 or Fig. 12 the difference between the left- and right-hand diagrams—wedge view versus space view—is not so much in where the viewpoint is located at any one moment. If the sun locus, halo point locus, and the halo itself are removed from the diagrams, leaving only a snapshot taken at a fixed moment, then the two diagrams hardly differ, being congruent by way of the rotation u. The essential difference between the left- and right-hand diagrams is in how the views change from moment to moment. In the left-hand diagram the viewpoint is fixed in the wedge, and so space vectors, like the sun vector, appear to move in circles about the zenith. In the right-hand diagram the viewpoint is fixed in space, and wedge vectors appear to move in circles about the zenith. The halo point is neither a wedge vector nor a space vector, and from either perspective it appears to move, tracing out the halo point locus from the wedge perspective and tracing out the halo itself from the space perspective. In general the two curves are not congruent.

To help in thinking about the creation of point halos, we imagine a more ambitious version of the nail and wooden wedge model of Subsection 1.B. It resembles a commercially available star globe—a large transparent plastic sphere with a rod extending diametrically through it from top to bottom. Instead of the rod skewering a miniature Earth at the center of the sphere, however, the rod skewers the wedge, and in such a way that, as seen from the wedge, the "up" end of the rod is in the direction of $\mathbf{k}_u$. The wedge, then, is at the center of the sphere, with both wedge and sphere fixed to the rod. On the sphere we paint the entry and exit regions, the minimum deviation entry and exit vectors, and the level curves of Δ and their images, making sure to locate them correctly with respect to the wedge (Fig. 9). We place the entire contraption inside a slightly larger transparent sphere fixed in space, and we are ready to create the halo. Wedge, inner sphere, and rod rotate together, with the rod remaining vertical. To find the halo point at some instant, we stop the rotation. A ray from the sun proceeding toward the center of the spheres will pierce both spheres at the sun point, the same point on both spheres. On each sphere we

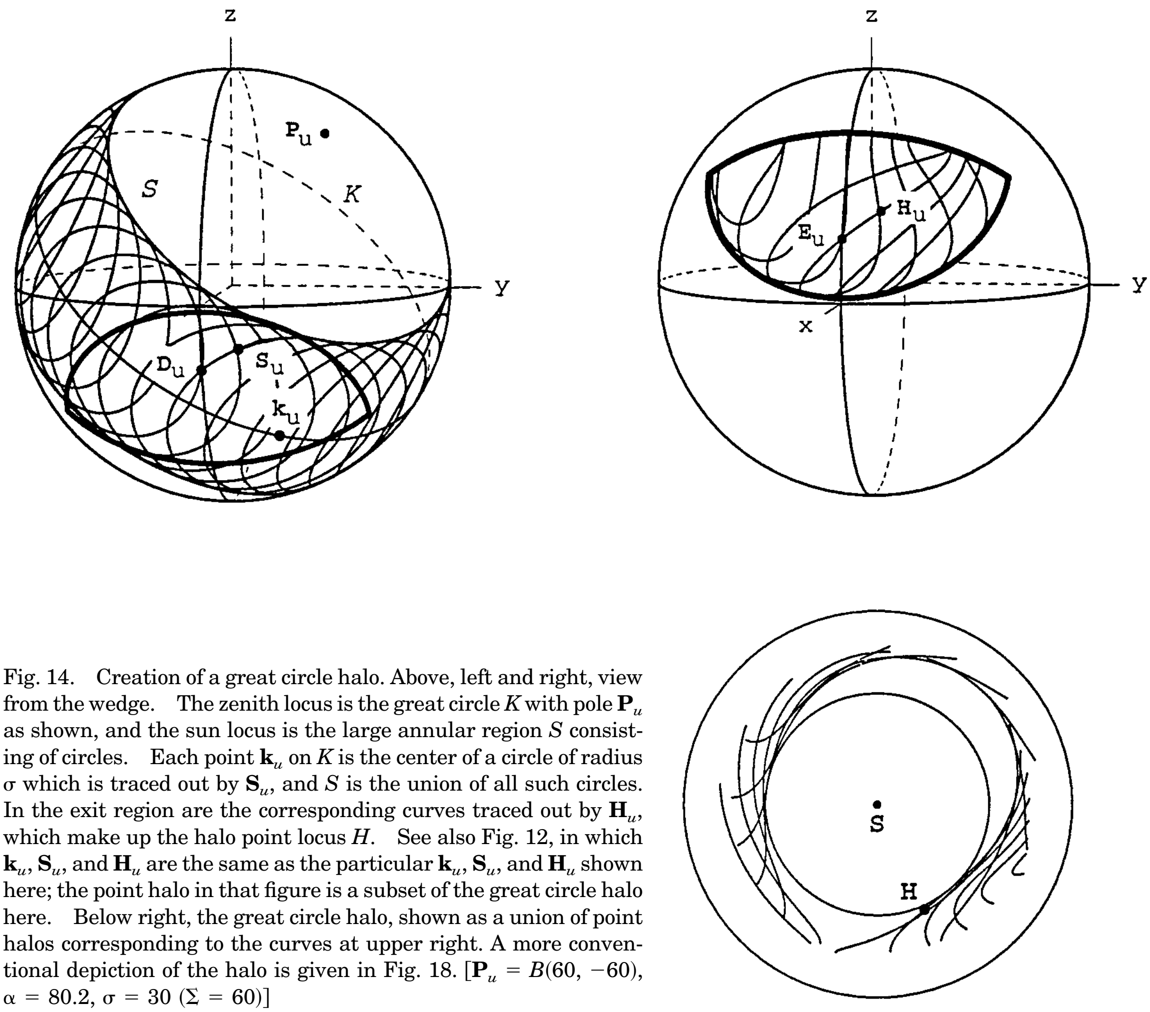

Fig. 14. Creation of a great circle halo. Above, left and right, view from the wedge. The zenith locus is the great circle K with pole $\mathbf{P}_u$ as shown, and the sun locus is the large annular region S consisting of circles. Each point $\mathbf{k}_u$ on K is the center of a circle of radius σ which is traced out by $\mathbf{S}_u$, and S is the union of all such circles. In the exit region are the corresponding curves traced out by $\mathbf{H}_u$, which make up the halo point locus H. See also Fig. 12, in which $\mathbf{k}_u$, $\mathbf{S}_u$, and $\mathbf{H}_u$ are the same as the particular $\mathbf{k}_u$, $\mathbf{S}_u$, and $\mathbf{H}_u$ shown here; the point halo in that figure is a subset of the great circle halo here. Below right, the great circle halo, shown as a union of point halos corresponding to the curves at upper right. A more conventional depiction of the halo is given in Fig. 18. [$\mathbf{P}_u = B(60, -60)$, $\alpha = 80.2$, $\sigma = 30$ ($\Sigma = 60$)]

mark the point with a black dot. Knowing the sun point, we then use the Bravais meridians and the level curves to locate the halo point, also the same on both spheres. We mark it with a red dot on each sphere. For the given instant that is all there is to it. Then the process is repeated for other instants giving other stages in the rotation. As more and more black and red dots accumulate, the black dots (sun points) on the outer sphere all coincide, and the black dots on the inner sphere form a circle, essentially the sun locus. The red dots (halo points) on the inner sphere form the halo point locus, and the red dots on the outer sphere form the halo.

We have seen how to construct point halos. Great circle halos, being unions of point halos, can in principle be constructed from the point halos, although in practice this can put some demands on the imagination. Figure 14 shows the creation of a great circle halo.

E. Other Ray Paths

The ray paths for halos that we consider in this paper enter the entry face of the wedge and directly exit the exit face, with no intervening internal reflections. Our methods, however, can easily be extended to certain ray paths involving internal reflections. Ray paths for subparhelia, Wegener arcs, and Hastings arcs, for example, have an internal reflection off the plane perpendicular to the entry and exit faces. How would such a reflection change a figure such as Fig. 11? In the left-hand diagram the halo point $\mathbf{H}_u$ and hence the halo locus H would be reflected across the Bravais equator $y = 0$. The halo itself, in the right-hand diagram, would change as well, but in a less transparent way. Thus for each halo in the existing atlas, Appendix A, there would be a new halo, with a simple connection between the two, although the two halos in general would look quite different from space. An entire new atlas of simulations would result. A new atlas would likewise result from any other new ray path considered.

F. Empty Halos

The halo simulations of Appendix A show many halos that are empty at the given sun elevation. Figure 11 shows how this can happen: if σ were somewhat smaller, then the sun locus S would miss the entry region entirely. So point halos can easily be empty, especially if the wedge angle is large, so that the entry region is small, or if the sun is high, so that the

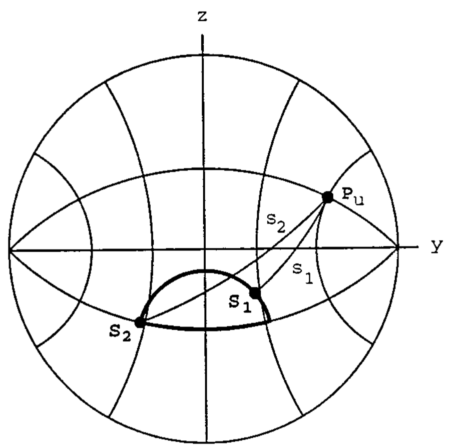

Fig. 15. Minimum and maximum angular distances s_1 and s_2 from $\mathbf{P}_u = B(30, -45)$ to the $\alpha = 90$ entry region. Here $s_1 = 58$ and $s_2 = 117$. The point halo with pole $\mathbf{P}_u$ and wedge angle α is nonempty for $s_1 \le \sigma \le s_2$. The great circle halo with this pole and wedge angle is never empty, since $s_1 \le 90 \le s_2$, so that the zenith locus passes through the entry region.

radius σ of S is small. Thus Fig. 41, with $\alpha = 90$, has several empty halos, and Fig. 36, with $\Sigma = 80$, has many. In Section 1 we mentioned that point halos with $\mathbf{P}_u$ ($= \mathbf{k}_u$) on the upper rear of the sphere tend to require the sun to be below the horizon in order to be nonempty. The reason is now clear: for such halos, σ must be large for S to reach the entry region.

Great circle halos are much less apt to be nonempty, because of their much larger sun locus, as in Fig. 14. In fact, the halo in that figure is never empty, regardless of sun elevation, since its zenith locus passes through the entry region. But the supralateral arc (Subsection 3.B) is a familiar great circle halo which is empty even for moderate sun elevations. And any great circle halo whose zenith locus misses the entry region will be empty for sufficiently high sun; two such empty halos can be seen in Fig. 45.

To summarize, a halo with zenith locus K, wedge angle α, and solar zenith angle σ is nonempty if and only if there is a point of K and a point in the entry region that are at angular distance σ from each other, since in this case the sun locus will intersect the entry region, and otherwise not. For point and great circle halos there is the following consequence:

Nonempty Halos Theorem

For a halo with pole $\mathbf{P}_u$ and wedge angle $\alpha \le \alpha_{\max}$, let s_1 and s_2 be the angular distances from $\mathbf{P}_u$ to the nearest and farthest points of the entry region ($0 \le s_1 \le s_2 \le 180$). Let σ be the solar zenith angle.

(i) If the halo is a point halo ($\psi = 0$), then it is nonempty if and only if $s_1 \le \sigma \le s_2$.

(ii) If the halo is a great circle halo, then either $s_1 \le 90 \le s_2$ (K passes through the entry region), in which case the halo is never empty, or, without loss of generality, $s_1 \le s_2 < 90$ (the entry region and $\mathbf{P}_u$ are on the same side of K), in which case the halo is nonempty if and only if $90 - s_2 \le \sigma \le 90 + s_2$, that is, $-s_2 \le \Sigma \le s_2$.

To apply the theorem we need to be able to calculate s_1 and s_2. A typical point on the upper boundary of the entry region is $\mathbf{Sx}(\theta)_u$, where $\theta_0 \le \theta \le 180 - \theta_0$ [Eq. (49)]. The angular distance from $\mathbf{P}_u$ to $\mathbf{Sx}(\theta)_u$ is $s(\theta) = \arccos[\mathbf{Sx}(\theta)_u \cdot \mathbf{P}_u]$. We evaluate $s(\theta)$ at closely spaced θ and take the minimum and maximum of the resulting finite set, and then proceed analogously with $\mathbf{Sn}(\theta)_u$ for the lower boundary. The smaller of the resulting two minima is s_1, except that $s_1 = 0$ if $\mathbf{P}_u$ is in the entry region. The larger of the two maxima is s_2, except that $s_2 = 180$ if $-\mathbf{P}_u$ is in the entry region.

For an illustration of the theorem see Fig. 15, where $\mathbf{P}_u = B(30, -45)$ and where the entry region is for wedge angle $\alpha = 90$. We compute $s_1 = 58$ and $s_2 = 117$. According to the theorem, the point halo with this pole and wedge angle is nonempty for $58 \le \sigma \le 117$, that is, for $-27 \le \Sigma \le 32$. The great circle halo with this pole and wedge angle is never empty, since $58 \le 90 \le 117$.

G. Contact Points with the Circular Halo

The contact points of a halo with the (inner boundary of the) relevant circular halo are important features. To analyze them, we introduce spherical coordinate

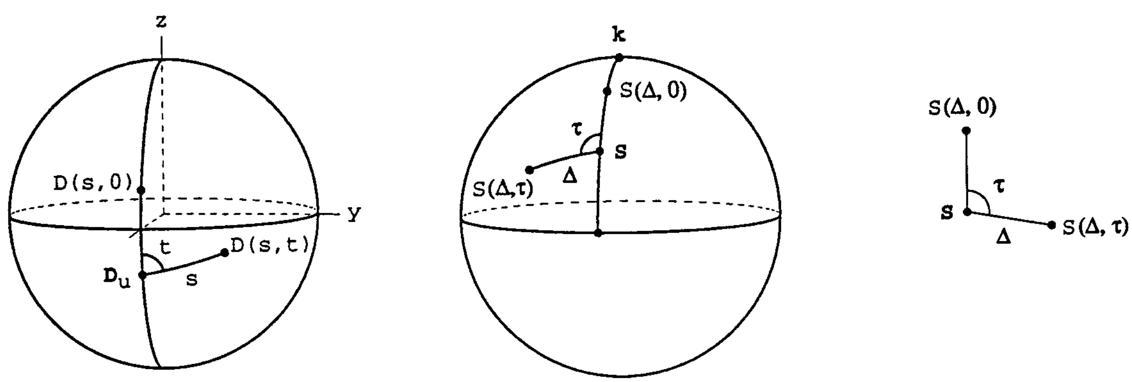

Fig. 16. Left, D-centered coordinates (s, t). Middle, S-centered coordinates (Δ, τ). Right, S-centered coordinates seen from inside the celestial sphere and looking directly at the sun.

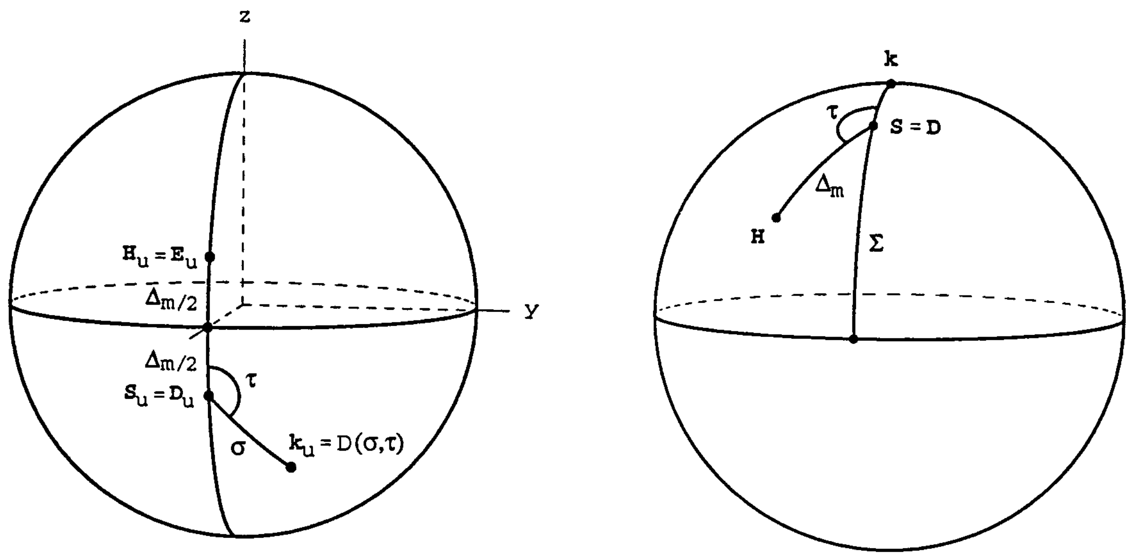

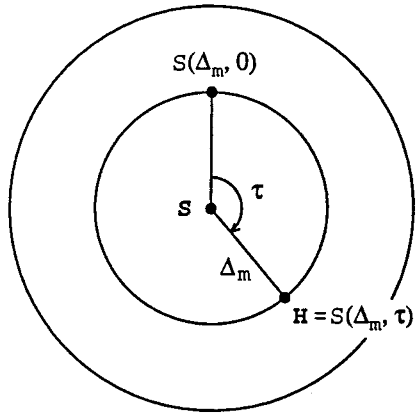

Fig. 17. Above left, the points $\mathbf{k}_u$, $\mathbf{S}_u$, and $\mathbf{H}_u$—the zenith point, sun point, and halo point as seen from the wedge—when u is a minimum deviation orientation, that is, when $\mathbf{S}_u = \mathbf{D}_u$. Compare with Fig. 12, in which $\mathbf{S}_u \neq \mathbf{D}_u$. [$\alpha = 80.2$, $\sigma = 30$ ($\Sigma = 60$), $\tau = 140$] Above right, the same three points but seen from the space frame. Right, same, but viewed from inside the celestial sphere. Note the identical bearings τ of $\mathbf{H}$ here and of $\mathbf{k}_u$ in the upper left diagram.

systems centered at the minimum deviation vector $\mathbf{D}_u$ and at the sun $\mathbf{S}$. The point $D(s, t)$ has *D-centered coordinates* (s, t) as shown in Fig. 16. The coordinate s is the angular distance from $D(s, t)$ to $\mathbf{D}_u$, and t is the bearing of $D(s, t)$ from $\mathbf{D}_u$, with positive bearing being clockwise. The point $S(\Delta, \tau)$ has *S-centered coordinates* (Δ, τ). The coordinate Δ is the angular distance from $S(\Delta, \tau)$ to $\mathbf{S}$, and τ is the bearing of $S(\Delta, \tau)$ from $\mathbf{S}$. Positive bearing is clockwise as viewed from inside the celestial sphere, as halos are normally viewed. We have

$$D(s, t) = \mathrm{rot}(-t, \mathbf{D}_u) \cdot D(s, 0) \tag{52}$$

$$S(\Delta, \tau) = \mathrm{rot}(\tau, \mathbf{S}) \cdot S(\Delta, 0), \tag{53}$$

where $\mathrm{rot}(t, \mathbf{Y})$ is rotation through angle t about the point $\mathbf{Y}$.

An orientation u is said to be a *minimum deviation orientation* if, for a wedge with orientation u, the deviation Δ between the incoming and outgoing rays is a minimum with respect to all orientations. In this case, there is a close and beautiful relation between $\mathbf{k}_u$ and $\mathbf{H}$, a relation that is perhaps already obvious from Figs. 11 and 12. We nevertheless offer a more elaborate approach, which focuses on the orientations.

From Eq. (45) an orientation u is a minimum deviation orientation exactly when $\mathbf{D} = \mathbf{S}$, or from Eq. (23), $u\mathbf{D}_u = \mathbf{S}$. One such orientation (Fig. 17) is the rotation u_0 such that $u_0\mathbf{D}_u = \mathbf{S}$ and $u_0\mathbf{E}_u = S(\Delta_m, 0)$, and then all such rotations are given by

$$u(\tau) = \mathrm{rot}(\tau, \mathbf{S})\, u_0 \tag{54}$$

$$= u_0\, \mathrm{rot}(\tau, \mathbf{D}_u). \tag{55}$$

Therefore

$$u(\tau)\mathbf{D}_u = \mathbf{S}, \tag{56}$$

$$u(\tau)\mathbf{E}_u = S(\Delta_m, \tau). \tag{57}$$

From Fig. 17 or from Eqs. (23) and (55),

$$\mathbf{k}_{u(\tau)} = D(\sigma, \tau), \tag{58}$$

so that σ is the angular distance from $\mathbf{k}_{u(\tau)}$ to $\mathbf{D}_u$, and τ is the bearing of $\mathbf{k}_{u(\tau)}$ from $\mathbf{D}_u$. As τ varies, the

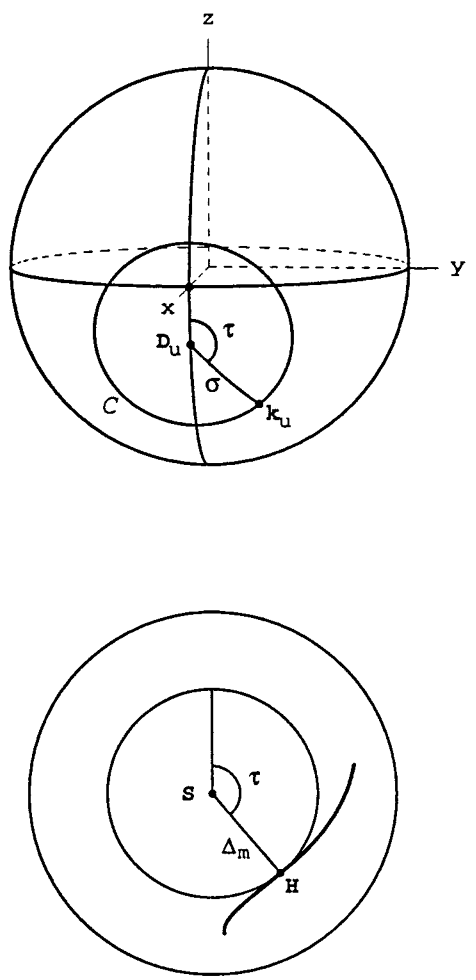

Fig. 18. Above left, contact circle $C = C(\alpha, \sigma)$, with radius σ and center $\mathbf{D}_u$. For the given wedge angle α and solar zenith angle σ, a halo with zenith locus K will contact the circular halo if and only if K intersects C. Below left, point halo with K consisting of the single point $\mathbf{k}_u$ shown at upper left. Since $\mathbf{k}_u$ is on C, the halo contacts the circular halo. The contact point $\mathbf{H}$ has the same bearing τ as $\mathbf{k}_u$. See also Fig. 17, which has the same α, σ, τ, and $\mathbf{k}_u$, and see Fig. 12, which has the same α, σ, and $\mathbf{k}_u$. Above right, same, but now K is the great circle with pole $\mathbf{P}_u$ as shown. Below right, the great circle halo with zenith locus K at upper right. Since K intersects C, the halo contacts the circular halo. The contact points $\mathbf{H}$ and $\mathbf{H}'$ with the circular halo correspond to the intersection points $\mathbf{k}_u$ and $\mathbf{k}_{u'}$ of K with C, with corresponding points having the same bearing. This is the same halo as in Fig. 14. The circular halo is the 35° halo.

point $\mathbf{k}_{u(\tau)}$ traces out the circle with center $\mathbf{D}_u$ and radius σ. This circle is the *contact circle* $C = C(\alpha, \sigma)$, the zenith locus of the set of minimum deviation orientations. (However, the set of minimum deviation orientations is not a halo-making set unless $\mathbf{S} = \pm\mathbf{k}$.)

As seen from the wedge with orientation $u(\tau)$, the halo point is $\mathbf{H}[u(\tau)]_{u(\tau)} = \mathbf{E}_u$, the same for all τ. From space it is $\mathbf{H}[u(\tau)] = u(\tau)\mathbf{E}_u$. Then from Eq. (57)

$$\mathbf{H}[u(\tau)] = S(\Delta_m, \tau), \tag{59}$$

so that Δ_m is the angular distance from $\mathbf{H}[u(\tau)]$ to $\mathbf{S}$, and τ is the bearing of $\mathbf{H}[u(\tau)]$ from $\mathbf{S}$. Since Δ_m is the minimum deviation, then as τ varies, $\mathbf{H}[u(\tau)]$ traces out the circular halo.

Conversely, if u is an orientation such that $\mathbf{H}(u) = S(\Delta_m, \tau)$, so that $\mathbf{H}(u)$ is on the circular halo, then $\mathbf{S}_u = \mathbf{D}_u$ and $\mathbf{H}(u)_u = \mathbf{E}_u$, from Eq. (45). Then

$$u\mathbf{D}_u = \mathbf{S}, \tag{60}$$

$$u\mathbf{E}_u = S(\Delta_m, \tau). \tag{61}$$

Since a rotation is determined by its values on any two independent points, in this case $\mathbf{D}_u$ and $\mathbf{E}_u$, comparison of Eqs. (60) and (61) with Eqs. (56) and (57) shows that $u = u(\tau)$. Thus

$$\text{if } \mathbf{H}(u) = S(\Delta_m, \tau) \text{ then } u = u(\tau). \tag{62}$$

Before collecting the above results in the Criterion for Contact, below, let us interpret them more concretely in the context of the wooden wedge. This time we place two nails in the wedge, with their heads in the direction of the minimum deviation entry and exit vectors $\mathbf{D}$ and $\mathbf{E}$. We orient the wedge so that one nail—$\mathbf{D}$—is fixed in the direction of the sun, and then we rotate the wedge about the fixed nail. The resulting wedge orientations are the minimum deviation orientations for the particular sun position and wedge angle. As the wedge rotates about the nail, the other nail—$\mathbf{E}$—traces out the circular halo. If we were to move our frame to the

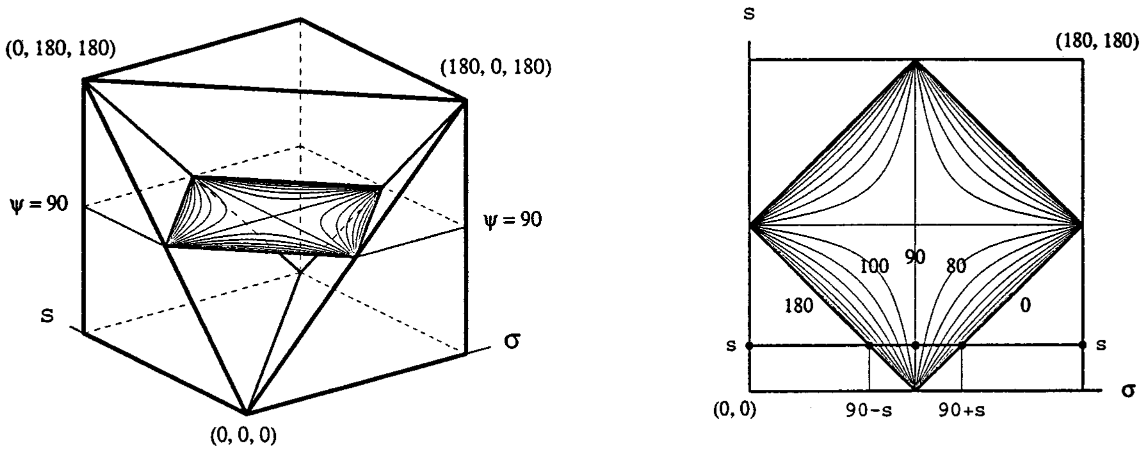

Fig. 19. Left, cube consisting of triples (σ, s, ψ), $0 \le \sigma \le 180$, $0 \le s \le 180$, $0 \le \psi \le 180$. The cube represents halos that satisfy the Spin Vector Assumption, with each triple (σ, s, ψ) representing all halos having solar zenith angle σ and zenith locus $K(\psi, \mathbf{P}_u)$, where $\mathbf{P}_u$ is at angular distance s from $\mathbf{D}_u$. All of the halos on the inner circle in Fig. 20, for example, would be represented by the single point $(\sigma, s, \psi) = (80, 30, 90)$. The regular tetrahedron having vertices (0, 0, 0), (180, 180, 0), (180, 0, 180), (0, 180, 180), consists of halos that contact the circular halo. Here the cube is truncated to show the tetrahedron, and the near upper face of the tetrahedron has been removed to expose the tetrahedron's $\psi = 90$ section, which consists of great circle halos that contact the circular halo. The $\psi = 0$ section, which consists of point halos that contact the circular halo, is the tetrahedron's bottom edge $\sigma = s$. Right, the $\psi = 90$ section in detail. Contours are lines of constant $\Delta\tau$—the half-spread between contact points. The bearing of the contact points from the sun is $\tau = t \pm \Delta\tau$, where t is the bearing of $\mathbf{P}_u$ from $\mathbf{D}_u$. The horizontal line shows the evolution of the contact points for a great circle halo as σ increases from 0 to 180.

wedge, we would see the zenith point rotating about the fixed nail, tracing out the contact circle. And so forth.

Criterion for Contact

For fixed wedge angle $\alpha \le \alpha_{\max}$ and solar zenith angle σ, we write $S(\tau) = S(\Delta_m, \tau)$ and $D(\tau) = D(\sigma, \tau)$ (see Fig. 16). Then

(i) The halo with zenith locus K contacts the (inner boundary of the) circular halo at $S(\tau)$ if and only if K intersects the contact circle at $D(\tau)$. More explicitly, $S(\Delta_m, \tau) \in \mathbf{H}[U(K)]$ if and only if $D(\sigma, \tau) \in K$.

(ii) If $\sigma \ne 0, 180$, then the mapping $S(\tau) \to D(\tau)$ is a 1–1 correspondence between the circular halo and the contact circle. The angle τ is the angular coordinate on both the circular halo and the contact circle, measured clockwise from the 12:00 position, with the halo being viewed from inside the celestial sphere.

(iii) If $\sigma = 0$ or 180, then the contact circle is just a point, and the mapping $S(\tau) \to D(\tau)$ takes all of the circular halo onto the single point. Thus when $\sigma = 0$ or 180, if the halo contacts the circular halo, it contacts it everywhere.

To prove (i), suppose $S(\tau) = \mathbf{H}(u)$ for some u in $U(K)$. Then $u = u(\tau)$ from Eq. (62) and $D(\tau) = \mathbf{k}_{u(\tau)} = \mathbf{k}_u \in K$ from Eqs. (58) and (37). Conversely, if $D(\tau) \in K$, then $\mathbf{k}_{u(\tau)} = D(\tau) \in K$, so that $u(\tau) \in U(K)$ and then $S(\tau) = \mathbf{H}[u(\tau)] \in \mathbf{H}[U(K)]$ from Eq. (59). Statements (ii) and (iii) are properties of the spherical coordinates shown in Fig. 16.

Two illustrations of the Criterion for Contact are given in Fig. 18. In the first illustration the zenith locus K is the one-point set $\{\mathbf{k}_u\}$, with $\mathbf{k}_u$ as shown in the upper left diagram, and the corresponding point halo is at the lower left. Since $\mathbf{k}_u$ is on the contact circle, the halo makes contact with its circular halo, at $\mathbf{H}$, and the points $\mathbf{k}_u$ and $\mathbf{H}$ have the same bearing τ. In the second illustration K is a great circle, shown in the upper right diagram, and the corresponding great circle halo is at the lower right. Again the contact points with the circular halo correspond to the intersections of K with the contact circle. Incidentally, the two points $\mathbf{k}_u$ in the right and left diagrams are identical, so the point halo is a subset of the great circle halo.

The Criterion for Contact is not restricted to point halos and great circle halos, since it does not rely on the Spin Vector Assumption, but in case the assumption does apply, we can say more. Suppose, then, that we have a halo with zenith locus $K = K(\psi, \mathbf{P}_u)$. Much can be inferred informally just by looking at the position of K with respect to the contact circle C, and we recommend doing so, but we also take the following complementary analytic approach:

Let $\mathbf{P}_u = D(s, t)$, so that s is the angular distance from $\mathbf{P}_u$ to $\mathbf{D}_u$, and t is the bearing of $\mathbf{P}_u$ from $\mathbf{D}_u$. From Fig. 16,

$$\mathbf{P}_u = (\cos s)\,\mathbf{D}_u + (\sin s \sin t)\,\mathbf{j} + (\sin s \cos t)\,\mathbf{D}_u \times \mathbf{j}. \tag{63}$$

According to the Criterion for Contact, the halo will contact the circular halo at $S(\tau)$ if and only if $D(\tau)$ is on K, that is, if and only if $\mathbf{P}_u \cdot D(\sigma, \tau) = \cos\psi$. From Eq. (63) the condition for contact is therefore

$$\cos\sigma \cos s + \sin\sigma \sin s \cos(\tau - t) = \cos\psi. \tag{64}$$

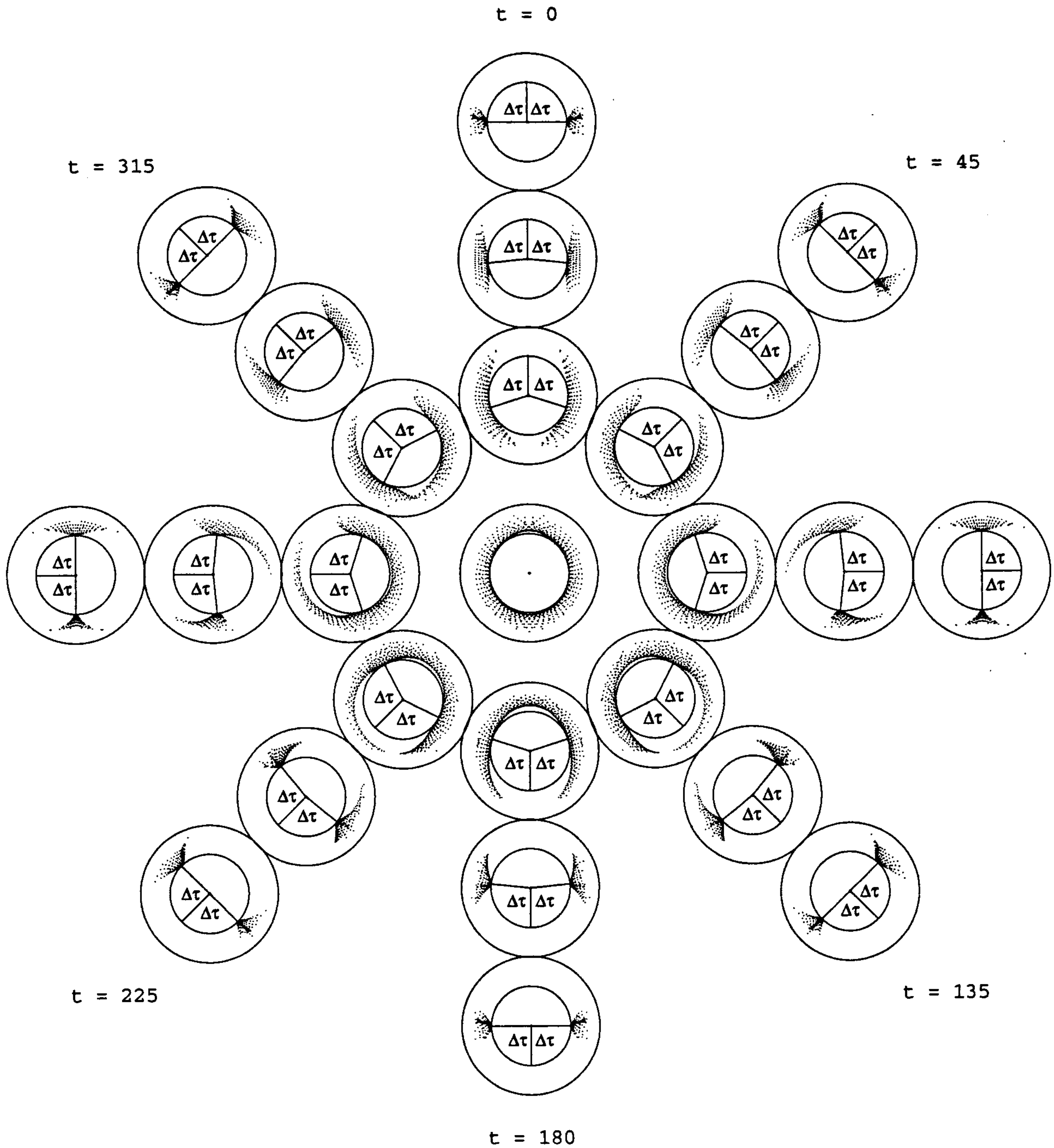

Fig. 20. Dependence of contact points on (s, t), the D-centered coordinates of poles $\mathbf{P}_u$ (Fig. 16, left). Great circle halos are shown for $\mathbf{P}_u$ having $s = 0, 30, 60, 90$, and $t = 0, 45, \ldots, 315$. For each halo the contact points are located symmetrically at angle $\Delta\tau$ on either side of the direction with bearing t, which is the direction from $\mathbf{D}_u$ ($s = 0$, center of figure) to $\mathbf{P}_u$. For a given ψ and Σ, as here, the half-spread $\Delta\tau$ depends only on s, the distance from $\mathbf{D}_u$ to $\mathbf{P}_u$. See the Contact Point Theorem, part (ii). [$\alpha = 80.2$ ($\Delta_m = 35$) and $\Sigma = 10$]

Hence

$$\tau = t \pm \Delta\tau, \tag{65}$$

where

$$\Delta\tau(\sigma, s, \psi) = \arccos[(\cos\psi - \cos\sigma\cos s)/\sin\sigma\sin s]. \tag{66}$$

The possibilities for contact are summarized in Fig. 19, where the cube consists of triples (σ, s, ψ) representing configurations of the two circles C and K, which have radii σ and ψ, and which have distance s between their centers. On the side faces of the cube, $\sin\sigma\sin s = 0$, and the argument of the arccosine in Eq. (66) is undefined; Eq. (64) has solutions τ if and only if $\cos\sigma\cos s = \cos\psi$, in which case all values of τ are solutions, and the halo contacts the circular halo everywhere. This is the case where (σ, s, ψ) is on a

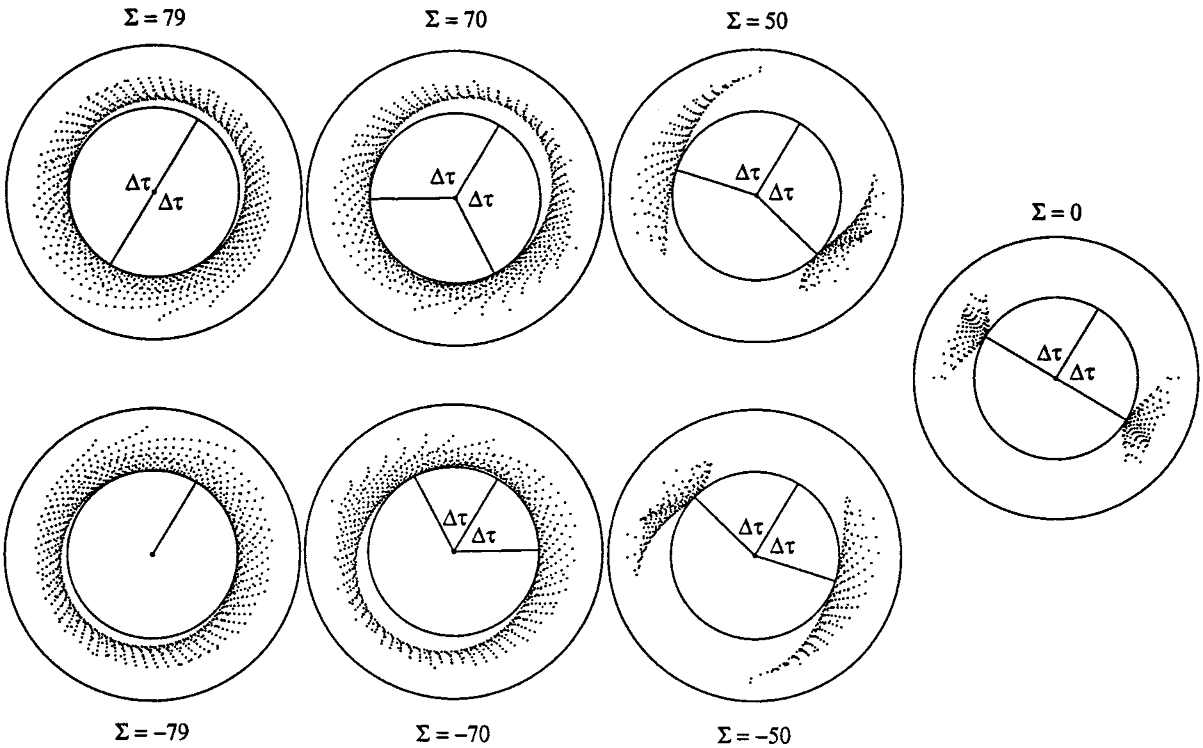

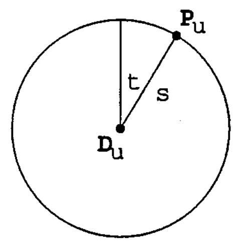

Fig. 21. Dependence of contact points on sun elevation Σ. The halo has pole $\mathbf{P}_u$ with D-centered coordinates $(s, t) = (79, 31)$. The halo has two contact points for each Σ with $-s < \Sigma < s$, one contact point for $\Sigma = \pm s$, and none otherwise. The contact points are located symmetrically at angle $\Delta\tau$ on either side of the direction with bearing t, which is the direction from $\mathbf{D}_u$ to $\mathbf{P}_u$. As Σ decreases from s to $-s$, the half-spread $\Delta\tau$ of the contact points decreases from 180 to 0 as shown. Here $\alpha = 80.2$ ($\Delta_m = 35$), but the results are essentially independent of α. Figure 18 shows the same halo for $\Sigma = 60$.

side edge of the regular tetrahedron having vertices (0, 0, 0), (180, 180, 0), (180, 0, 180), (0, 180, 180). Elsewhere on the faces of the tetrahedron, $\Delta\tau = 0$ or 180, from Eq. (66), and there is exactly one contact point. On the top two faces $\Delta\tau = 180$, and the direction of the contact point from the sun is therefore opposite that of $\mathbf{P}_u$ from $\mathbf{D}_u$. On the bottom faces $\Delta\tau = 0$, and the direction of the contact point is the same as that of $\mathbf{P}_u$ from $\mathbf{D}_u$. At each point within the tetrahedron there are two contact points, which from Eq. (65) are symmetrically located about the direction from $\mathbf{D}_u$ to $\mathbf{P}_u$. Outside the tetrahedron there is no contact. Again, most of this is also clear informally. In particular, the faces of the tetrahedron correspond to tangencies of C with K.

The upper half ($\psi > 90$) of the left-hand diagram in Fig. 19 can be ignored if desired, since $K(\psi, \mathbf{P}_u) = K(180 - \psi, -\mathbf{P}_u)$. In particular, for point halos we

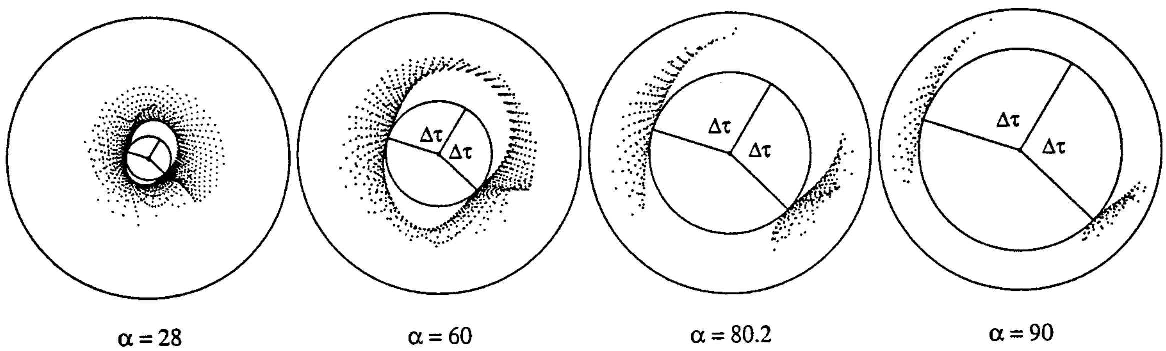

Fig. 22. Dependence of contact points on wedge angle α. Great circle halos are shown for wedge angle $\alpha = 28$, 60, 80.2, and 90. Each halo has pole $\mathbf{P}_u$ with the same D-centered coordinates $(s, t) = (79, 31)$, the same as in Fig. 21. The bearing of the contact points is independent of α. Note, however, that the four poles are not the same, since D-centered coordinates depend on α. ($\Sigma = 50$)

normally assume $\psi = 0$ rather than $\psi = 180$, so that $\mathbf{P}_u = \mathbf{k}_u$ rather than $\mathbf{P}_u = -\mathbf{k}_u$. And the upper half of the right-hand diagram can be ignored since $K(90, \mathbf{P}_u) = K(90, -\mathbf{P}_u)$.

The following theorem makes explicit some of the information contained in the figure and in previous calculations. Most of the theorem can also be verified geometrically by drawing the contact circle and the zenith locus. See also Figs. 20–22.

Contact Point Theorem

Let $\mathbf{P}_u = D(s, t)$, so that s is the angular distance from $\mathbf{P}_u$ to $\mathbf{D}_u$, and t is the bearing of $\mathbf{P}_u$ from $\mathbf{D}_u$. Let $\alpha \le \alpha_{\max}$.

(i) For a point halo with pole $\mathbf{P}_u$: The halo will have a contact point for exactly one solar zenith angle, namely, $\sigma = s$. When contact occurs,

(a) if $0 < s < 180$, then there is exactly one contact point, with bearing $\tau = t$;

(b) if $s = 0$ or 180 ($\mathbf{P}_u = \pm\mathbf{D}_u$), then every point on the circular halo is a contact point.

(ii) For a great circle halo with pole $\mathbf{P}_u$:

(a) If $s \ne 0, 90, 180$, then choose $\mathbf{P}_u$ to be the pole of K closest to $\mathbf{D}_u$, so that $s < 90$. Then the halo has two contact points for each Σ with $-s < \Sigma < s$, one contact point for $\Sigma = \pm s$, and none otherwise. The bearing of the two contact points is $\tau = t \pm \Delta\tau$, with the half-spread $\Delta\tau$ decreasing from 180 to 0 as Σ decreases from s to $-s$. The half-spread is given quantitatively in Eq. (66) and qualitatively by a horizontal line like the one shown in the right-hand diagram of Fig. 19.

(b) If $s = 0$ or 180 ($\mathbf{P}_u = \pm\mathbf{D}_u$), then the halo does not contact the circular halo unless $\Sigma = 0$, in which case it contacts it everywhere.

(c) If $s = 90$ (K passes through $\mathbf{D}_u$), then the halo contacts the circular halo for all Σ. Contact occurs everywhere on the circular halo if $\Sigma = \pm 90$, and otherwise at the diametrically opposite points with bearing $\tau = t \pm 90$.

Thus the bearing τ of contact points is independent of wedge angle α in the following sense: If, for example, two great circle halos have different wedge angles but have poles with the same D-centered coordinates (s, t), then the range of sun elevations Σ for which contact occurs is the same for both halos, namely, $-s \le \Sigma \le s$, and for a given Σ in this range the bearing τ of the contact points is the same for both halos, namely, $\tau = t \pm \Delta\tau$ (if $s \ne 0, 90, 180$). Thus for fixed Σ all great circle halos whose poles $\mathbf{P}_u$ have the same D-centered coordinates share a common skeleton of contact points, with only the distance Δ_m to the sun depending on α (Fig. 22). The amount of flesh—the noncontact points—on the skeleton will decrease with increasing α, until at $\alpha = \alpha_{\max}$ the entry and exit regions consist only of the single points $\mathbf{D}$ and $\mathbf{E}$, respectively, and the halo consists only of contact points, with no flesh. Halos with small α are no richer in contact points than those with large α.

The D-centered coordinates are natural spherical coordinates related to the frame of wedge vectors $\mathbf{D}$, $\mathbf{B}$, $\mathbf{D} \times \mathbf{B}$. This frame is usually a better frame than $\mathbf{A}$, $\mathbf{B}$, $\mathbf{C}$ for studying contact points.

An interesting consequence of the theory is that for a point halo, knowledge of the contact point and the relevant solar zenith angle σ is enough to determine the halo. For if (Δ_m, τ) are the S-centered coordinates of the contact point, then (σ, τ) are the D-centered coordinates of $\mathbf{k}_u$. The point $\mathbf{k}_u$ itself is then known, since Δ_m determines $\mathbf{D}_u$. The halo is then known, since K and α are both known, K consisting of the single point $\mathbf{k}_u$, and α being known from Δ_m. See the left-hand diagrams in Fig. 18.

For a great circle halo, the two distinct contact points at a single solar zenith angle $\sigma \ne 0, 90, 180$, are enough to determine the halo. The two contact points together with σ determine two intersection points of K with C. The intersection points are distinct, since $\sigma \ne 0, 180$, and they therefore determine the great circle K, since they are not antipodal. Thus K and α are known. See the right-hand diagrams in Fig. 18.

H. Halo Transformation Rules

We will see that there are essentially four natural ways to move a halo shape on the celestial sphere without deforming it. Rules 1–4, below, show how these changes arise from changes in the zenith locus of the halo. Then in Section 3 we will see how the changes in zenith locus arise in real crystals. Rule 1 is less important than Rules 2–4, since most of us quite reasonably take it for granted.

Rule 1, Azimuth Change

Leaving the zenith locus K unchanged and rotating the sun through angle ϕ about the z-axis corresponds to rotating the halo shape in the same way. That is,

$$\mathbf{H}[U(K), \mathrm{zrot}(\phi)\, \mathbf{S}] = \mathrm{zrot}(\phi)\, \mathbf{H}[U(K), \mathbf{S}]. \quad (67)$$

Rule 1 is a precise formulation of the idea that the shape of a halo is essentially independent of solar azimuth. As we said, most people take it for granted, and we, too, often ignore the distinction between $\mathrm{zrot}(\phi)\, \mathbf{H}[U(K), \mathbf{S}]$ and $\mathbf{H}[U(K), \mathbf{S}]$. Logically, Rule 1 depends on the azimuth invariance of halo-making sets [Eq. (29)].

Rule 2, x-Rotation of a Halo

Replacing K by $-K$ and rotating the sun 180° about the x-axis corresponds to rotating the halo shape in the same way. That is,

$$\mathbf{H}[U(-K), \mathrm{xrot}\, \mathbf{S}] = \mathrm{xrot}\, \mathbf{H}[U(K), \mathbf{S}], \quad (68)$$

where xrot is rotation through 180° about the x-axis.

We say that halos with zenith loci K and K' are *x-rotations* of each other if

$$\mathbf{H}[U(K'), w\mathbf{S}] = w\mathbf{H}[U(K), \mathbf{S}] \quad \text{for all } \mathbf{S}, \quad (69)$$

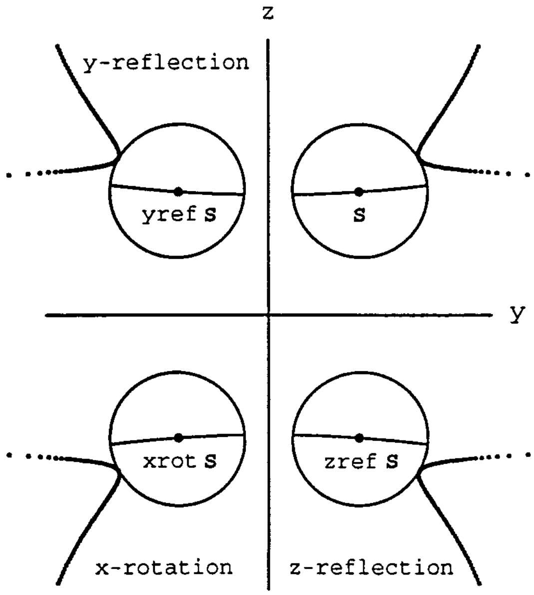

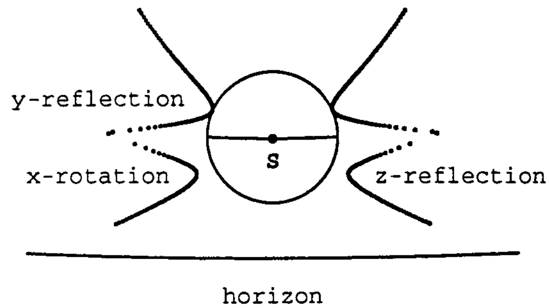

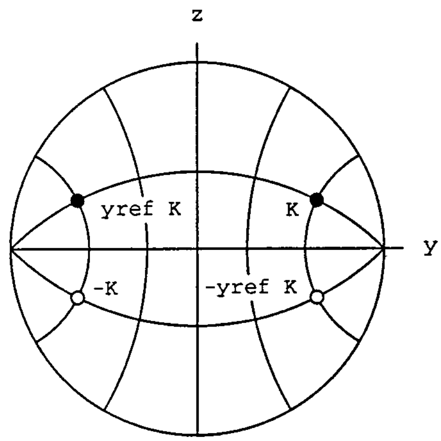

Fig. 23. Left, halo with the sun at **S**. Also shown are the halo's x-rotation when the sun is at xrot **S**, its y-reflection when the sun is at yref **S**, and its z-reflection when the sun is at zref **S**. The four halo shapes do not appear in the sky simultaneously. This view is of the rear of the celestial sphere, seen from inside. Above right, the same four halos but with the sun at **S**. The x-rotation is no longer a rotation of the original halo, and the z-reflection is no longer a reflection of the original halo. Below right, zenith loci of the halos. Here K consists of the single point $\mathbf{k}_u = B(30, -45)$; the sets K and yref K are on the front hemisphere, and $-K$ and $-$yref K are on the rear. ($\alpha = 40$, $\Sigma = 25$)

where w = xrot. That is, the shape of one halo when the sun is at xrot **S**, is the same as the shape of the other when the sun is at **S**, but rotated 180° about the x-axis. Rule 2 says that two halos with zenith loci K and $-K$ (and with the same wedge angle) are x-rotations of each other; see Fig. 23.

If halos with zenith loci K and K' are x-rotations of each other, then Rule 1 shows that Eq. (69) is satisfied not only by w = xrot but also by $w = \mathrm{zrot}(\phi) \cdot \mathrm{xrot}$, which is the form for a 180° rotation about an arbitrary horizontal axis. For example, the shape of one halo when the sun is at zref **S**, is the same as the shape of the other when the sun is at **S**, but rotated 180° about the point on the horizon below the sun. (The transformation zref is reflection in the plane $z = 0$.) If the shape of a halo is known for sun elevation Σ, then the shape of its x-rotation is known for sun elevation $-\Sigma$.

Rule 2 can be used to infer halos on the rear hemisphere from halos on the front. From the point halos in, say, Fig. 35, which have poles on the front hemisphere and have $\Sigma = 50$, one can infer the point halos with poles on the rear hemisphere for $\Sigma = -50$. In general the rear hemisphere is redundant if one has the front hemisphere halos for all Σ. Similarly, all negative Σ are redundant if one has the front and rear hemisphere halos for all positive Σ.

Rules 1–4 are proved analytically in the theorem following their discussion. For some geometric insight into Rule 2, simply observe that, to rotate the halo point 180° about the x-axis, one does the same for the sun and the wedge, thus turning the wedge upside down; the effect on the zenith point as seen from the wedge is to change its sign. Or one can examine Fig. 24, left, which shows $\mathbf{k}_u$, $\mathbf{S}_u$, and $\mathbf{H}(u, \mathbf{S})_u = \mathbf{H}(e, \mathbf{S}_u)$ [Eqs. (13) and (23)] for a typical u; this is the usual view from the wedge with orientation u. The orientation $v = \mathrm{xrot} \cdot u$ satisfies $-\mathbf{k}_v = \mathbf{k}_u$ and $\mathbf{S}'_v = \mathbf{S}_u$, where $\mathbf{S}' = \mathrm{xrot}\ \mathbf{S}$. The two configurations $\{-\mathbf{k}_v, \mathbf{S}'_v, \mathbf{H}(e, \mathbf{S}'_v)\}$ and $\{\mathbf{k}_u, \mathbf{S}_u, \mathbf{H}(e, \mathbf{S}_u)\}$ therefore coincide as shown. When they are rotated by u and v to show the view from space as in the right-hand diagram, then $\mathbf{H}(v, \mathbf{S}') = \mathrm{xrot}\ \mathbf{H}(u, \mathbf{S})$.

Rule 3, y*-Reflection of a Halo*

Reflecting both K and the sun in the plane $y = 0$ corresponds to reflecting the halo shape in the same way. That is,

$$\mathbf{H}[U(\mathrm{yref}\,K), \mathrm{yref}\,\mathbf{S}] = \mathrm{yref}\,\mathbf{H}[U(K), \mathbf{S}], \quad (70)$$

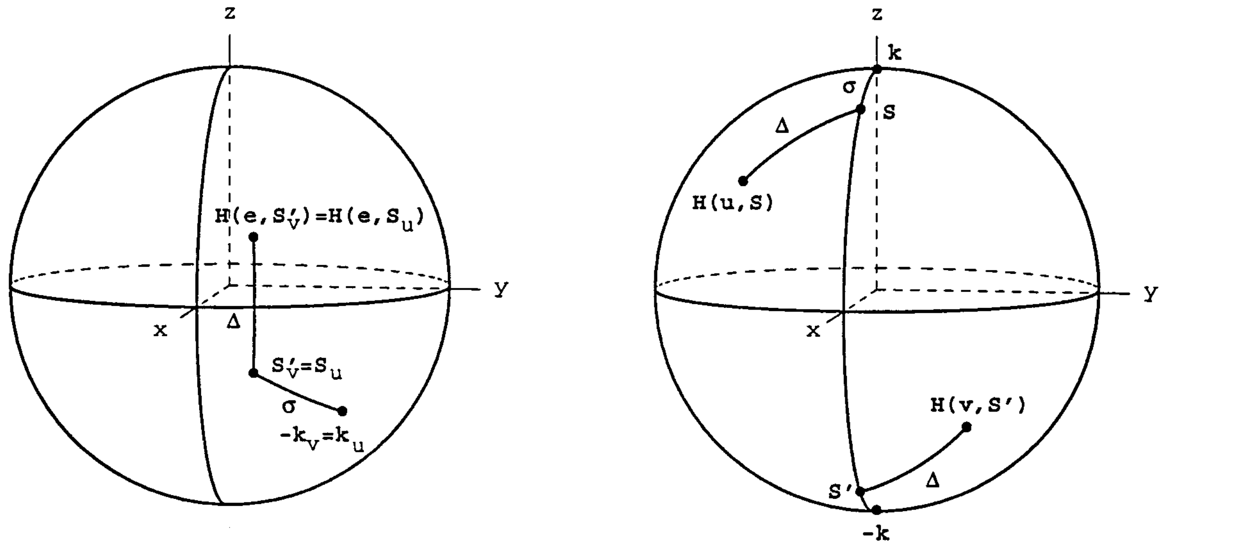

Fig. 24. Geometry of Rule 2, showing views from the wedge at left and from space at right. For each orientation u, the orientation v = xrot $\cdot$ u satisfies $-\mathbf{k}_v = \mathbf{k}_u$ and $\mathbf{S}'_v = \mathbf{S}_u$, where $\mathbf{S}'$ = xrot $\mathbf{S}$. At left, therefore, $\mathbf{H}(e, \mathbf{S}'_v) = \mathbf{H}(e, \mathbf{S}_u)$, and at right, $\mathbf{H}(v, \mathbf{S}')$ = xrot $\mathbf{H}(u, \mathbf{S})$. The right-hand diagram is drawn for the special case where $\mathbf{S}$ is in the plane $y = 0$.

where yref is reflection in the plane $y = 0$. This symmetry is displayed clearly in the halo atlas, Appendix A.

Halos with zenith loci K and K' are *y-reflections* or *left–right reflections* of each other if Eq. (69) is satisfied with w = yref. Rule 3 says that two halos with zenith loci K and yref K are y-reflections of each other.

If halos with zenith loci K and K' are y-reflections of each other, then Eq. (69) is satisfied not only by w = yref but also by w = zrot(ϕ) $\cdot$ yref, which is the form for a reflection about an arbitrary vertical plane. For example, when the sun positions of the two halos are the same, their shapes are reflections of each other in the solar vertical.

For geometric insight into Rule 3, refer to the left-hand diagram in Fig. 25, which shows $\mathbf{k}_u$, $\mathbf{S}_u$, and $\mathbf{H}(u)_u = \mathbf{H}(u, \mathbf{S})_u = \mathbf{H}(e, \mathbf{S}_u)$ for a typical wedge orientation u. For the case shown, where $\mathbf{S}$ is in the plane $y = 0$, the orientation v = yref $\cdot$ u $\cdot$ yref satisfies $\mathbf{k}_v$ = yref $\mathbf{k}_u$ and $\mathbf{S}_v$ = yref $\mathbf{S}_u$, and the two configurations $\{\mathbf{k}_u, \mathbf{S}_u, \mathbf{H}(e, \mathbf{S}_u)\}$ and $\{\mathbf{k}_v, \mathbf{S}_v, \mathbf{H}(e, \mathbf{S}_v)\}$ are therefore reflections of each other as shown. When they are rotated by u and v to show the view from space as in the right-hand diagram, then $\mathbf{H}(v)$ = yref $\mathbf{H}(u)$, as claimed.

The two wedge orientations u and v differ by a rotation whose axis is the intersection of the normal plane of the wedge and the plane of the solar vertical,

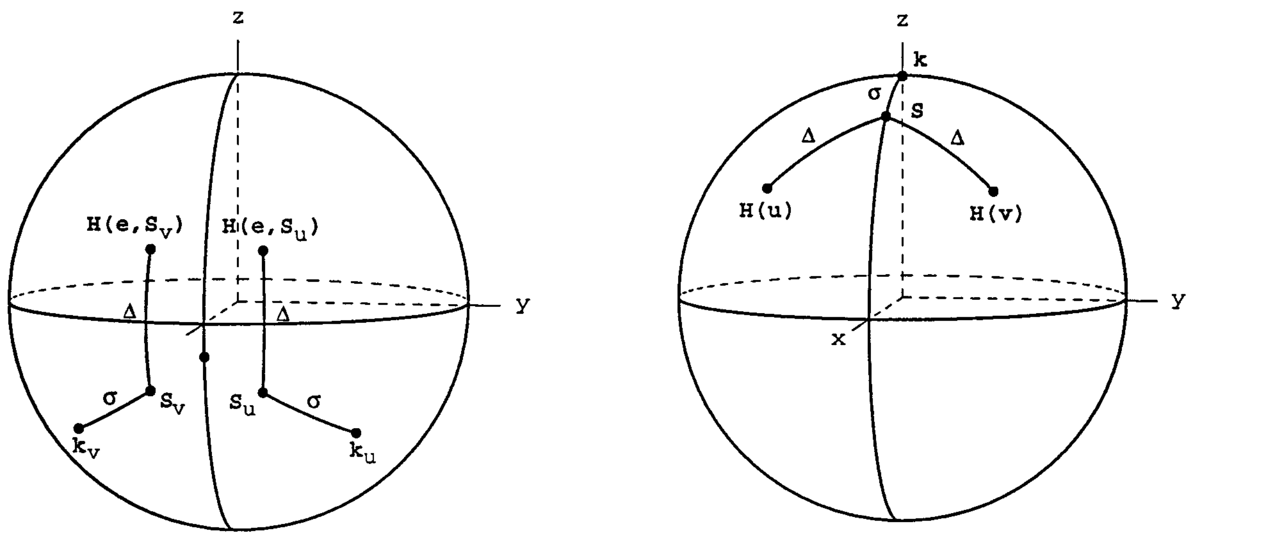

Fig. 25. Geometry of Rule 3, showing views from the wedge at left and from space at right. For each orientation u the orientation v = yref $\cdot$ u $\cdot$ yref satisfies $\mathbf{k}_v$ = yref $\mathbf{k}_u$ and $\mathbf{S}_v$ = yref $\mathbf{S}_u$, as shown. At left, therefore, $\mathbf{H}(e, \mathbf{S}_v)$ = yref $\mathbf{H}(e, \mathbf{S}_u)$, and at right, $\mathbf{H}(v)$ = yref $\mathbf{H}(u)$. The orientations u and v differ by a rotation whose axis, as seen from the wedge, is the solid dot shown on $y = 0$. Here $\mathbf{S}$ is in the plane $y = 0$, so that yref $\mathbf{S} = \mathbf{S}$.

Table 1. Orthogonal Transformations[a] w such that $w\mathbf{k} = \pm\mathbf{k}$

w	$\det w$	$w\mathbf{k}$	K' [Eqs. (72)]	Geometric Description of w
$\mathrm{zrot}(\phi) \cdot e$	1	$\mathbf{k}$	K	Rotation about the vertical axis
$\mathrm{zrot}(\phi) \cdot \mathrm{xrot}$	1	$-\mathbf{k}$	$-K$	180° rotation about a horizontal axis
$\mathrm{zrot}(\phi) \cdot \mathrm{yref}$	-1	$\mathbf{k}$	$\mathrm{yref}\, K$	Reflection in a vertical plane
$\mathrm{zrot}(\phi) \cdot \mathrm{zref}$	-1	$-\mathbf{k}$	$-\mathrm{yref}\, K$	Reflection in the horizontal plane, followed by rotation about the vertical axis

[a]See also Ref. 5.

and whose angle of rotation is twice the angle between the two planes. This is clear when viewed from the wedge with orientation u, where the solar vertical is the great circle through $\mathbf{k}_u$ and $\mathbf{S}_u$, and the normal plane is $y = 0$. The intersection of the two planes, giving the axis of rotation, is indicated by a solid dot in Fig. 25, but not labeled.

Rule 4, z-Reflection of a Halo

Rotating K by 180° about the y-axis and reflecting the sun in the plane $z = 0$ corresponds to reflecting the halo in the same way. That is,

$$\mathbf{H}[U(\mathrm{yrot}\, K), \mathrm{zref}\, \mathbf{S}] = \mathrm{zref}\, \mathbf{H}[U(K), \mathbf{S}]. \quad (71)$$

of the solar vertical. It is easy to recognize the y-reflection of a halo.

There is a situation that helps one to think about x-rotation and z-reflection. The situation is rare, but it does happen, namely, when sunlight reflects off the calm water or level ice surface of a lake, and when there are low level ice crystals in the atmosphere at the same time. The result is a halo display from a sun at $\mathbf{S}$ and a sun at zref $\mathbf{S}$.

Rules 1–4 are instances of the following theorem.

Theorem

Let w be an orthogonal transformation with $w\mathbf{k} = \pm\mathbf{k}$ (see Table 1). For any subset K of the sphere, let

$$K' = \begin{array}{rllll} K & \text{if } w\mathbf{k} = \mathbf{k} & \text{and} & \det w = 1 & (\text{e.g., } w = \mathrm{zrot}(\phi), \text{ Rule 1}) \\ -K & \text{if } w\mathbf{k} = -\mathbf{k} & \text{and} & \det w = 1 & (\text{e.g., } w = \mathrm{xrot}, \text{ Rule 2}) \\ \mathrm{yref}\, K & \text{if } w\mathbf{k} = \mathbf{k} & \text{and} & \det w = -1 & (\text{e.g., } w = \mathrm{yref}, \text{ Rule 3}) \\ -\mathrm{yref}\, K & \text{if } w\mathbf{k} = -\mathbf{k} & \text{and} & \det w = -1 & (\text{e.g., } w = \mathrm{zref}, \text{ Rule 4}) \end{array} \quad (72)$$

Halos with zenith loci K and K' are *z-reflections* of each other if Eq. (69) is satisfied with $w = \mathrm{zref}$. Rule 4 says that two halos with zenith loci K and yrot K (= $-$yref K) are z-reflections of each other. Rule 4 can be used to infer rear hemisphere halos from front hemisphere halos, much like Rule 2. Rule 4 is a consequence of Rules 2 and 3.

The concept of z-reflection is subtle. To grasp it, one should regard halos in the fundamental sense of Eq. (18), so that a halo is not attached to any one particular sun position. Suppose, then, that a halo display, with the sun at position $\mathbf{S}$, contains some given halo. The z-reflection of the halo may well be present, as will be seen in Section 3. The subtlety is that at this particular moment, with the sun still at $\mathbf{S}$, the shape of the z-reflection and that of the original halo may not be simply related, and in particular are not apt to be reflections of each other (Fig. 23, upper right diagram). It is the shape of the one halo when the sun is at $\mathbf{S}$, and the shape of the other if the sun should happen to pass through the point zref $\mathbf{S}$, that are reflections of each other.

The concept of x-rotation is similar, but y-reflection is more straightforward. With the sun at $\mathbf{S}$, the shape of the y-reflection and the shape of the given halo are indeed reflections of each other, in the plane

Then with α fixed,

$$\mathbf{H}[U(K'), w\mathbf{S}] = w\mathbf{H}[U(K), \mathbf{S}] \text{ for all } \mathbf{S}. \quad (73)$$

Proof

For each wedge orientation u define the orientation $w'(u)$ by Eqs. (14) and (15). From Eq. (17),

$$\mathbf{H}[w'(u), w\mathbf{S}] = w\mathbf{H}(u, \mathbf{S}). \quad (74)$$

For the fourth case in Eq. (72),

$$\begin{aligned} \mathbf{k}_{w'(u)} &= w'(u)^{-1}\mathbf{k} = \mathrm{yref} \cdot u^{-1} \cdot w^{-1}\mathbf{k} \\ &= -\mathrm{yref} \cdot u^{-1}\mathbf{k} = -\mathrm{yref}\, \mathbf{k}_u, \end{aligned} \quad (75)$$

so that from Eq. (37)

$$w'(u) \in U(-\mathrm{yref}\, K) \Leftrightarrow u \in U(K). \quad (76)$$

Equation (74) then gives Eq. (73). The other three cases are similar.

No Other Orthogonal Halo Transformations

Could there be other rules similar to Rules 1–4? To formulate the problem more precisely, we reexamine the general form of the existing rules, each of which is characterized by an orthogonal transformation w which moves the halo shape. The transformation w

also associates to each wedge orientation u a second wedge orientation $w'(u)$ by Eqs. (14) and (15), and if U is a set of wedge orientations, then as in Eq. (74):

$$\mathbf{H}[w'(U), w\mathbf{S}] = w\mathbf{H}(U, \mathbf{S}), \tag{77}$$

where $w'(U) = \{w'(u) : u \in U\}$. So if a halo shape is moved without deformation, as specified by w, the same result can be achieved by using w to move the sun and the set of wedge orientations.

All of the above is true for any orthogonal transformation w. What is special about the existing four rules—and what is natural to require of any analogous rules—is that $w'(U)$ is a halo-making set whenever U is also, so that Eq. (77) can be expressed in the form of Eq. (73). Thus our original problem is really to find all such w. But if we consider the simplest halo-making set $U = Zu$, for a point halo, then according to Eq. (30) the set $w'(U)$ will be a halo-making set if and only if $Z \cdot w'(Zu) \subseteq w'(Zu)$, which simplifies to $Zw \subseteq wZ$. Then $\zeta \cdot w\mathbf{k} = w\mathbf{k}$ for all ζ in Z. Taking $\zeta \neq e$, we conclude that $w\mathbf{k} = \pm\mathbf{k}$. The resulting possibilities for w are listed in Table 1. They are essentially those of Rules 1–4; no other w is possible.

The orthogonal transformations w satisfying $w\mathbf{k} = \pm\mathbf{k}$ are exactly those such that $Zw = wZ$. Let us interpret the condition $Zw = wZ$ more concretely, in the context of a point halo arising in a particular wedge of a spinning crystal. If the wedge at some moment has orientation u, then the set of all of its orientations as the crystal spins is Zu. If at the same moment another wedge on the crystal has orientation wu (assume $\det w = 1$), then the set of orientations for the second wedge is Zwu. This is the meaning given to w in Section 3. Here in the present subsection, however, in order to move the halo in the manner specified by w, one attempts to get the orientations for the second wedge by applying w, thought of as fixed in space, to each orientation of the first wedge as it occurs. The result is the set wZu. For most w this attempt fails—the resulting orientations are simply not the orientations of the second wedge, if the wedge is truly fixed in the crystal. But for w with $Zw = wZ$, the two sets of orientations Zwu and wZu coincide.

Face Interchange Rule

Rotating K through an angle of 180° about the z-axis corresponds to interchanging the entry and exit faces of the wedge. In this case we say that the two halos are the *face interchanges* of each other. Such halos are always associated with each other, although they need not be simultaneously nonempty. The Face Interchange Rule is a consequence of the Wedge Change Rule, Subsection 3.O.

At first glance the Face Interchange Rule resembles Rules 1–4, because it speaks of a change in the zenith locus. But it does not give the effect on the halo that is due to the change, as do Rules 1–4, rather it tells how the change in zenith locus arises. The Face Interchange Rule logically belongs in Section 3, but we need it sooner, as in the following discussion.

When the Spin Vector Assumption is Satisfied

For a halo satisfying the Spin Vector Assumption, applying a reflection or rotation to K is the same as applying the same operation to $\mathbf{P}_u$. For such a halo we can therefore summarize Rules 1–4 and the Face Interchange Rule as follows: For each halo with pole $\mathbf{P}_u$ there are eight related halos, all with the same ψ and α. The first four are illustrated in Fig. 23.

(i) The given halo, with pole $\mathbf{P}_u$.
(ii) The halo with pole $-\mathbf{P}_u$. It is the x-rotation of the given halo.
(iii) The halo with pole yref $\mathbf{P}_u$. It is the y-reflection of the given halo.
(iv) The halo with pole $-$yref $\mathbf{P}_u$ = yrot $\mathbf{P}_u$. It is the z-reflection of the given halo.
(v) The halo with pole zrot $\mathbf{P}_u$. It is the face interchange of the given halo.
(vi) The halo with pole $-$zrot $\mathbf{P}_u$ = zref $\mathbf{P}_u$. It is the x-rotation of the face interchange of the given halo.
(vii) The halo with pole yref zrot $\mathbf{P}_u$ = xref $\mathbf{P}_u$. It is the y-reflection of the face interchange of the given halo.
(viii) The halo with pole $-$yref zrot $\mathbf{P}_u$ = xrot $\mathbf{P}_u$. It is the z-reflection of the face interchange of the given halo.

If the shape of the given halo is known for all Σ, then the shapes of halos (i)–(iv) can easily be found. But we know of no simple way of describing the shape of the face interchange of a halo in terms of the shape of the given halo. The shapes of halos (v)–(viii) therefore, although easily described in terms of each other, do not seem to be simply related to those of halos (i)–(iv).

For great circle halos, the halos (i) and (ii) are the same, since their poles are antipodal and hence their zenith loci coincide. Likewise, halos (iii) and (iv) are the same, (v) and (vi) are the same, and (vii) and (viii) are the same.

I. Additional Properties

A halo can have special features if its zenith locus K is suitably located. Many such features have already been mentioned. Following are several more.

(i) If K is invariant under the antipodal map (i.e., $-K = K$), then the halo is its own x-rotation. In the halo atlas illustrations, these halos would be the great circle halos. If a halo is its own x-rotation, then changing the sun elevation from Σ to $-\Sigma$ has the effect of rotating the halo 180° about the point on the horizon below the sun (see, e.g., Fig. 21). When the sun is on the horizon, such a halo must be symmetric with respect to the sun; this is shown beautifully in Fig. 42.

If a halo is its own x-rotation, and in particular if a halo is a great circle halo, then its z-reflection is the same as its y-reflection, since zref = yref · xrot. For a great circle halo with pole $\mathbf{P}_u$ the result is easy to remember by recalling that the relevant poles yrot $\mathbf{P}_u$ and yref $\mathbf{P}_u$ are antipodal. Similar results hold for halos that are their own y-reflections or their own z-reflections.

(ii) If K is left–right symmetric (i.e., yref $K = K$), then so is the halo itself—it is its own y-reflection. In the halo atlas these halos would be point halos with $\mathbf{P}_u$ on $y = 0$ and great circle halos with $\mathbf{P}_u$ on $y = 0$ or with $\mathbf{P}_u = (0, \pm 1, 0)$.

(iii) If K is invariant under 180° rotation about the y-axis (i.e., yrot $K = K$), then the halo is its own z-reflection. In the atlas these halos would be point halos with $\mathbf{P}_u = (0, \pm 1, 0)$ and great circle halos with $\mathbf{P}_u$ on $y = 0$ or with $\mathbf{P}_u = (0, \pm 1, 0)$. If a halo is its own z-reflection, then changing the sun elevation from Σ to $-\Sigma$ has the effect of reflecting the halo about the plane $z = 0$, the plane of the horizon. When the sun is on the horizon, such a halo must be symmetric with respect to the horizon; some examples appear among the halos in Fig. 42.

(iv) If K is invariant under 180° rotation about the z-axis (i.e., zrot $K = K$), then interchanging the entry and exit faces does not change the halo—the halo is its own face interchange. In the atlas these halos would be point halos with $\mathbf{P}_u = (0, 0, \pm 1)$ and great circle halos with $\mathbf{P}_u$ on $z = 0$ or with $\mathbf{P}_u = (0, 0, \pm 1)$.

(v) If all of K is on the equator $z = 0$ (upper hemisphere $z > 0$, lower hemisphere $z < 0$), then the contact points of the halo with the circular halo are on (above, below) the parhelic circle. This is obvious from Fig. 11, where if $\mathbf{k}_u$ is moved to the equator and if $\mathbf{S}_u$ and $\mathbf{H}_u$ are moved to $\mathbf{D}_u$ and $\mathbf{E}_u$, then $\eta = \sigma$, so that the zenith angle of the contact point $\mathbf{H}$ equals the zenith angle of $\mathbf{S}$. In the atlas the halos with all of K on the equator would be the point halos with $\mathbf{P}_u$ on the equator and the great circle halos with $\mathbf{P}_u = (0, 0, \pm 1)$, the latter being well shown in Figs. 42–49.

(vi) If all of K is on the great circle $x = 0$ (front hemisphere $x > 0$, rear hemisphere $x < 0$), then the contact points of the halo with the circular halo are on (above, below) the subparhelic circle. Again this is clear from Fig. 11. In the atlas the halos with all of K on $x = 0$ would be the point halos with $\mathbf{P}_u$ on $x = 0$ and the great circle halos with $\mathbf{P}_u = (\pm 1, 0, 0)$.

(vii) If all of K is on (within, outside) the great circle centered at $\mathbf{E}_u$, then the contact points of the halo with the circular halo are on (above, below) the horizon.

(viii) If all of K is on (within, outside) the great circle centered at $\mathbf{D}_u$, then contact with the circular halo occurs only when the sun is on (above, below) the horizon.

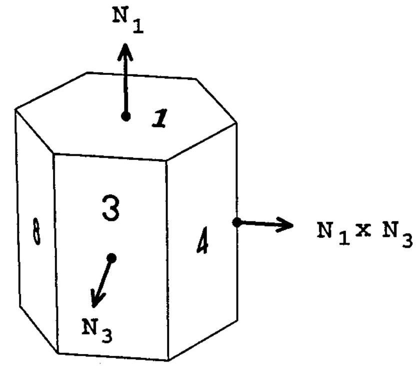

Fig. 26. Hexagonal prismatic crystal and crystal frame vectors $\mathbf{N}_3$, $\mathbf{N}_1 \times \mathbf{N}_3$, $\mathbf{N}_1$.

3. Realizable Halos in the Atlas

Anyone who has thought about halos arising in pyramidal crystals is apt to be baffled by the seemingly endless variety of exotic shapes that these halos can assume. If the Spin Vector Assumption is satisfied, however, then we know the variety cannot be endless, and by examining the halo atlas, Appendix A, we even have a good idea of what the possibilities are, before ever looking at the specific crystal shapes and orientations dictated by real crystals. The possibilities are narrowed further if the crystal shapes and orientations are known, since the shapes and orientations limit the possible poles. We will now examine known and plausible halos and see where their poles appear on the sphere and hence where the halos appear in the atlas. We start with a crystal together with one of six crystal orientation classes to be described momentarily. A choice of entry and exit faces for the ray path—hence a specification of a wedge on the crystal—will determine the halo.

A. Crystal Orientation Classes

The crystal is at first assumed to be a hexagonal prism. The crystal faces are numbered as in Fig. 26, with the basal faces being 1 and 2, and the prism faces being 3, 4, . . . , 8. The outward unit normal to face i is $\mathbf{N}_i$, and the *crystal frame* vectors are $\mathbf{N}_3$, $\mathbf{N}_1 \times \mathbf{N}_3$, $\mathbf{N}_1$. In terms of the crystal frame vectors, the outward normals are

$$\begin{aligned}
&\mathbf{N}_1 = \mathbf{N}_1, \quad \mathbf{N}_2 = -\mathbf{N}_1, \quad \mathbf{N}_3 = \mathbf{N}_3,\\
&\mathbf{N}_4 = (\cos 60)\, \mathbf{N}_3 + (\sin 60)\, \mathbf{N}_1 \times \mathbf{N}_3,\\
&\mathbf{N}_5 = (\cos 120)\, \mathbf{N}_3 + (\sin 120)\, \mathbf{N}_1 \times \mathbf{N}_3,\\
&\mathbf{N}_6 = (\cos 180)\, \mathbf{N}_3 + (\sin 180)\, \mathbf{N}_1 \times \mathbf{N}_3,\\
&\mathbf{N}_7 = (\cos 240)\, \mathbf{N}_3 + (\sin 240)\, \mathbf{N}_1 \times \mathbf{N}_3,\\
&\mathbf{N}_8 = (\cos 300)\, \mathbf{N}_3 + (\sin 300)\, \mathbf{N}_1 \times \mathbf{N}_3.
\end{aligned} \tag{78}$$

We consider a particular wedge, say wedge $i\,j$, whose entry and exit faces are i and j, respectively. The entry and exit normals $\mathbf{N} = \mathbf{N}_i$ and $\mathbf{X} = -\mathbf{N}_j$, together with the spin vector $\mathbf{P}$, determine the pole $\mathbf{P}_u$ with respect to the wedge. To get $\mathbf{P}_u$ informally, one orients the crystal so that the wedge determined by $\mathbf{N}$ and $\mathbf{X}$ is in standard orientation; wherever $\mathbf{P}$ ends up—this is the desired vector $\mathbf{P}_u$. Formally, $\mathbf{P}_u$ is found from Eqs. (8) and (21), with $\mathbf{N}$, $\mathbf{X}$, and $\mathbf{P}$ expressed as linear combinations of the crystal frame vectors. The spin vector $\mathbf{P}$ is found from the crystal orientation classes.

Following are the six crystal orientation classes. Refer to Fig. 26 for $\mathbf{N}_3$, $\mathbf{N}_1 \times \mathbf{N}_3$, and $\mathbf{N}_1$.

(1) *Plate*, the class of plate orientations; an orientation u is a *plate orientation*[6] if and only if $\mathbf{N}_1(u) = \mathbf{k}$. In Eq. (1) we can therefore take $\mathbf{P} = \mathbf{N}_1$ and $\psi = 0$. Examples of halos arising in plate orientations would be the common parhelia, with wedge angle $\alpha = 60$ and therefore associated with the 22° circular halo, and the circumzenith arc, with $\alpha = 90$ and associated with the 46° circular halo. (It is not necessary that the rotations about the spin vector be achieved in each crystal, only in the population of crystals as a whole; individual crystals need not be spinning. Nor is it necessary that the shapes of the crystals be plates.)

(2) *Par*, the class of Parry orientations; u is a *Parry orientation* if and only if $\mathbf{N}_3(u) = \mathbf{k}$. We can therefore take $\mathbf{P} = \mathbf{N}_3$ and $\psi = 0$. Examples would be the Parry arcs ($\alpha = 60$) and the Parry infralateral and Parry supralateral arcs ($\alpha = 90$).

(3) *AP*, the class of alternate Parry orientations; u is an *alternate Parry orientation* if and only if $\mathbf{N}_1(u) \times \mathbf{N}_3(u) = \mathbf{k}$. We can therefore take $\mathbf{P} = \mathbf{N}_1 \times \mathbf{N}_3$ and $\psi = 0$. Examples would be the alternate Parry arcs ($\alpha = 60$) and the 46° parhelia ($\alpha = 90$).

(4) *Col*, the class of column orientations; u is a *column orientation* if and only if $\mathbf{N}_1(u)$ is horizontal. We can therefore take $\mathbf{P} = \mathbf{N}_1$, the same as for plate orientations, but now $\psi = 90$. Examples would be the upper and lower tangent arcs of the 22° circular halo ($\alpha = 60$) and the infralateral and supralateral arcs ($\alpha = 90$).

(5) *Low*, the class of Lowitz orientations; u is a *Lowitz orientation* if and only if $\mathbf{N}_1(u) \times \mathbf{N}_3(u)$ is horizontal. We can therefore take $\mathbf{P} = \mathbf{N}_1 \times \mathbf{N}_3$, the same as for alternate Parry orientations, but now $\psi = 90$. Lowitz orientations would occur if the crystal were spinning about a long diagonal of one of the hexagonal cross sections, with the spin axis remaining horizontal. Examples would be the Lowitz arcs ($\alpha = 60$) and the upper and lower tangent arcs to the 46° halo ($\alpha = 90$).

(6) *AL*, the class of alternate Lowitz orientations; u is an *alternate Lowitz orientation* if and only if $\mathbf{N}_3(u)$ is horizontal. We can therefore take $\mathbf{P} = \mathbf{N}_3$, the same as for Parry orientations, but now $\psi = 90$. Alternate Lowitz orientations would occur if the crystal were spinning about a short diagonal of one of the hexagonal cross sections, with the spin axis remaining horizontal. Examples would be the alternate Lowitz arcs ($\alpha = 60$).

Thus all six crystal orientation classes satisfy the Spin Vector Assumption. And $\mathbf{P} = \mathbf{N}_1$ for plate and column orientations, $\mathbf{P} = \mathbf{N}_3$ for Parry and alternate Lowitz orientations, and $\mathbf{P} = \mathbf{N}_1 \times \mathbf{N}_3$ for Lowitz and alternate Parry orientations; see Table 2.

Table 2. Spin Vector P and Its Zenith Angle ψ for the Six Classes of Crystal Orientations

Crystal Orientation Class	$\mathbf{P}$	ψ
Plate orientations	$\mathbf{N}_1$	0
Column orientations	$\mathbf{N}_1$	90
Parry orientations	$\mathbf{N}_3$	0
Alternate Lowitz orientations	$\mathbf{N}_3$	90
Alternate Parry orientations	$\mathbf{N}_1 \times \mathbf{N}_3$	0
Lowitz orientations	$\mathbf{N}_1 \times \mathbf{N}_3$	90

Of the six crystal orientation classes, only the existence of plate orientations, Parry orientations, and column orientations is firmly established. There are no unequivocal published photographs of Lowitz arcs, although some recent unpublished photographs—the 31 August 1994 Finnish halo display,[7] for example—suggest that Lowitz orientations may also be real. Observational evidence for alternate Parry orientations is scanty, and observational evidence for alternate Lowitz orientations is lacking altogether. We nevertheless include these latter three classes of crystal orientations, for three reasons: First, they seem plausible, especially if the hexagonal faces of the crystals need not be regular. Second, halo observers, ourselves included, tend to be afflicted with a kind of blindness to new halos, so that absence of observations in the halo record is no proof of nonexistence. Third and perhaps most important, inclusion of these three classes gives balance and completeness to the presentation.

We are now prepared to describe all possible refraction halos arising in hexagonal prismatic crystals having orientations given by any one of the six orientation classes above. To list the halos, we need only list the poles (coordinate vectors) of the spin vectors $\mathbf{N}_1$, $\mathbf{N}_3$, and $\mathbf{N}_1 \times \mathbf{N}_3$ with respect to the wedges of the crystal. For hexagonal prismatic crystals the wedges to be considered are those with wedge angle $\alpha = 90$ or $\alpha = 60$. [Wedge angles larger than $\alpha_{\max} = 99.5$ do not allow the wedge to pass light.] We refer to the halos with $\alpha = 90$ as 46° arcs, since they tend to be associated with the 46° circular halo. Similarly, the halos with $\alpha = 60$ are 22° arcs. The term arc does not imply any particular shape; we use "arc" and "halo" nearly interchangeably, except that "46° halo", for example, usually refers to the 46° circular halo.

B. The 46° Arcs

Figure 59, Appendix B, is the pole diagram for 46° arcs; it shows the poles $\mathbf{P}_u$ for all 46° arcs. From the figure and from the halo atlas, imagined to be extended to cover all sun elevations, one can find the appearance of any 46° arc. In particular, among the halos of Figs. 41 and 49 would be all 46° arcs with a sun elevation of 20°.

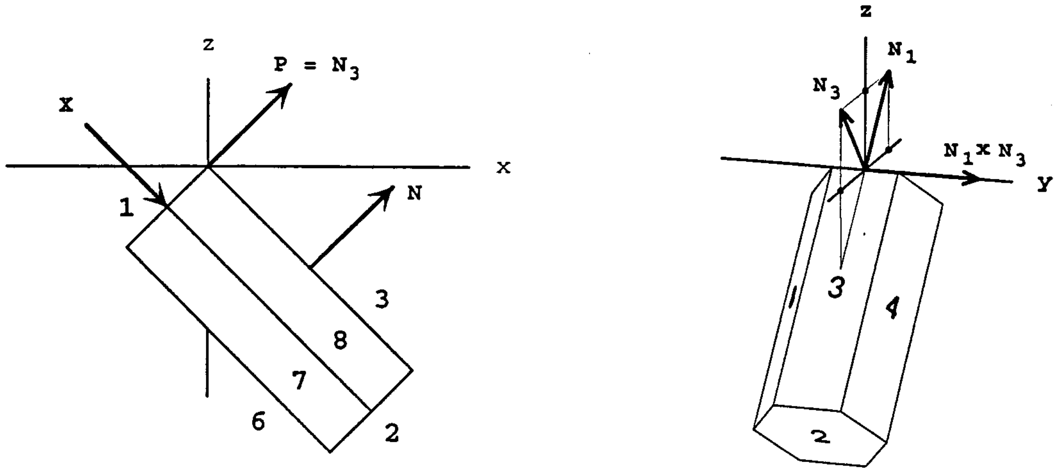

Fig. 27. Left, geometric derivation of the pole Par 3 1, the coordinate vector of the Parry spin vector $\mathbf{P} = \mathbf{N}_3$ with respect to wedge 3 1. The crystal is oriented so that wedge 3 1 is in standard orientation (Fig. 5), and in this orientation the vector $\mathbf{P}$ coincides with the desired pole. The pole Par 3 1 is therefore $(1/\sqrt{2}, 0, 1/\sqrt{2}) = B(90, -45)$. Right, same crystal orientation but with the x-axis pointing nearly out of the paper, so that the diagram can be more easily related to Fig. 59. The spin vectors $\mathbf{N}_1$ and $\mathbf{N}_1 \times \mathbf{N}_3$ for plate orientations and alternate Parry orientations, respectively, have been added. From the diagram here, the pole Plate 3 1 is $(-1/\sqrt{2}, 0, 1/\sqrt{2}) = B(90, -135)$ and the pole AP 3 1 is $(0, 1, 0) = B(0, \delta)$.

Consider, for example, the circumzenith arc arising in Parry oriented crystals, whose ray path enters face 3 and exits face 1. Table 2 gives $\mathbf{P} = \mathbf{N}_3$ and $\psi = 0$. Then with $\mathbf{N} = \mathbf{N}_3$ and $\mathbf{X} = -\mathbf{N}_1$, Eqs. (8), (21), and (26) give $\mathbf{P}_u = (1/\sqrt{2}, 0, 1/\sqrt{2}) = B(90, -45)$, indicated by "Par 3 1" in Fig. 59. In Fig. 41, which is the halo atlas figure for point halos with $\alpha = 90$ and $\Sigma = 20$, the halo at $(\theta, \delta) = (90, -45)$ is therefore the circumzenith arc with $\Sigma = 20$.

As mentioned previously, a less formal and more enlightening approach to finding $\mathbf{P}_u$ can replace the preceding calculations. Simply orient the crystal so that the relevant wedge is in standard orientation, and see where the spin vector falls. For the circumzenith arc just considered, the relevant wedge is wedge 3 1. The resulting crystal orientation is shown in Fig. 27; again $\mathbf{P}_u = (1/\sqrt{2}, 0, 1/\sqrt{2}) = B(90, -45)$.

Par 3 1, above, is the pole[8] (coordinate vector) of the Parry spin vector $\mathbf{P} = \mathbf{N}_3$ with respect to the wedge 3 1. More generally, Par $i\,j$ is the pole of $\mathbf{N}_3$ with respect to wedge $i\,j$. We also refer to the corresponding halo itself as Par $i\,j$; it is the halo arising in Parry orientations and wedge $i\,j$. Similarly, Plate $i\,j$ is the pole of the plate spin vector $\mathbf{P} = \mathbf{N}_1$ with respect to wedge $i\,j$, and it is also the halo arising in plate orientations and wedge $i\,j$. Similar conventions apply to the other four crystal orientation classes.

Although the poles in Fig. 59 are labeled for point halos, they are equally valid for great circle halos. Since $\mathbf{P} = \mathbf{N}_1$ for both plate and column orientations, then for each wedge $i\,j$ the poles Plate $i\,j$ and Col $i\,j$ are the same, and in the figure each pole labeled "Plate $i\,j$" can be relabeled "Col $i\,j$." Similarly, "Par $i\,j$" can be relabeled "AL $i\,j$," and "AP $i\,j$" can be relabeled "Low $i\,j$." Calculations and informal geometric derivations of poles for point halos apply verbatim to the corresponding great circle halos. Of course, to see what the great circle halos look like, one must refer to Fig. 49, whereas for point halos, refer to Fig. 41.

Wedges that Make the Same Halo

In Fig. 59 the first table, which is for plate orientations, lists all 24 wedges having wedge angle $\alpha = 90$. The table groups together wedges that make the same halo for plate orientations. Thus one finds six wedges that make the circumzenith arc, namely, wedges 1 3, 1 4, . . . , 1 8. All six have the same pole, located at the solid dot labeled "Plate 1 3" on the front hemisphere. The second table, which is for Parry orientations, lists the same 24 wedges but groups together wedges that make the same halo for Parry orientations. The third table does the same for alternate Parry orientations.

The first table also applies to column orientations, which give great circle halos, as well as to plate orientations, which give point halos. To get a grouping of wedges for column orientations, one need only merge two of the groups for plate orientations that face each other in the right and left columns. Whereas for plate orientations the table shows four groups of wedges and hence four halos, for column orientations it shows only two groups and hence two halos—12 wedges are for the infralateral arcs and 12 are for the supralateral arc. The second and third tables are similar.

To see how the groupings of wedges are arrived at, one needs to realize, from Eqs. (18) and (45), that two halos (with $\alpha \leq \alpha_{\max}$) are the same if and only if the two wedge angles are the same and the two sets of wedge orientations are the same. The latter happens if and only if the two zenith loci are the same, that is, if and only if $\psi_1 = \psi_2$ and the two poles are the same, or if $\psi_1 + \psi_2 = 180$ and the two poles are antipodal. Thus point halos (hence for plate, Parry, and alternate Parry orientations) are the same if and only if they have the same wedge angles and the same poles. (For point halos we have $\psi = 0$, not $\psi = 180$.) Great circle halos (hence for column, Lowitz, and alternate Lowitz orientations) are the same if and only if they have the same wedge angles and the same or antipodal poles. Thus the construction of the tables in Fig. 59, as well as the tables in the rest of Appendix B, is just a computer sorting of wedges according to wedge angle and pole.

In the tables, any wedge with pole on the front hemisphere appears in the left column, and any wedge with pole on the rear appears in the right. Two wedges with antipodal poles appear on the same line. According to Rule 2, their halos are x-rotations of each other. If the halos are great circle halos, they are the same.

Discussion of the Individual 46° Arcs

We treat the 46° arcs in some detail, both to illustrate previous results and to serve as a basis for comparison later with other arcs. First, the point halos:

Par 8 1, the right Parry supralateral arc. $\mathbf{P}_u$ ($=\mathbf{k}_u$) $= B(30, -45)$. We begin with this little known halo because it is among the 46° arcs that have the fewest special features and is more typical of many of the halos to follow. Figure 41 shows the halo for $\Sigma = 20$, and a complete atlas would of course show it for all Σ. The halo was also used as an example in Figs. 11 and 15.

The table in Fig. 59 gives the angular distances s_1 and s_2 from $\mathbf{P}_u$ to the nearest and farthest points of the entry region; $s_1 = 58$ and $s_2 = 117$ as shown in Fig. 15. According to the Nonempty Halos Theorem, Subsection 2.F, the halo is therefore nonempty for $58 \le \sigma \le 117$, that is, for $-27 \le \Sigma \le 32$. The table also shows $\mathbf{P}_u$ to have D-centered coordinates $(s, t) = (79, 62)$, and so from the Contact Point Theorem, Subsection 2.G, contact with the 46° circular halo occurs when $\sigma = s = 79$, i.e., $\Sigma = 11$, and the bearing of the contact point from the sun is $\tau = t = 62$.

Par 4 1, the left Parry supralateral arc. $\mathbf{P}_u = B(150, -45)$. From Rule 3 and Fig. 59, this halo is the left–right reflection of Par 8 1.

Par 1 7 and Par 1 5, left and right Parry infralateral arcs. $\mathbf{P}_u = B(150, 45)$ and $\mathbf{P}_u = B(30, 45)$. From the table the arcs are nonempty when $-2 \le \Sigma \le 62$, and contact with the 46° halo occurs when $\Sigma = 28$.

Par 5 1 and Par 7 1, unnamed arcs on the rear hemisphere. $\mathbf{P}_u = B(150, 135)$ and $\mathbf{P}_u = B(30, 135)$. Nonempty when $-32 \le \Sigma \le 27$, and contact with the 46° halo when $\Sigma = -11$. Since Par 5 1 is on the same line in the table as the right Parry supralateral arc Par 8 1, then it is the x-rotation of the right Parry supralateral arc and hence the z-reflection of the left Parry supralateral arc. Similarly, Par 7 1 is the x-rotation of the left Parry supralateral arc and the z-reflection of the right Parry supralateral arc. See Fig. 23, where the four halos have the same poles as Par 4 1, Par 8 1, Par 5 1, and Par 7 1, but have wedge angle $\alpha = 40$. Either from the Face Interchange Rule or from the wedge notation, Par 5 1 is the face interchange of the right Parry infralateral arc Par 1 5. And Par 7 1 is likewise the face interchange of the left Parry infralateral Par 1 7.

The concepts of x-rotation, y-reflection, and z-reflection are closely related, with any one of them expressible in terms of the other two. From here on we generally state things in terms of y-reflection and z-reflection.

Par 1 8 and Par 1 4; rear hemisphere halos, the z-reflections of the Parry infralateral arcs, and the face interchanges of the Parry supralateral arcs. $\mathbf{P}_u = B(150, -135)$ and $\mathbf{P}_u = B(30, -135)$. Nonempty when $-62 \le \Sigma \le 2$, and contact with the 46° halo when $\Sigma = -28$.

Plate 1 3, Par 3 1, the circumzenith arc. $\mathbf{P}_u = B(90, -45)$. From the table, $s_1 = 58$ and $s_2 = 90$, so the halo is nonempty when $0 \le \Sigma \le 32$. And $(s, t) = (68, 0)$, so contact with the 46° halo occurs when $\Sigma = 22$, with the contact point directly above the sun, in the solar vertical. The values of s_1, s_2, s, and t are easier to confirm than for the arcs considered above, because of the symmetric position of $\mathbf{P}_u$ with respect to the entry region. In the analog of Fig. 15 the pole $\mathbf{P}_u$ would now be at $B(90, -45)$, and $\mathbf{S}_1$ and $\mathbf{S}_2$ would change accordingly. The location of $\mathbf{S}_1$ is obvious, and s_1 is then found from the figure and from Eq. (49) to be 58° (again). And $s_2 = 90$, directly from the figure, but note $\mathbf{S}_2$ can now be anywhere on the grazing entry curve. Also, the angular distance from $\mathbf{P}_u$ to $\mathbf{D}_u$ is $s = 45 + \Delta_m/2 = 68$. (Most of these results for the circumzenith arc can be obtained more directly and more physically; we are trying to show how the halo fits into the general scheme and how it compares with the Parry supralateral arc considered previously.) The halo is left–right symmetric according to (ii) of Subsection 2.I. The symmetry and the uniqueness of the contact point show again that the contact point is in the solar vertical.

Plate 3 2, Par 1 6, the circumhorizon arc. $\mathbf{P}_u = B(90, 45)$. Nonempty when $58 \le \Sigma \le 90$, and contact with the 46° halo when $\Sigma = 68$. Left–right symmetric. Contact point in the solar vertical but below the sun.

Plate 2 3, Par 6 1; rear hemisphere halo, the z-reflection of the circumzenith arc, and the face interchange of the circumhorizon arc. $\mathbf{P}_u = B(90, 135)$. Nonempty when $-32 \le \Sigma \le 0$, and contact with the 46° halo when $\Sigma = -22$. Left–right symmetric. Contact point in the solar vertical.

Plate 3 1, Par 1 3; rear hemisphere halo, the z-reflection of the circumhorizon arc, and the face interchange of the circumzenith arc. $\mathbf{P}_u = B(90, -135)$. Nonempty when $-90 \le \Sigma \le -58$, and contact with the 46° halo when $\Sigma = -68$. Left–right symmetric. Contact point in the solar vertical.

AP 1 3 and AP 3 1, left and right 46° parhelia. $\mathbf{P}_u = B(180, \delta)$ and $\mathbf{P}_u = B(0, \delta)$. Nonempty when $-32 \le \Sigma \le 32$, and contact with the 46° halo when $\Sigma = 0$. From Fig. 11, suitably modified, these halos lie entirely on the parhelic circle: The point $\mathbf{k}_u$ would now be at one of the Bravais poles $(0, \pm 1, 0)$, and the sun locus S would coincide with a Bravais circle. The point $\mathbf{H}_u$ would be on the same circle, and hence $\eta = \sigma$ in the figure, that is, the zenith angle of $\mathbf{H}$ would be the zenith angle of $\mathbf{S}$, as claimed. Either from the wedge notation or from the Face Interchange Rule, the right parhelion is the face interchange of the left. Each is its own z-reflection, from (iii) of Subsection 2.I.

AP 5 1, AP 4 1, etc. The remaining 46° arcs from alternate Parry orientations.

Great circle halos:

AL 8 1. $\mathbf{P}_u = B(30, -45)$, the same as for the right Parry supralateral arc Par 8 1. [But the antipode $\mathbf{P}_u = B(150, 135)$ is now a pole as well.] We treat this obscure and probably nonexistent halo first, because of its relation to the right Parry supralateral arc and because of its relative lack of special features. From the table, $s_1 = 58$ and $s_2 = 117$, and since $s_1 \le 90 \le s_2$, then from the Nonempty Halos Theorem the halo is never empty. Also from the table, the D-centered coordinates of $\mathbf{P}_u$ are $(s, t) = (79, 62)$, so by the Contact Point Theorem the halo contacts the 46° halo when $-79 \le \Sigma \le 79$, and the contact points have bearing $\tau = 62 \pm \Delta\tau$ as described in the theorem.

AL 4 1, the y-reflection and z-reflection of AL 8 1. $\mathbf{P}_u = B(150, -45)$.

AL 1 5, the face interchange of AL 8 1. $\mathbf{P}_u = B(30, 45)$. Never empty (K just nicks the entry region near the left corner). Contact with the 46° halo when $-62 \le \Sigma \le 62$.

AL 1 7, the y-reflection and z-reflection of AL 1 5, and the face interchange of AL 4 1. $\mathbf{P}_u = B(150, 45)$.

Col 1 3, AL 3 1; infralateral arcs. $\mathbf{P}_u = B(90, -45)$. Never empty; in fact, the lower boundary of the entry region forms an arc of K. Contact with the 46° halo occurs when $-68 \le \Sigma \le 68$. The halo is its own y-reflection (i.e., it is left–right symmetric) and hence is its own z-reflection, since for great circle halos the two properties are equivalent [or use (iii) of Subsection 2.I].

Col 3 2, AL 1 6; supralateral arc. The face interchange of the infralateral arcs. $\mathbf{P}_u = B(90, 45)$. Nonempty when $-32 \le \Sigma \le 32$, and contact with the 46° halo when $-22 \le \Sigma \le 22$. The halo is its own y-reflection and its own z-reflection.

AL 4 1, AL 8 1, AL 1 7, AL 1 5; the remaining 46° arcs from alternate Lowitz orientations.

Low 3 1; upper and lower tangent arcs to the 46° halo. $\mathbf{P}_u = B(0, \delta)$. Also known as Galle's halo, this halo is one of five 46° arcs from Lowitz orientations. Since $s = 90$, this halo is an instance of the special case ii(c) of the Contact Point Theorem. The halo is also its own y-reflection, z-reflection, and face interchange, the latter from (iv) of Subsection 2.I.

Low 5 1, Low 4 1, Low 1 8, Low 1 7; the remaining 46° arcs from Lowitz orientations.

Where in this list is the 46° circular halo? Nowhere, since the halo does not satisfy the Spin Vector Assumption and hence has no pole. If, however, we were representing halos by their zenith loci rather than by their poles, then the circular halo would be included, and its zenith locus would be the entire sphere. By analogy with point halos and great circle halos, the circular halo would be a "sphere halo".

$\alpha = 90$ is Special

The wedge angle $\alpha = 90$, giving rise to the 46° arcs, is special. From Fig. 10 we see that circles (not shown) on the inner sphere and centered at point $\mathbf{N}$ will $\mathbf{N}$-project to circles on the outer sphere, and each of the image circles will be in a (different) plane perpendicular to $\mathbf{N}$; this is true regardless of α. For $\alpha = 90$, however, each of the planes is parallel to $\mathbf{X}$, and so the image circles $\mathbf{X}$-project back to circles on the inner sphere. The resulting circles, in fact, all have center at point $\mathbf{N}$. Thus the composite projection, which gives the halo point as a function of the sun point (Fig. 3), takes each circle centered at $\mathbf{N}$ to a concentric circle, and the same is true for each circle centered at $\mathbf{X}$. This remarkable property is responsible for many peculiarities of $\alpha = 90$ halos. In Fig. 59, for example, the Bravais meridian $\delta = -45$ and the upper boundary of the entry region are arcs of concentric circles centered at $\mathbf{X}$, thus explaining the recurring values of s_1 in the tables of the figure (e.g., $s_1 = 58$). And the reason that the circumzenith arc is indeed a circular arc centered at the zenith is now evident in the analog of Fig. 11: the sun locus S would be a circle centered at $\mathbf{k}_u = \mathbf{N}_u$, and the halo point locus H would therefore be (part of) a concentric circle, so the zenith angle η of $\mathbf{H}$ would be constant.

Another interesting feature of $\alpha = 90$ is that the circumzenith arc, for example, can arise in two different crystal orientation classes; the circumzenith arc is Plate 1 3, and it is also Par 3 1. The same of course holds for the corresponding great circle halo; it is Col 1 3 and it is also AL 3 1.

C. The 22° Arcs

Figure 55 is the pole diagram for 22° arcs. The calculations used in making the figure are exactly the same as for the 46° arcs but with $\mathbf{N}$ and $\mathbf{X}$ now chosen so that $\alpha = 60$ instead of $\alpha = 90$. This change produces new poles and hence new halos. Figures

33–37 and 42–45 in the halo atlas can be used to find the appearance of the halos if the sun elevation is 0, 20, 50, or 80°. The results will be approximate, however, since not all of the poles in Fig. 55 have a corresponding halo shown in the atlas figures. The upper suncave Parry arc, for example, which is at $B(90, -30)$ and indicated by "Par 3 5" in Fig. 55, is not shown in the atlas figures, but it is apt to resemble the nearby halo at $B(90, -45)$ in Figs. 33–36. Of course, one can always calculate the arc exactly, using the methods of Section 1.

We now list the 22° arcs, starting with the point halos. Of the point halos all but the parhelia are left–right symmetric and have their contact points in the solar vertical (Rule 3 and the Contact Point Theorem).

Plate 3 5 and Plate 3 7, the familiar left and right 22° parhelia. Like the 46° parhelia, they are part of the parhelic circle. Each is its own z-reflection. They are face interchanges of each other, and of course they are left–right reflections of each other.

Par 8 4 and Par 5 7, the upper and lower sunvex Parry arcs. Each is the z-reflection of the other, and each is its own face interchange. Contact points with the 22° halo are on the subparhelic circle, from (vi) of Subsection 2.I.

Par 3 5 and Par 4 6, the upper and lower suncave Parry arcs. Par 4 6, being within the entry region, is a closed loop when the sun is high enough, that is, when the solar zenith angle σ is less than the angular distance from the pole to the boundary.

Par 7 3 and Par 6 8, unnamed Parry arcs on the rear hemisphere. Par 7 3 is the z-reflection of Par 4 6 and the face interchange of Par 3 5, and Par 6 8 is the z-reflection of Par 3 5 and the face interchange of Par 4 6.

AP 4 6, AP 5 7, AP 6 8, AP 7 3, AP 8 4, and AP 3 5, the alternate Parry arcs. The most interesting of these is AP 5 7, with $\mathbf{P}_u = (1, 0, 0)$. Its contact point with the 22° halo must be on the parhelic circle, from (v) of Subsection 2.I. But the contact point must also have bearing $\tau = t = 0$, so when contact occurs the parhelic circle is a circle of radius 11° tangent to the 22° halo at the top. Figure 36 shows the arc when $\Sigma = 80$, which is very nearly the solar elevation for contact. AP 8 4 is analogous.

In general, the Parry and alternate Parry arcs are akin to the circumzenith and circumhorizon arcs and their rear hemisphere relatives, since all are located on the Bravais equator $y = 0$.

Next are the great circle halos. Each is its own y-reflection and z-reflection.

Col 3 5, the familiar upper and lower tangent arcs to the 22° halo. Since $s = 90$, this halo is an instance of the special case ii(c) of the Contact Point Theorem.

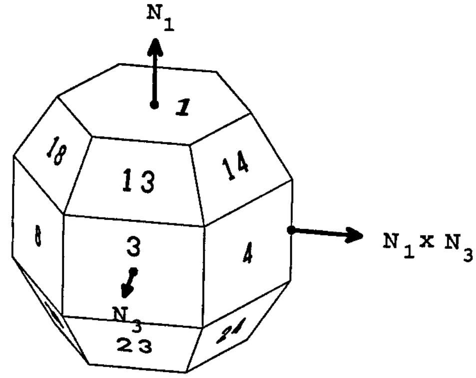

Fig. 28. Pyramidal crystal and crystal frame vectors $\mathbf{N}_3$, $\mathbf{N}_1 \times \mathbf{N}_3$, $\mathbf{N}_1$.

In fact, the zenith locus K is the Bravais equator $y = 0$, which always intersects the contact circle in the vertical, and so the halo contacts the 22° halo for all sun elevations, and it does so at the two points in the solar vertical. (With $\Sigma = \pm 90$, contact occurs everywhere.) The halo is its own face interchange, from (iv) of Subsection 2.I.

Low 4 6, Low 6 8, Low 5 7, the lower, upper, and unnamed Lowitz arcs. Low 5 7, with its pole at $(\pm 1, 0, 0)$, has its contact points located on the subparhelic circle, from (vi) of Subsection 2.I. Contact can therefore occur only for $-11 \le \Sigma \le 11$, which is consistent with $s = 11$ in the table in Fig. 55. The halo is its own face interchange. It has its pole fairly close to $\mathbf{D}_u$, which makes it approximately circular at low sun elevations, in contrast to halos far from $\mathbf{D}_u$. Low 4 6 and Low 6 8 are face interchanges of each other. Since the zenith loci of the Lowitz arcs pass through $(0, \pm 1, 0)$, the Lowitz arcs contain the parhelia.

AL 8 4, AL 3 5, and AL 4 6, the alternate Lowitz arcs. AL 8 4, with its pole at $(0, 0, \pm 1)$, has its contact points always on the parhelic circle, from (v) of Subsection 2.I; see Figs. 42–45. AL 8 4 is its own face interchange, and AL 3 5 and AL 4 6 are face interchanges of each other.

The Lowitz and alternate Lowitz arcs are akin to the infralateral and supralateral arcs, since all are located on the Bravais equator.

Comparison of the pole diagram for the 22° arcs (Fig. 55) with the pole diagrams for, say, the 24° or 35° arcs to be discussed later (Figs. 57 and 58), shows that the 22° arcs are remarkably simple—their poles are all on the Bravais equator $y = 0$ or at the Bravais poles $(0, \pm 1, 0)$, and their zenith loci are therefore conveniently located with respect to the entry region and the minimum deviation vector. The same is true of the 46° arcs that are normally found in the classical halo literature. (The Parry infralateral and supralateral arcs, their rear hemisphere and alternate Parry relatives, and the corresponding great circle halos are virtually unknown in all but the most recent literature.) Classical halo theorists were dealt a lucky hand.

D. Nomenclature Defect

Figures 42–45 show that for low sun the halo Col 3 5, with pole $\mathbf{P}_u = (0, \pm 1, 0)$, consists of two separate components—the upper tangent arc and the lower tangent arc—whereas for high sun the halo is a single component—the circumscribed halo. From our point of view in this paper, however, there is only one halo, not two or three, and the existence of the three names is unfortunate and misleading.

A similar though less serious nomenclature defect occurs for the infralateral arcs Col 1 3 and for each of the three Lowitz arcs Low 4 6, Low 6 8, and Low 5 7: from our point of view each is a single halo, but its name is plural. In this paper we nevertheless use the traditional nomenclature.

The disconnection in various halos, as in Col 3 5 for low sun, for example, can be roughly understood by viewing the creation of the halo from the wedge, as was done in Fig. 14 for another great circle halo.

E. Pyramidal Crystals

Each of the six crystal orientation classes can apply not only to prismatic crystals but also to pyramidal crystals, that is, to crystals having pyramidal faces as well as, perhaps, prism and basal faces. Pyramidal crystals thus can give rise to a large number of halos. These halos provide much of the motivation for this paper.

To treat halos arising in pyramidal crystals, we need only add the appropriate normal vectors to the list given in Eq. (78). The face numbering for pyramidal crystals is shown in Fig. 28. Basal faces are 1 and 2, and prism faces are 3, 4, . . . , 8, as for prismatic crystals. Pyramidal faces are 13, 14, . . . , 18 and 23, 24, . . . , 28. As before, the vector $\mathbf{N}_i$ is the outward normal to face i. We assume that the pyramidal faces have Miller indices $\{1, 0, -1, 1\}$ and that the crystallographic axial ratio c/a is the conventional value 1.63, in which case the pyramidal faces are inclined at an angle of 28° with the (principal) crystal axis. Therefore

$$\begin{aligned}
&\mathbf{N}_{13} = (\cos 28)\mathbf{N}_3 + (\sin 28)\mathbf{N}_1, \quad && \mathbf{N}_{23} = (\cos 28)\mathbf{N}_3 + (\sin 28)\mathbf{N}_2,\\
&\mathbf{N}_{14} = (\cos 28)\mathbf{N}_4 + (\sin 28)\mathbf{N}_1, \quad && \mathbf{N}_{24} = (\cos 28)\mathbf{N}_4 + (\sin 28)\mathbf{N}_2,\\
&\mathbf{N}_{15} = (\cos 28)\mathbf{N}_5 + (\sin 28)\mathbf{N}_1, \quad && \mathbf{N}_{25} = (\cos 28)\mathbf{N}_5 + (\sin 28)\mathbf{N}_2,\\
&\ldots && \ldots\\
&\text{with } \mathbf{N}_1, \mathbf{N}_2, \ldots, \mathbf{N}_8 \text{ as before.}
\end{aligned} \tag{79}$$

For the pyramidal crystal under consideration, Table 3 shows the wedge angles α that give rise to halos. For each α there is a pole diagram in Appendix B. The calculations of the poles are the same as for halos from prismatic crystals, but visualizing the results geometrically is sometimes more difficult.

Table 3. Wedge Angles and Corresponding Circular Halos[a]

Wedge Angle α	Radius Δ_m of Circular Halo	Name of Circular Halo	Example of Wedge (Entry and Exit Faces)
28.0	9.0	9°	18 5
52.4	18.3	18°	18 24
56.0	19.9	20°	18 15
60.0	21.8	22°	8 4
62.0	22.9	23°	1 24
63.8	23.8	24°	18 4
80.2	34.9	35°	18 14
90.0	45.7	46°	1 4

[a]These arise in pyramidal crystals having prism faces, basal faces, and $\{1, 0, -1, 1\}$ pyramidal faces, as shown in Fig. 28.

F. The 9° Arcs

For the 9° arcs the wedge angle is 28° and a typical wedge is 18 5. The poles for the 9° arcs are shown in Fig. 52. As usual, the halos can be estimated from their poles and from the halo atlas; see Fig. 38 for the point halos and Fig. 46 for the great circle halos, if $\Sigma = 20$.

We would be surprised if we ever observed halos arising in pyramidal crystals having alternate Parry orientations or Lowitz orientations, and from here on we omit their poles from the diagrams and from the discussion, in the interest of simplification. Their poles can always be added to the diagrams if desired, since the poles Par $i\,j$, AP $i\,j$, and Plate $i\,j$ form a (right-handed) frame. Halos from pyramidal crystals having alternate Lowitz orientations also seem highly unlikely, but their poles are automatically included, since they coincide with the poles for Parry orientations.

We have discussed the 22° and 46° arcs in some detail, and we now regard them as familiar, even though some are rare or even nonexistent. From here on, when introducing a new halo, we look for a 22° or 46° arc whose pole and wedge angle are close to those of the new halo, and whose appearance can therefore be expected to be similar; when possible, this seems preferable to treating each new halo in isolation. The 9° arc Par 4 27, for example, should bear some resemblance to the 46° arc Par 8 1, the right Parry supralateral arc, which by now we understand quite well. Here, however, the resemblance should not be overly close, since the poles of the two arcs are not overly close, and the wedge angles are not close at all.

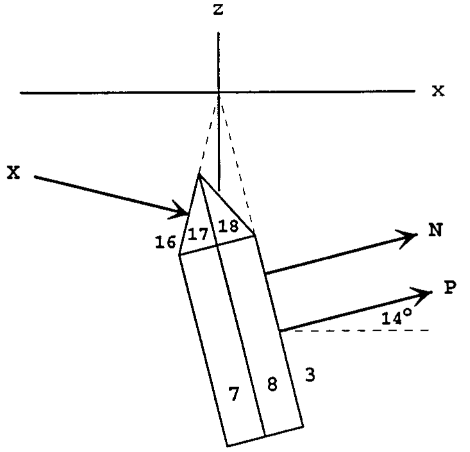

Fig. 29. Geometric derivation of the pole Par 3 16, the coordinate vector of the Parry spin vector $\mathbf{P} = \mathbf{N}_3$ with respect to wedge 3 16. The crystal is oriented so that wedge 3 16 is in standard orientation, and in this orientation the vector $\mathbf{P}$ coincides with the desired pole. The wedge angle is 28°, so face 3 is inclined 14° from the vertical. The pole Par 3 16 is therefore (cos 14, 0, sin 14) = B(90, −14), in agreement with the table in Fig. 52.

The eight 9° point halos with poles on the Bravais equator $y = 0$ should as a group resemble the 22° and 46° point halos on the Bravais equator, namely, the Parry and alternate Parry arcs and the circumzenith and circumhorizon arcs and their rear hemisphere relatives. In particular, they are all left–right symmetric and have their contact points in the solar vertical. Similarly, the 9° great circle halos Col 13 6 and Col 3 26 resemble the Lowitz arcs and the infralateral and supralateral arcs.

The poles in Fig. 52 can be verified geometrically by putting the relevant wedge in standard orientation. Figure 29 shows the derivation of the pole Par 3 16. The result there, incidentally, is an instance of the more general but simple observation that Par 3 j = $\mathbf{N}_0(\alpha)$ and Plate 1 j = $\mathbf{N}_0(\alpha)$ [Eq. (10)], since then $\mathbf{P} = \mathbf{N}$; see Figs. 52, 55, 56, 57, and 59.

Crystals are not Wedges

Sections 1 and 2 apply to an isolated wedge. Their results can be far off the mark when, as in the present section, the wedge is part of a crystal having other faces that can interfere with the prescribed ray path. The 9° arcs present extreme examples of this shielding of one crystal face by another. Note that in Fig. 28, for example, if the sun vector $\mathbf{S}$ makes an angle less than 90° with $\mathbf{N}_1$, then the light ray cannot travel the path 3 16. Thus in Fig. 52 the entry region for the wedge—if the wedge is considered as a part of the crystal rather than as an isolated wedge—is no longer the entire entry region as shown but rather has a bite taken out, the bite being (at least) the region inside the great circle centered at the point Plate 3 16.

Drawing the analog of Fig. 11 for the 9° arc Par 3 16 shows that for very high sun approximately half of the sun locus is in the missing bite, and the halo itself is no longer a complete loop, as if the wedge were isolated, but rather is about half a loop. (The entry region for the wedge Par 3 26, which makes the same halo, should be considered as well, but the region turns out to be the same.)

Similarly, the 9° arc Plate 3 16 is now empty (at least) when the zenith angle σ is less than 90, whereas the values of s_1 and s_2 in Fig. 52 imply that, if the wedge were in isolation, the arc would be nonempty whenever $\sigma \geq 61$. Some of our results, as here, need to be substantially qualified if applied to real crystals instead of to isolated wedges.

G. The 18° Arcs

For the 18° arcs the wedge angle is 52.4° and a typical wedge is 18 24. The poles are shown in Fig. 53, and the halos are shown in Figs. 39 and 47. The 18° arc Par 14 28 should be similar to the 22° arc Par 8 4, the upper sunvex Parry arc, because the poles of the two halos are identical and their wedge angles are close. The same is true for the arc Par 15 27 and the lower sunvex Parry arc. The 18° arcs Par 13 25 and Par 14 26 should resemble the 46° arcs AP 4 1 and AP 1 7, respectively. The 18° arc Plate 13 27 is not particularly close to any 22° or 46° arc, but it is almost identical to the point halo with pole at B(30, 0), which is shown in the atlas; see Fig. 39. According to (v) of Subsection 2.I, its contact point with the 18° circular halo is on the parhelic circle. The 18° arc Col 13 27 is its own face interchange, from (iv) of Subsection 2.I.

H. The 20° Arcs

For the 20° arcs the wedge angle is 56° and a typical wedge is 18 15. The poles are shown in Fig. 54. The 20° arc Plate 13 16 is very similar to the 22° arc Par 8 4, the upper sunvex Parry arc, and Plate 23 26 is likewise similar to the lower sunvex Parry arc. The 20° arc Par 13 16 is very similar to the 22° arc AP 5 7 and of course also shares its peculiarities. The 20° arcs Par 14 17 and Par 18 15 are very close to the 18° arcs Plate 13 25 and Plate 13 27.

We hope that by now it will go without saying that, if two point halos are close, then the corresponding great circle halos are also close. Thus, for example, Col 13 16 is close to AL 8 4. Incidentally, each of these halos has its contact point on the parhelic circle, from (v) of Subsection 2.I.

I. The 23° Arcs

For the 23° arcs the wedge angle is 62° and a typical wedge is 1 24. The poles are shown in Fig. 56. The 23° arc Plate 1 23 is close to the 22° arc Par 3 5, the upper suncave Parry arc, and Plate 13 2 is close to the lower suncave Parry arc. The 23° arc Par 13 2 is close to the 22° arc AP 4 6, and the other five 23° arcs on the Bravais equator also have their near twins among the 22° arcs. The 23° arcs Par 14 2 and Par 1 25 should be somewhat similar to the 46° arcs Par 8 1 and Par 1 5, the right Parry supralateral and infralateral arcs, respectively, but the two wedge angles are not especially close. The remaining 23° arcs are likewise similar to various 46° arcs.

J. The 24° Arcs

For the 24° arcs the wedge angle is 63.8° and a typical wedge is 18 4. The poles are shown in Fig. 57. The 24° arc Par 3 25 is close to the 22° arc Par 3 5, the upper suncave Parry arc, and Par 14 6 is close to the lower suncave. The 24° arcs Plate 13 7 and Plate 3 27 are somewhat similar to the 46° arcs Par 8 1 and Par 1 5, the right Parry supralateral and infralateral arcs. The 24° arc Par 4 28 is not close to any familiar 22° or 46° arc, but it is close to the $\alpha = 60$ point halo with pole at $B(60, -90)$ in the halo atlas; see Figs. 33–36.

K. The 35° Arcs

For the 35° arcs the wedge angle is 80.2° and a typical wedge is 18 14. The poles are shown in Fig. 58, and the halos are shown in Figs. 40 and 48. None of the poles in Fig. 58 is especially close to poles of 22° or 46° arcs. Plate 13 17 and Par 18 14 are on the great circle $x = 0$ and so have their contact points on the subparhelic circle, from (vi) of Subsection 2.I.

L. Halo Containments in the Pole Diagrams

A point halo is a subset of a great circle halo if their poles are orthogonal. But the poles Par $i\,j$, AP $i\,j$, and Plate $i\,j$ are always mutually orthogonal, since they are just the crystal frame vectors $\mathbf{N}_3$, $\mathbf{N}_1 \times \mathbf{N}_3$, $\mathbf{N}_1$ as seen from wedge $i\,j$. This orthogonality therefore creates a wealth of halo containments. Each pair $i\,j$ gives rise to six containments: The halo Plate $i\,j$ is a subset of the halos Low $i\,j$ and AL $i\,j$. The halo Par $i\,j$ is a subset of Col $i\,j$ and Low $i\,j$. And AP $i\,j$ is a subset of Col $i\,j$ and AL $i\,j$. In Fig. 59, for example, the infralateral arcs Col 1 3 must contain all the halos Par 1 3, . . . , Par 1 8, as well as AP 1 3, . . . , AP 1 8. And the circumzenith arc Plate 1 3 must be a subset of each of the halos AL 1 3, AL 1 4, AL 1 5, as well as Low 1 3, Low 1 4, Low 1 5. And so forth. In the discussions of the individual halos, we usually did not mention the containments, but they were always there.

M. Halo Identification Problems

We have seen several examples of halos having poles close to one another. If the wedge angles are close as well, the halos can be difficult to distinguish. To summarize: The 18° arc Par 14 28, the 20° arc Plate 13 16, and the 22° arc Par 8 4—the upper sunvex Parry arc—have identical poles and nearly identical wedge angles, thus making for a complicated region of sky where identifications must be made with caution. The 18° arc Par 15 27, the 20° arc Plate 23 26, and the lower sunvex Parry arc are likewise close. The 23° arc Plate 1 23 and the 24° arc Par 3 25 are close to the 22° arc Par 3 5—the upper suncave Parry arc. The 23° arc Plate 13 2 and the 24° arc Par 14 6 are likewise close to the lower suncave Parry arc. The 18° arc Plate 13 27 and the 20° arc Par 18 15 are very close. The 18° arc Par 13 25, the 24° arc Par 13 5, and the 35° arc Par 13 15 are somewhat similar, although perhaps not so similar as to cause confusion. The 35° arcs Plate 13 17 and Par 18 14 are close to each other, as are Plate 23 27 and Par 17 15.

Another potential source of confusion lies in the many halo containments. For fixed i and j, as explained earlier, the halo Par $i\,j$ is always a subset of Col $i\,j$. Even though Par $i\,j$ is a point halo and Col $i\,j$ is a great circle halo, there is the possibility of confusing the two, especially if the sun elevation is close to that for which the point halo contacts the circular halo. Among 22° arcs an example would be the lower sunvex Parry arc Par 5 7 and the upper and lower tangent arcs Col 5 7; the lower sunvex Parry arc and the lower tangent arc can be confused for $\Sigma \approx 11$. Similarly, the halo Plate $i\,j$ could perhaps be confused with Low $i\,j$ for appropriate sun elevations; an example would be the 22° parhelia Plate 4 6 and Plate 5 3 and the lower Lowitz arcs Low 4 6, if $\Sigma \approx 0$. The upper Lowitz arcs Low 6 8 are slightly less likely to be confused with the parhelia, and the unnamed Lowitz arcs Low 5 7 not at all likely, because of its proximity to $\mathbf{D}_u$.

We do not wish to overstate the identification problem. When there are two or more competing identifications for a halo, the presence of other, known halos is often enough to decide among them. Simple polarization observations or careful radiance observations may also be able to decide, as explained in Refs. 9 and 10. Confusion in the past has often arisen simply out of ignorance of the multiple possibilities. The lone label at hand got applied.

N. Reality of the Halos

What is the evidence for the existence of odd radius ($\Delta_m \neq 22, 46$) halos arising in preferentially oriented crystals? Some of the published photographs can be found in Refs. 2 and 11–16. There are many unpublished photographs as well, some spectacular, especially among the collection of the Finnish Halo Observers Network. Of the published photographs, the one by Sturm in Ref. 11, p. 92, is the best. It shows the 9° arc Plate 3 26, the 24° arcs Plate 3 25 and Plate 3 27, the 35° arcs Plate 23 25 and Plate 23 27, and probably faint 18° arcs Plate 13 25 and Plate 13 27. Thus the Sturm photo suggests that plate orientations are a real orientation mode for pyramidal crystals. Many other photos, most unpublished, seem to offer confirmation. In addition to the arcs already mentioned, we find among our Antarctic and Alaskan photographs the 20° arcs Plate 13 16 and Plate 23 26, the 23° arc Plate 1 23, perhaps the 35° arcs Plate 13 15 and Plate 13 17, and what appear to be the 18° arcs Plate 13 25 and Plate 13 27, and perhaps Plate 23 15 and Plate 23 17. These 18° arcs, however, are just above the horizon, in the confused murk where the low-level crystal swarm is concentrated, and the identifications are not certain.

Can column orientations be a real orientation mode for pyramidal crystals? The photographic evidence is much weaker than that for plate orientations, but there is some, mostly unpublished. The best published evidence is for the 9° arcs Col 13 6 and Col 3 26 and is from a display photographed by O. Richard

Norton and shown in Ref. 13. In that display what appears at first to be the 9° circular halo is in fact strongly enhanced on the sides, and this enhancement persists and indeed is better shown in several of Norton's other photographs of the display.[17] We predict that, with increased awareness, more photographs of odd radius arcs from column orientations will be forthcoming. In our crystal samples we sometimes find columnar crystals with pyramidal ends; sufficient numbers of these crystals, if large enough, ought to produce the desired arcs.

The case for Parry orientations as an orientation mode for pyramidal crystals is still weaker, for we know of no supporting halo photographs whatsoever. But we know that Parry orientations can occur—in Antarctica they are rather common—and we know that pyramidal crystals occur. We think that in the best displays from Parry orientations we will eventually see an odd radius arc from Parry orientations.

Odd radius arcs from alternate Parry orientations, or Lowitz orientations, or alternate Lowitz orientations are quite another matter. As mentioned earlier, we doubt that they will ever be seen.

One thing that is not in doubt is the reality of pyramidal crystals. They dominate many of our crystal samples collected at low temperatures. The crystals are usually too small for the interfacial angles to be accurately measured and thus to confirm our assumptions that the crystallographic axial ratio is 1.63 and that the pyramidal faces have Miller indices $\{1, 0, -1, 1\}$. The few crystals for which the measurements have been made do, however, support the assumptions; see Refs. 11, 18, and 19. Monte Carlo simulations of odd radius halo displays made using the same assumptions are good matches for the actual displays, but they are not perfect.

O. Crystal Symmetries, Pole Symmetries, and Halo Symmetries

Wedge Change Rule

Suppose two congruent wedges are located on the same crystal, and suppose that w is one of the two orthogonal transformations that take the first wedge to the second, that is, that take the entry and exit normals of the first wedge to the respective entry and exit normals of the second. Suppose also that $\mathbf{P}$ is a vector fixed in the crystal. In what follows, we can, without loss of generality, freeze the crystal at some moment, so that w becomes a constant matrix and $\mathbf{P}$ a constant vector. If at this same moment the frame of the first wedge is v, then the frame of the second is $w'(v)$ [Eqs. (14) and (15)], and the coordinate vectors $\mathbf{P}_v = v^{-1}\mathbf{P}$ and $\mathbf{P}_{w'(v)} = w'(v)^{-1}\mathbf{P}$ with respect to the two wedges are related by

$$\mathbf{P}_{w'(v)} = \begin{cases} w_v^{-1}\,\mathbf{P}_v & \text{if } \det w = 1, \quad (80) \\ \text{yref}\, w_v^{-1}\,\mathbf{P}_v & \text{if } \det w = -1, \quad (81) \end{cases}$$

where $w_v = v^{-1}wv$ is the matrix of w with respect to the frame v or, equivalently, w_v is the transformation w when the crystal is oriented so that the first wedge is in standard orientation. Equations (80) and (81) constitute the *Wedge Change Rule*. The Wedge Change Rule gives the relation between poles for different wedges on the same crystal.

Here the vector $\mathbf{P}$ is fixed, and $\mathbf{P}_v$ depends on v. The matrix v should be thought of as specifying a frame on the fixed crystal, rather than as specifying the frame of a particular wedge as the crystal moves, as did u in Sections 1 and 2. Equation (21) is still correct, however.

Wedge Change Corollary

Again suppose that two congruent wedges are located on the same crystal and that w is one of the two orthogonal transformations that take the first wedge to the second. Let v be the frame for the first wedge, so that $w'(v)$ is the frame for the second. Suppose that the Spin Vector Assumption is satisfied, with $\mathbf{P}$ the spin vector, and with $\mathbf{P}_v$ and $\mathbf{P}_{w'(v)}$ therefore the poles with respect to the two wedges.

If $\det w = 1$, then

(i) $\mathbf{P}_{w'(v)} = \mathbf{P}_v$ (the two point halos arising in the wedges are the same) if and only if $w\mathbf{P} = \mathbf{P}$. That is, w should be a rotation about an axis parallel to $\mathbf{P}$.

(ii) $\mathbf{P}_{w'(v)} = -\mathbf{P}_v$ (the two point halos are x-rotations of each other) if and only if $w\mathbf{P} = -\mathbf{P}$. That is, w should be a 180° rotation about an axis perpendicular to $\mathbf{P}$.

If $\det w = -1$, then

(iii) $\mathbf{P}_{w'(v)} = \text{yref}\,\mathbf{P}_v$ (the two point halos are y-reflections of each other) if and only if $w\mathbf{P} = \mathbf{P}$. That is, w should be a reflection in a plane parallel to $\mathbf{P}$.

(iv) $\mathbf{P}_{w'(v)} = -\text{yref}\,\mathbf{P}_v$ (the two point halos are z-reflections of each other) if and only if $w\mathbf{P} = -\mathbf{P}$. That is, w should be a reflection in a plane perpendicular to $\mathbf{P}$, perhaps followed by a rotation about $\mathbf{P}$. Equivalently, w should be an inversion, perhaps followed by a rotation about $\mathbf{P}$. So if the two wedges happen to be inversions of each other, then the two halos are z-reflections of each other.

For the proof of (iv), Eq. (81) gives $-\text{yref}\,\mathbf{P}_v = \mathbf{P}_{w'(v)} \Leftrightarrow -\text{yref}\,\mathbf{P}_v = \text{yref}\,w_v^{-1}\mathbf{P}_v \Leftrightarrow w_v\mathbf{P}_v = -\mathbf{P}_v \Leftrightarrow w\mathbf{P} = -\mathbf{P}$. Parts (i), (ii), and (iii) are similar.

Halo Symmetries from Crystal Symmetries

A crystal symmetry is an orthogonal transformation that permutes the face normals of a crystal, and a pole symmetry is an orthogonal transformation that permutes poles. According to the Wedge Change Corollary, a crystal symmetry w satisfying $w\mathbf{P} = \pm\mathbf{P}$ induces a pole symmetry, one of the transformations e, $-e$, yref, or $-$yref. These four pole symmetries in turn give rise to halo symmetries—the identity,

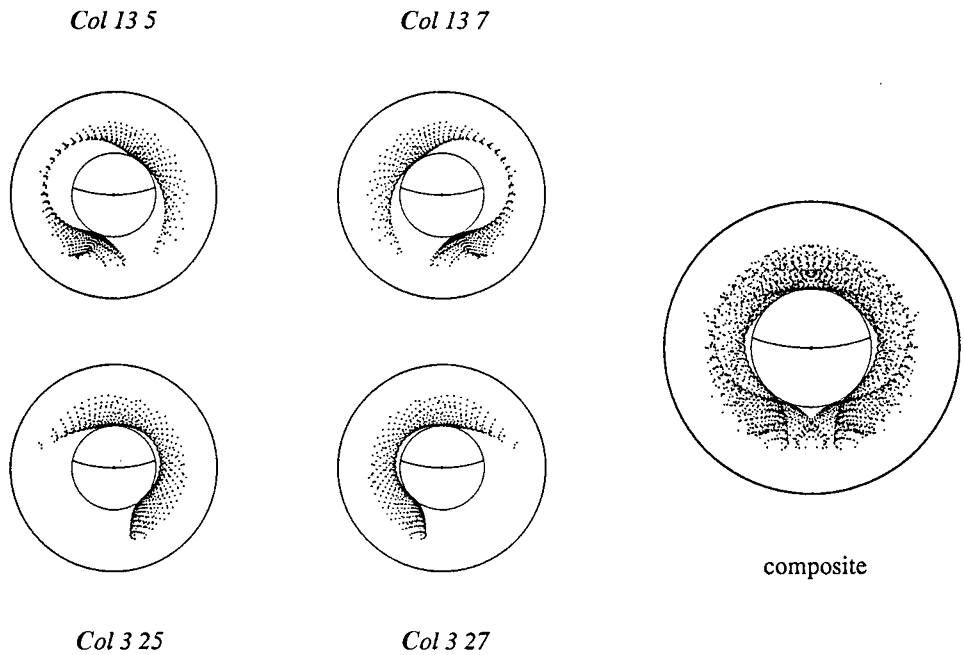

Fig. 30. The 24° arcs Col 13 5, Col 13 7, Col 3 25, and Col 3 27, shown individually and then as a composite. The composite is *mmm* symmetric. At this sun elevation it has a total of eight contact points with the 24° circular halo, one pair of contact points coming from each of the four component halos. Also see Fig. 57 and recall that the pole for Col $i\,j$ is the same as that for Plate $i\,j$. ($\Sigma = 40$)

x-rotation, y-reflection, or z-reflection, respectively, as indicated in Fig. 23.

For the crystal shapes of Figs. 26 and 28 and for the plate spin vector $\mathbf{P} = \mathbf{N}_1$, the induced pole symmetries are all of e, $-e$, yref, and $-$yref, since each of the four relevant conditions of the Wedge Change Corollary is satisfied for some crystal symmetry w. Actually it is enough to verify any two of the last three conditions. But the crystal has mirror planes parallel to $\mathbf{P}$, so the condition of part (iii)—det $w = -1$ and $w\mathbf{P} = \mathbf{P}$—is satisfied. And the crystal has a mirror plane perpendicular to $\mathbf{P}$, so the condition of part (iv) is also satisfied. The same conclusions hold for the Parry and alternate Parry spin vectors $\mathbf{N}_3$ and $\mathbf{N}_1 \times \mathbf{N}_3$.

What happens if we consider other crystal shapes or other spin vectors? Often the induced pole symmetries will be all of e, $-e$, yref, and $-$yref, as above, but it need not always be so. If in Fig. 28 the top tier of pyramid faces were missing—a common feature—then for the plate spin vector $\mathbf{P} = \mathbf{N}_1$ the induced pole symmetries would be just e and yref. Of the halo symmetries x-rotation, y-reflection, and z-reflection, the point halo display from this crystal would be symmetric only under y-reflection. This low symmetry apparently appears in the halo display photographed by Sturm and reproduced in Ref. 11.

For a more exotic example, consider the orthorhombic disphenoidal crystal whose four face normals are a unit vector $\mathbf{N}$ in the direction of, say, $2\mathbf{i} + 3\mathbf{j} + 4\mathbf{k}$, together with xrot $\mathbf{N}$, yrot $\mathbf{N}$, and zrot $\mathbf{N}$. The only crystal symmetries are the identity and the three 180° rotations about the crystal axes, the crystal axes being the xyz-coordinate axes when the crystal is oriented as given. If the crystal were to spin about the z-axis, then the induced pole symmetries would be e and $-e$. The resulting point halo display would be symmetric only under x-rotation. There would not even be left–right symmetry.

In the preceding two examples we spoke as if the pole symmetries e, $-e$, yref, and $-$yref could only arise as symmetries induced from crystal symmetries. In those examples this turns out to be true, but one needs to look at the pole diagram for each wedge angle to be sure. Consider, for example, a triangular prism whose cross section is a scalene triangle and whose spin vector is in the direction of the prism axis. The only crystal symmetries are the identity and a reflection in a plane perpendicular to the prism axis, and so the induced pole symmetries are only e and $-$yref. But the poles for $\alpha = 90$ are $(\pm 1/\sqrt{2},\ 0,\ \pm 1/\sqrt{2})$, the same as the plate poles in Fig. 59, and the poles for the other three wedge angles are $(0, \pm 1, 0)$, the same as the plate poles in Fig. 55. All four transformations e, $-e$, yref, and $-$yref are therefore symmetries of the pole diagrams. The point halo display from this crystal would give no clue as to the low symmetry of the crystal. From a halo display, one can sometimes infer the absence of crystal symmetry, but not its presence, at least not without additional assumptions.

mmm Symmetry of the Pole Diagrams

The group *mmm* consists of the eight orthogonal transformations e, $-e$, xref, yref, zref, xrot, yrot, zrot.

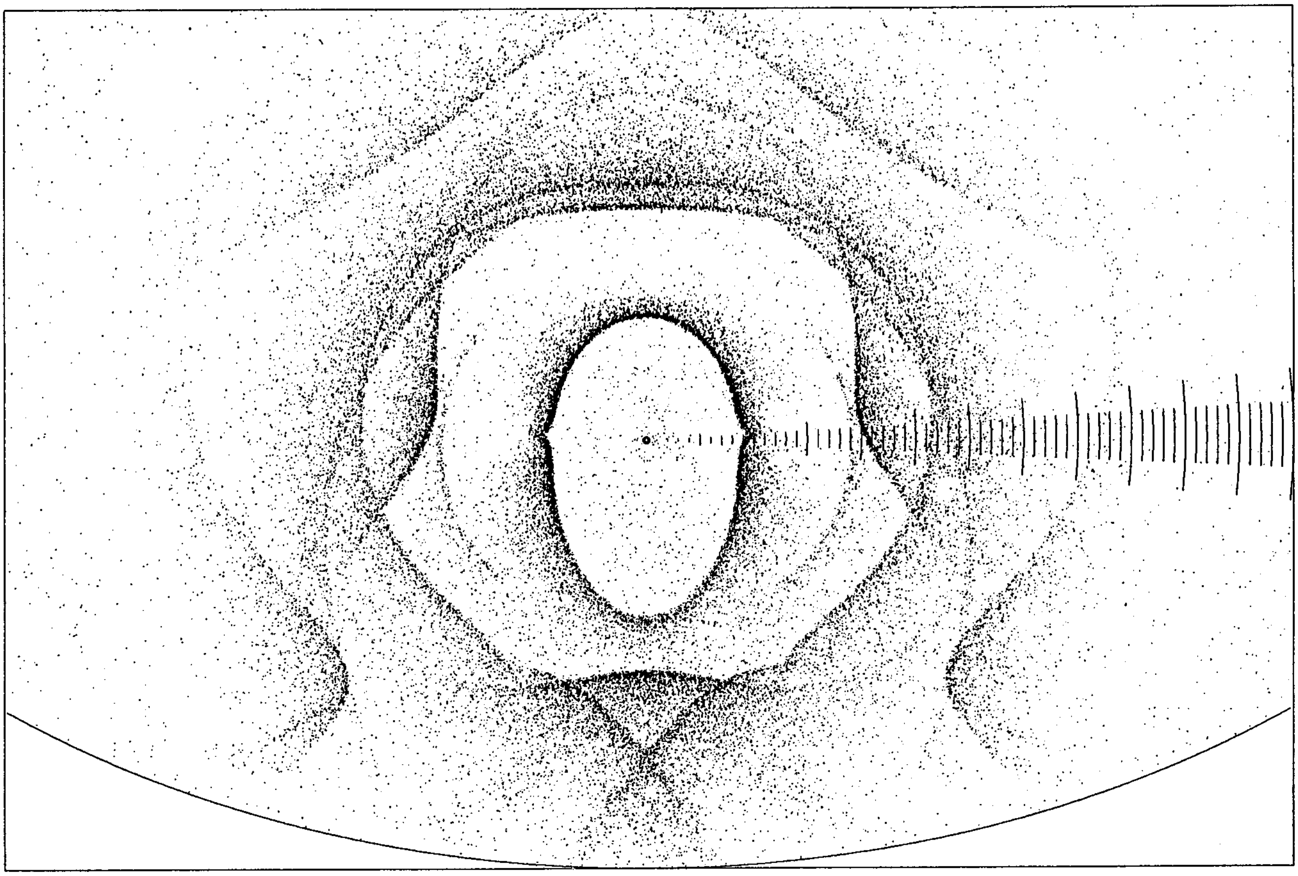

Fig. 31. Monte Carlo simulation made using pyramidal crystals having column orientations. The crystals have pyramidal faces and prism faces, but not basal faces; all the faces in Fig. 28 are present except faces 1 and 2. With study, the halos of Fig. 30 can be discerned among the many halos here. The tick marks are at 1° intervals. (Σ = 40, the same as for Fig. 30)

For any crystal shape and spin vector, the induced pole symmetries, together with zrot (Face Interchange Rule), generate a subgroup of *mmm* consisting of pole symmetries. For the crystals of Figs. 26 and 28 and for the Parry, alternate Parry, and plate spin vectors, the subgroup is all of *mmm*. For the hemimorphic crystal considered above, the subgroup would consist of e, xref, yref, and zrot, and for the disphenoid the subgroup would consist of e, $-e$, zrot, and zref.

The "*mmm* symmetry" of each of the pole diagrams of Appendix B is obvious; if any one of the eight transformations in the group *mmm* is applied to any of the plate (Parry, alternate Parry) poles of the diagram, the result is also a plate (Parry, alternate Parry) pole of the diagram. The pole diagrams for the hemimorphic crystal and the disphenoidal crystal would of course exhibit lower symmetry.

Two halos whose poles differ by one of the transformations e, $-e$, yref, or $-$yref bear a simple relation to each other according to Rules 1–4 (Fig. 23). Two halos whose poles differ by zrot are inextricably associated with each other, by the Face Interchange Rule, but we know of no simple relation between their shapes. The group of pole symmetries generated by zrot and the induced pole symmetries therefore splits into two halves, with the halo shapes in each half closely related to each other by Rules 1–4, but with no clear relation between shapes of halos from different halves.

Halo Displays are Usually Composites

The halos shown in the halo atlas are halos in their most rudimentary form. Few of them occur in isolation, and almost every simulation in the atlas must ordinarily be combined with other simulations in order to simulate a real halo display. Real halo displays are composites of the atlas halos.

One natural composite is that dictated by *mmm* symmetry. Consider, for example, the 24° arc Col 13 5, whose pole is shown in Fig. 57 (but labeled Plate 13 5). The halo itself is shown at the upper left in Fig. 30 for Σ = 40. One would not expect to see this halo in isolation but rather as part of a composite consisting of the four 24° arcs Col 13 5, Col 13 7, Col 3 25, and Col 3 27—the four great circle halos resulting from Col 13 5 by *mmm* symmetry of the pole diagram. The four poles are shown in Fig. 57, and the composite halo is shown at the right in Fig. 30. The composite bears little resemblance to any one of its components; it is left–right symmetric and has eight contact points with the 24° circular halo. In fact, it could easily be mistaken for the circular halo, unless it were superbly developed.

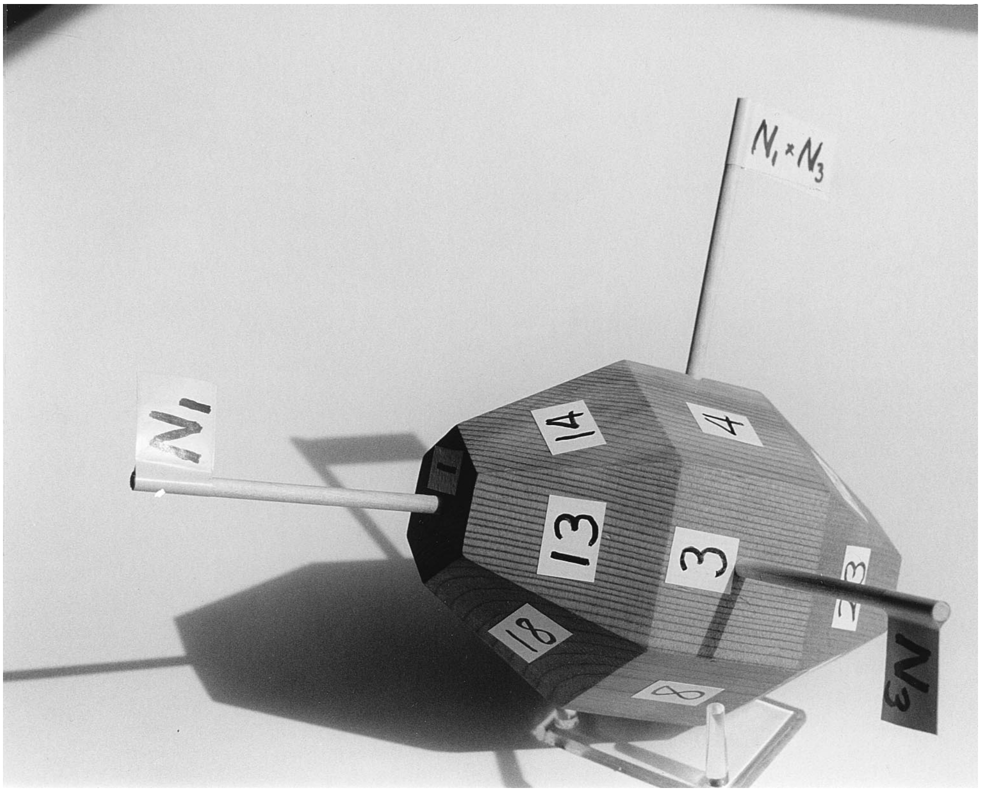

Fig. 32. Wooden model of the pyramidal crystal in Fig. 28. If the model is at the origin of coordinates, then the x-axis is pointing toward and below the camera. The wedge 13 5 is in standard orientation. The dowel with flag $\mathbf{N}_1$ therefore points in the direction of Plate 13 5, and the dowel with flag $\mathbf{N}_3$ points in the direction of Par 13 5. Compare with Fig. 57. The model was made by Jack Corbin.

If the reasoning of the preceding paragraph is applied instead to the 35° arc Col 13 15, one is led to a composite of only two halos, not four, because of the location of the pole of Col 13 15 in a coordinate plane. The composite has four contact points, not eight (for $-77 < \Sigma < 77$, from Fig. 58). The same reasoning applied to the 20° arc Col 13 16 finds a "composite" consisting only of the original arc itself, because of the special location of the pole on two coordinate planes. The composite therefore has two contact points (for $-80 < \Sigma < 80$, from Fig. 54).

Figure 31 is a traditional Monte Carlo simulation as described in Ref. 11, pp. 132–133. Compared with the other simulations in this paper it is highly realistic. This is not to say that anyone has ever seen a real display that looks like the simulation. But the intensities are presumably correct, given the assumptions regarding crystal shapes and orientations. The simulation is included to make two points. First, even the composite simulation of Fig. 30 would be only one ingredient in a real display. Second, the intensities of the halo atlas simulations are often quite far off the mark, as can be seen by comparing Figs. 30 and 31. Probably the least realistic aspect of the simulation in Fig. 31 is that the crystal orientations are assumed to be perfect, with no allowed departures of the crystal axis from its assumed horizontal position—this is done so that the halos are more easily distinguished from each other. The simulation is also simplified by the absence of basal faces on the crystals—otherwise 23° arcs further complicate the picture.

Figure 51, with $\alpha = 60$ and $\Sigma = 20$, is like Fig. 43 except that each halo diagram is now a composite analogous to the right-hand diagram in Fig. 30. Used in conjunction with the pole diagrams of Figs. 53–57, which all have α close to 60, the figure gives some indication of the composite 18, 20, 22, 23, and 24° arcs from column orientations for $\Sigma = 20$.

Figure 50 is similar to Fig. 51 but is for point halos instead of great circle halos. Each halo diagram is a composite of the eight (not necessarily distinct) halos dictated by *mmm* symmetry. Used in conjunction with Figs. 53–57, the figure gives an indication of the composite 18, 20, 22, 23, and 24° arcs from plate or Parry orientations for $\Sigma = 20$.

Many crystal shapes and orientations will lead to pole diagrams having *mmm* symmetry, since it is enough, for example, that the crystal be symmetric under inversion and have a mirror plane containing the spin vector. And for great circle halos, either of the above two conditions is enough to give *mmm* symmetry.

P. Structure of the Pole Diagrams

To understand the structure of the pole diagrams of Appendix B we recommend constructing a wooden crystal shaped as in Fig. 28 and with nails or dowels appropriately placed to represent the crystal frame vectors (Fig. 32). Then to reconstruct Fig. 59, for example, which is the pole diagram for $\alpha = 90$, first orient the crystal so that the wedge 3 1 is in standard orientation (Fig. 27); the crystal frame vectors $\mathbf{N}_3$, $\mathbf{N}_1 \times \mathbf{N}_3$, $\mathbf{N}_1$, which are the spin vectors for the Parry, alternate Parry, and plate orientation classes, respectively, then coincide with the vectors Par 3 1, AP 3 1, Plate 3 1, which can be recorded in the diagram. Next rotate the crystal so that wedge 4 1 is in standard orientation; the crystal frame vectors now coincide with Par 4 1, AP 4 1, Plate 4 1. Continue in this fashion for all 24 of the $\alpha = 90$ wedges, and the pole diagram is complete.

Induced Pole Symmetries

To understand the pole diagrams in detail, we need to generalize and to make precise the notion of a pole symmetry induced by a crystal symmetry w and spin vector $\mathbf{P}$. As before, we regard the crystal as fixed at some moment, so that w and $\mathbf{P}$ are constants. Suppose a set V consists of wedge frames $v_1, v_2, \ldots, v_k$ for certain wedges on the crystal, and suppose that w' [Eqs. (14) and (15)] maps V to itself. If an orthogonal transformation w^* satisfies

$$w^*\mathbf{P}_v = \mathbf{P}_{w'(v)} \quad \text{for all } v \in V, \tag{82}$$

then w^* is an *induced pole symmetry*[20] for V. The transformation w^* is indeed a pole symmetry, of the poles $\mathbf{P}_{v_1}, \ldots, \mathbf{P}_{v_k}$. It expresses the effect, on poles, of the crystal symmetry w.

Here we do not distinguish carefully between a wedge and its wedge frame. We therefore regard V either as a set of wedge frames or as the set of wedges themselves.

We have already seen one way that induced pole symmetries can arise: according to the Wedge Change Corollary, Subsection 3.O, a crystal symmetry w satisfying $w\mathbf{P} = \pm\mathbf{P}$ induces a pole symmetry, one of the transformations e, $-e$, yref, or $-$yref. These transformations are special in that they are induced pole symmetries for the set of all wedges of the crystal. They are subtle, however, in that the action of w^* can be quite different from that of w.

Induced pole symmetries can arise in a more straightforward way as follows. If the matrices w_v and w_u of w with respect to wedge frames v and u are the same, then we say that the frames are *equivalent* with respect to w. The collection of all wedge frames is naturally partitioned into equivalence classes of equivalent frames, and, if $\det w = 1$, then w' maps each equivalence class to itself. Then for each equivalence class V there is an induced pole symmetry w^* for V. This is clear by using the Wedge Change Rule to rewrite Eq. (82) as

$$w^*\mathbf{P}v = \begin{cases} w_v^{-1}\mathbf{P}_v & \text{if } \det w = 1, \quad (83) \\ \text{yref}\, w_v^{-1}\mathbf{P}_v & \text{if } \operatorname{def} w = 1, \quad (84) \end{cases}$$

since w^* can be taken to be the common value of w_v^{-1} for $v \in V$. So here the action of w^* is essentially the same as that of w, but reversed.

Consider, for example, the crystal of Fig. 26 or Fig. 28 and the 60° rotational symmetry $w = r$ whose axis is $\mathbf{R} = \mathbf{N}_1$ and which takes wedge 3 1 to wedge 4 1. The six wedges 3 1, 4 1, . . . , 8 1 make up one equivalence class. This can be verified algebraically, but the wooden crystal model (Fig. 32) gives more geometric insight. If any one of the six wedges is selected and put in standard orientation, and if the rotation r then acts on the crystal, the action of r looks the same, regardless of which wedge was selected—this is w_v. In fact, in each case the action is a 60° rotation about the axis $\mathbf{R}_{3\,1}$, the vector $\mathbf{R}$ as seen from wedge 3 1 (i.e., the coordinate vector of $\mathbf{R}$ with respect to wedge 3 1). According to Eq. (83), the 60° rotation about the same axis but in the opposite sense is an induced pole symmetry r^* for the set of wedges 3 1, 4 1, . . . , 8 1. The rotation permutes the poles $\mathbf{P}_{3\,1}$, $\mathbf{P}_{4\,1}, \ldots, \mathbf{P}_{8\,1}$, but the rotation itself is independent of $\mathbf{P}$. It therefore gives information about the structure of pole diagrams for all $\mathbf{P}$.

For the crystal symmetry r there are, in all, four equivalence classes of wedges for $\alpha = 90$, with each of the wedges 3 1, 3 2, 1 3, and 2 3 determining a separate equivalence class containing six wedges, and with an induced pole symmetry r^* for each equivalence class. The four induced pole symmetries are 60° rotations about $\mathbf{R}_{3\,1}$ = Plate 3 1, $\mathbf{R}_{3\,2}$ = Plate 3 2, $\mathbf{R}_{1\,3}$ = Plate 1 3, and $\mathbf{R}_{2\,3}$ = Plate 2 3 (Fig. 59), with the sense of rotation opposite to that of r.

Finally, if w is a crystal symmetry such that $w^2 = e$, and if v is any wedge frame of the crystal, then there are at least two induced pole symmetries of $V = \{v, w'(v)\}$. For in this case w' maps V to itself. And the orthogonal transformation w^* need only interchange the points $\mathbf{P}_v$ and $\mathbf{P}_{w'(v)}$. Still, we recommend trying some examples.

Reconstructing the Pole Diagrams

Although the pole diagrams of Appendix B may at first appear chaotic, they have a simple structure. In each, we can find two antipodal plate poles that are the centers of a great circle on which six Parry poles are equally distributed, and from this configuration we can construct the entire diagram using only *mmm* symmetry. In Fig. 52, for example, which is the pole diagram for the 9° arcs, the antipodal plate poles 13 6 and 23 6 are the centers of the great circle containing the six Parry poles 13 6, 14 7, . . . , 18 5. Then *mmm* symmetry gives another pair of antipodal plate poles and another great circle containing six Parry poles.

A feature of the 9° arcs is that the pole Plate 13 6 lies on exactly one of the coordinate planes $x = 0$, $y = 0$, $z = 0$; by *mmm* symmetry it therefore gave rise to two pairs of antipodal plate poles and two great circles containing the Parry poles. But for the 24° arcs a single plate pole, which is now on none of the coordinate planes, gives rise to four—not two—pairs of antipodal plate poles and four great circles (Fig. 57). And for the 22° arcs, a single plate pole, which is on two coordinate planes, gives rise to only one pair of plate poles and one great circle (Fig. 55). The 18, 23, 35, and 46° arcs are similar to the 9° arcs—a plate pole is on one coordinate plane—and the 20° arcs are similar to the 22° arcs—a plate pole is on two coordinate planes.

To see why all this should be so, and especially to see which wedges go with which poles, we first construct a pole diagram for the crystal of Fig. 28 but for an arbitrary spin vector $\mathbf{P}$, starting with a single pair of poles $\mathbf{P}_{ij}$ and Plate ij. The pole diagram will contain poles of $\mathbf{P}$ with respect to all wedges having the same wedge angle as wedge ij. We make use of three crystal symmetries: the 60° rotation r about $\mathbf{R} = \mathbf{N}_1$ described above, the reflection m in the plane perpendicular to $\mathbf{N}_1$, and the 180° rotation ρ about $\mathbf{N}_3$. Given any pair of congruent wedges on the crystal, we can take the one wedge to the other by applying r an appropriate number of times, then perhaps applying m, and then perhaps applying ρ (for the moment not distinguishing the face interchange of a wedge from itself). The desired pole diagram can therefore be constructed from the given pole $\mathbf{P}_{ij}$ by applying the induced pole symmetries r^*, m^*, ρ^*, followed by zrot to account for face interchanges. After applying r^* successively, we have a diagram with six poles equally distributed on a circle with center $\mathbf{R}_{ij}$ = Plate ij and with radius equal to the angle β between $\mathbf{P}$ and $\mathbf{R} = \mathbf{N}_1$. Applying m^*, ρ^*, and zrot then gives a final diagram with 48 (not necessarily distinct) poles.

For an arbitrary $\mathbf{P}$, the induced pole symmetries m^* and ρ^* may not be simple, but if $\mathbf{P} = \mathbf{N}_1$ (the plate spin vector), then $m^* = -$yref and $\rho^* = -e$ by the Wedge Change Corollary, and so m^*, ρ^*, and zrot generate mmm, nothing more. And $\beta = 0$, with the above circle of radius β collapsing to the point Plate ij. The resulting pole diagram for plate orientations therefore consists of just the eight (not necessarily distinct) points resulting from Plate ij by mmm symmetry.

If $\mathbf{P} = \mathbf{N}_3$ (the Parry spin vector), then $m^* =$ yref and $\rho^* = e$. And $\beta = 90$, so the circle is now a great circle centered at Plate ij and containing six equally distributed Parry poles. Applying m^*, ρ^*, and zrot gives a diagram of four great circles, each containing six equally distributed Parry poles, for a total of 24. The mmm symmetry may not be obvious from this construction, but it is there; one way to see it is to note that the original six equally distributed Parry poles are symmetric under $-e$.

The above bounds of 48, 8, and 24 on the number of poles can be lowered in case $\alpha \neq 63.8$, for then not all of r^*, m^*, ρ^*, and zrot are needed to construct the pole diagram. Given any two wedges with $\alpha = 60$, for example, we can take the one wedge to the other using only r and ρ, even if face interchanges are distinguished (Fig. 26 or Fig. 28). The pole diagram for an arbitrary $\mathbf{P}$ and for the $\alpha = 60$ wedges can therefore be constructed from a pair of ($\alpha = 60$) poles $\mathbf{P}_{ij}$ and Plate ij using only r^* and ρ^*. The result is a pole diagram with 12 (not necessarily distinct) poles, rather than 48. The plate pole diagram now has two poles, rather than eight, and the Parry pole diagram has six, rather than 24. Since the plate pole diagram must be mmm symmetric, we again see that the plate poles for $\alpha = 60$ must lie on a coordinate axis. Similarly, two Parry poles must lie on a coordinate axis.

Alternate Parry poles can always be found from the plate and Parry poles, since Par ij, AP ij, and Plate ij are a (right-handed) frame. The pole diagrams for an arbitrary $\mathbf{P}$ are then easily found. Rather than struggling with m^* and ρ^*, we can use the existing pole diagrams, since if the coordinates of $\mathbf{P}$ with respect to the crystal frame vectors $\mathbf{N}_3$, $\mathbf{N}_1 \times \mathbf{N}_3$, $\mathbf{N}_1$, are x, y, z, then $\mathbf{P}_{ij} = x$ Par $ij + y$ AP $ij + z$ Plate ij. For a randomly chosen $\mathbf{P}$ and for a given wedge angle, there are apt to be as many distinct poles as there are wedges having the given wedge angle.

Section 3 is supposed to be about real and plausible halos, and in one sense it is. But in another sense, it is hardly about halos at all; the understanding of halos was developed in Sections 1 and 2. Section 3 is about the geometry of crystals, and mostly about the geometry of the pyramidal crystal in Fig. 28. Its main theme: Given a vector $\mathbf{P}$ fixed in the crystal, and given a wedge of the crystal, what does $\mathbf{P}$ look like from the wedge? That is all.

Q. Two Summaries

We—Tape and Können—view this article differently, or at least we emphasize different aspects. We decided that this was not all bad, and that readers might benefit from two different summaries.

Summary by Tape

We have presented a conceptual framework for the systematic study of refraction halos arising in preferentially oriented crystals. The framework not only permits the calculation of shapes for all such halos, it helps to explain intuitively why the halos look the way they do. Included as a small part of the system are all known refraction halos.

Perhaps another look at, say, Fig. 59 will serve as a partial summary. The sphere in Fig. 59 represents and thus conveniently organizes the set of point halos with wedge angle $\alpha = 90$, but how does it do so? It does so by representing orientations—the orthogonal matrices with determinant 1. In fact, each point $\mathbf{k}_u$ on the sphere represents all of the rotations (orientations) that take $\mathbf{k}_u$ to the zenith point $\mathbf{k}$. A halo's zenith locus, which is a subset of the sphere, is a means of specifying the set of wedge orientations that make the halo; a rotation is a wedge orientation for the halo if it takes some point in the zenith locus and makes it vertical. The pole $\mathbf{P}_u$ of the halo is in turn a means of specifying the zenith locus. For a point halo the zenith locus consists of the single point $\mathbf{k}_u = \mathbf{P}_u$. So by giving the pole $\mathbf{P}_u = B(30, -45)$ for the right Parry supralateral arc Par 8 1, for example, we are telling how to orient the ($\alpha = 90$) wedge in order to produce the halo: Starting with the wedge in standard orientation, for which the wedge vector $\mathbf{P}$

coincides with $\mathbf{P}_u$, one just tips the wedge so that $\mathbf{P}$ becomes vertical, and then one gives the wedge all possible rotations about the vertical. Sunlight passing through these variously oriented wedges makes the halo. And how do we find $\mathbf{P}_u$ for this halo in the first place? We simply orient the crystal so that the wedge with entry and exit faces 8 and 1 is in standard orientation; wherever the (Parry, in this case) spin vector $\mathbf{P}$ ends up—this is $\mathbf{P}_u$.

The scheme of this paper is based on what at first may have seemed an unnatural viewpoint: Each rotation acting on a specified wedge of a crystal is regarded as starting not with the crystal in some standard crystal orientation but rather with the crystal oriented so that the wedge is in standard orientation. Whether a given rotation is, say, a Parry orientation therefore depends on the wedge that is specified. Thus, for example, Fig. 59 shows that the Parry orientations for the wedge 8 1 are the same as the Parry orientations for 4 2 but are disjoint from the Parry orientations for 3 1. In general, the figure gives the plate orientations, the Parry orientations, etc., for each wedge with $\alpha = 90$. Figure 55 does the same for $\alpha = 60$, Fig. 52 for $\alpha = 28$, etc.

In this spotty review I have not stressed the view of halo formation as seen from the wedge frame, but it is this view that lets us see conceptually, rather than just computationally, why a given halo looks the way it does. Figure 11 is a good example. Much of the success of the wedge frame view is due to the relatively simple way that light passes through the wedge, as indicated in Fig. 3 or Fig. 9.

Summary by Können

We have found a natural halo parameter $\mathbf{P}_u$—the crystal spin vector expressed in the reference frame of the refracting wedge—that leads to a classification of all the halos that result from preferentially oriented crystals. Based on this parameter we formulate a comprehensive conceptual theory of halos. The theory is worked out under the crucial but plausible Spin Vector Assumption, which postulates the spin vector to be fixed in a halo-generating wedge and to be constrained to a constant zenith angle. The wedge is free to rotate about the spin vector, and the spin vector is free to rotate about the vertical. We find under this assumption that the variety in halo shapes is not endless. The theory creates order in halos and helps us to understand why halos look the way they do. See, for example, Figs. 11 and 20.

To organize halos, we introduce a sphere on which each point represents a value of the vector $\mathbf{P}_u$. I call the sphere the *halo sphere* and points on it *halo poles*. If wedge angle, refractive index, solar elevation, and the spin vector's zenith angle are fixed, then the position of the halo pole on the halo sphere determines uniquely the shape of the halo arising from the wedge. For two types of refraction halo, namely, spin vector vertical (point halos) and spin vector horizontal (great circle halos), we calculate halo shapes that are due to wedges consisting of ice, using a scheme that ignores intensity factors but calculates the shapes correctly. We present the results in the form of an atlas of "all possible halos". This atlas shows, for selected wedge angles and selected solar elevations, the halo shapes corresponding to representative halo poles on the sphere.

The combination of a known crystal shape and a known crystal orientation class results in a discrete set of halo poles. For hexagonal ice crystals with low-index pyramidal faces on both ends and no missing faces (Fig. 28), we calculate the halo poles for all halo-generating wedge angles (Table 3), taking into consideration six orientation classes—plate, column, Parry, Lowitz, alternate Parry, and alternate Lowitz—and we present in various diagrams the positions of these poles on the halo sphere. The actual halo display that would show up for a given orientation class is the composite of all halo shapes in the atlas represented by all halo poles of that orientation. Although the halos in the atlas usually lack symmetry with respect to the solar vertical, the actual composites from any of the six orientation classes considered here always bear this symmetry. Figures 50 and 51 show how an atlas of left–right symmetric composites might appear.

Applications of the theory extend well beyond those explicitly considered in the paper. First, the theory is capable of organizing halos from ray paths other than those involving refractions alone, and it can be applied to other crystal shapes and to other crystal orientation classes. Second, the organizing properties of $\mathbf{P}_u$ provide a basis for designing a systematic nomenclature for halos that are due to preferentially oriented crystals, based on the special features of halos arising from poles at certain positions on the halo sphere. Third, our results provide new tools for solving the inverse halo problem, namely, the problem of inferring refractive indices, shapes, and orientations of halo-making crystals from halo observations. See, for example, Subsection 2.I and the Wedge Change Corollary, Subsection 3.O.

The conceptual approach to halos presented in this paper complements the computational Monte Carlo ray tracing approach for simulating halos. Both approaches seem invaluable in reaching real understanding of halos from preferentially oriented crystals of complicated shapes, and likewise both are invaluable tools for solving inverse halo problems.

Appendix A: The Halo Atlas

A complete halo atlas would contain every halo that satisfies the Spin Vector Assumption. There would be a halo for every value of ψ, $\mathbf{P}_u$, and α, and the appearance of each halo would be illustrated for every sun elevation Σ. In this appendix halos are shown only for $\psi = 0$ and $\psi = 90$ and for selected values of $\mathbf{P}_u$, α, and Σ. The resulting atlas is obviously far from complete, but it is enough to suggest what a more complete version might look like. The layout in the halo atlas figures (Figs. 33–51) is that of Fig. 7, right.

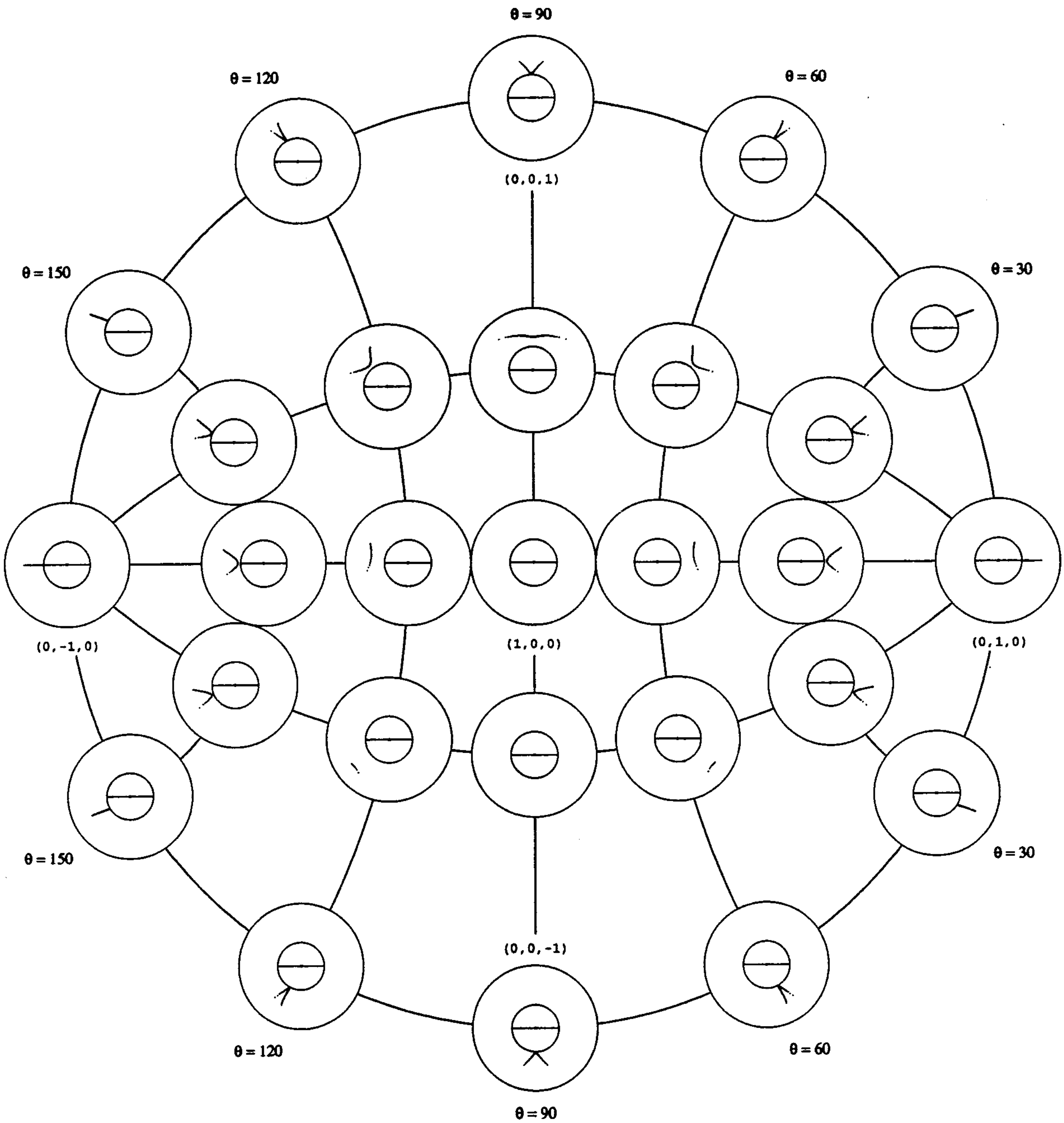

Fig. 33. Point halos ($\psi = 0$) with wedge angle $\alpha = 60$ and sun elevation $\Sigma = 0$. The corresponding circular halo is the common circular halo, with radius $\Delta_m = 22$. Halos are shown for the 27 poles $\mathbf{P}_u$ shown in Fig. 7, all of which are on the front hemisphere. In the halo diagrams the inner circle is the circular halo, and the line within it is part of the parhelic circle, which is included as a reminder of sun elevation. Some halos can be empty, depending on sun elevation.

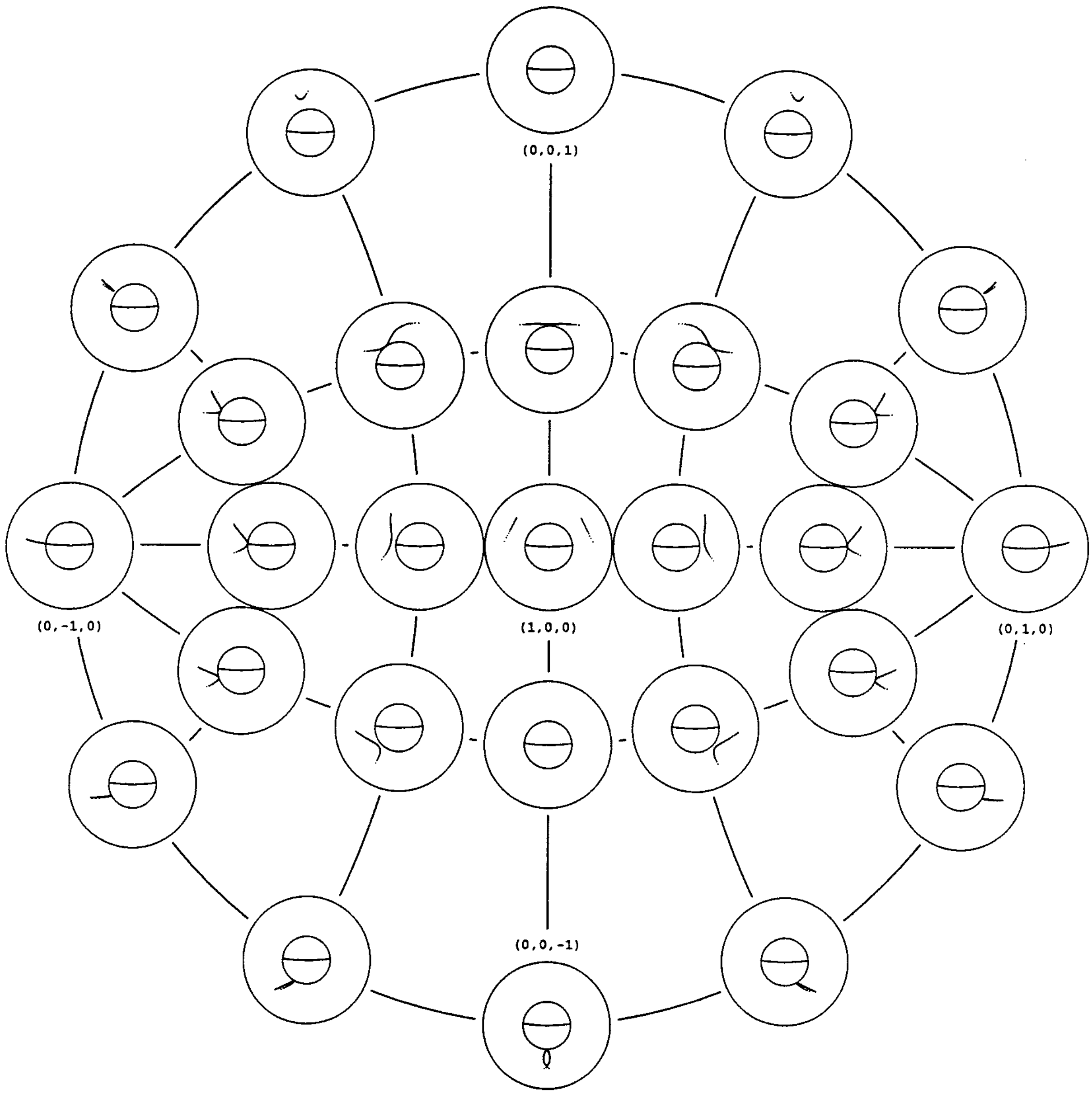

Fig. 34. Point halos with wedge angle $\alpha = 60$ ($\Delta_m = 22$) and sun elevation $\Sigma = 20$. Same as Fig. 33 except for Σ.

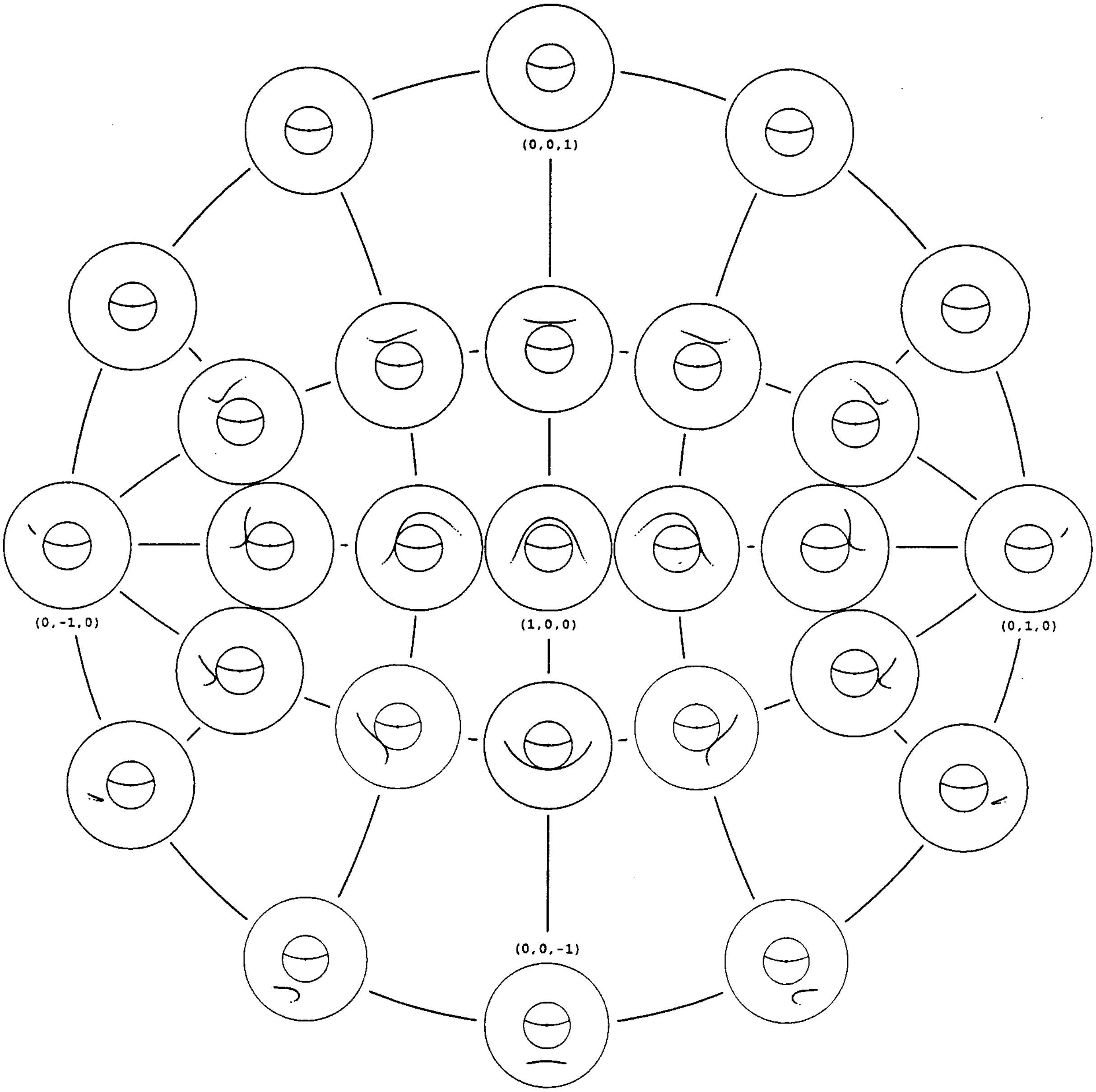

Fig. 35. Point halos with $\alpha = 60$ ($\Delta_m = 22$) and $\Sigma = 50$. Same as Figs. 33 and 34 except for Σ.

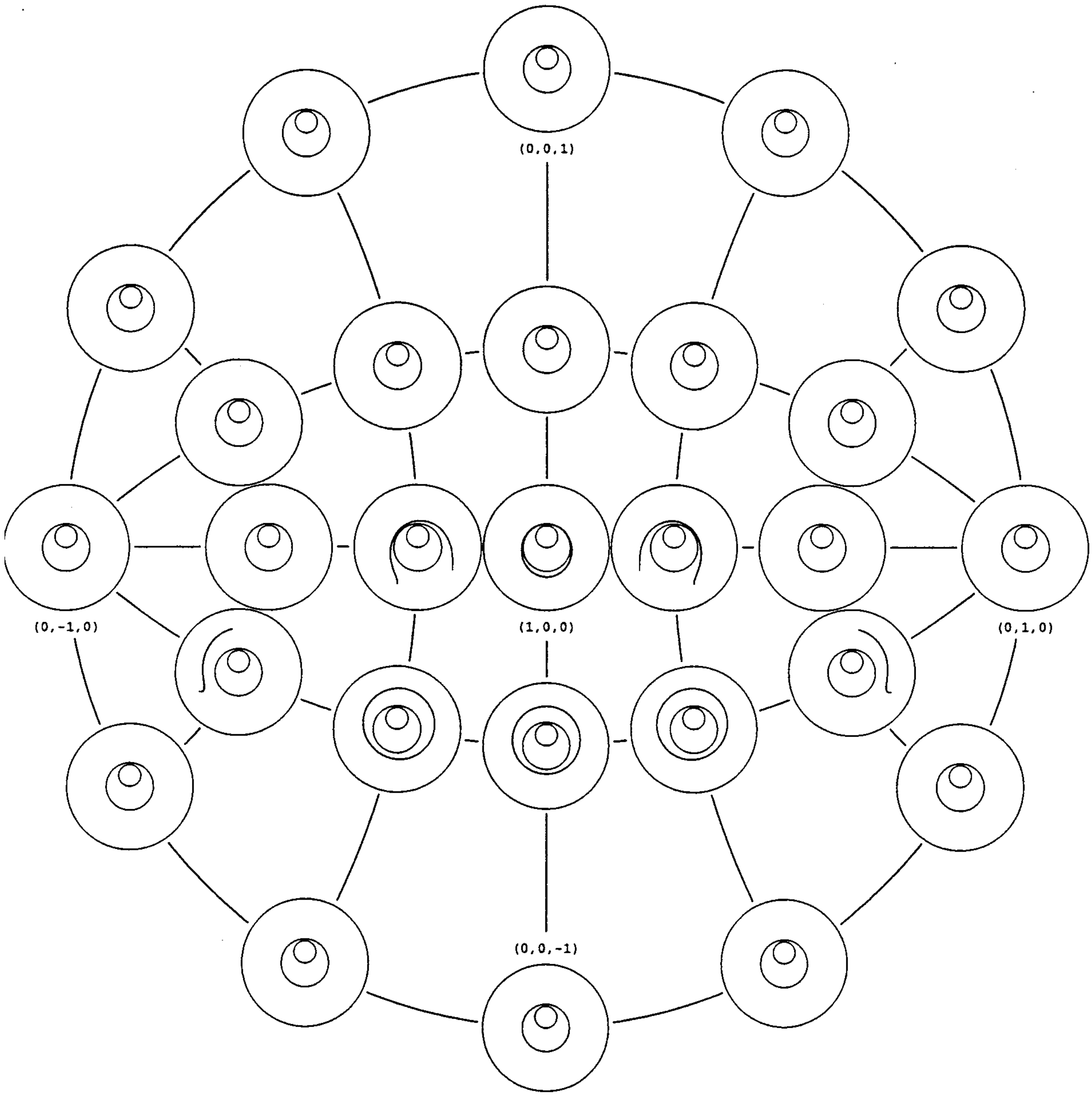

Fig. 36. Point halos with $\alpha = 60$ ($\Delta_m = 22$) and $\Sigma = 80$. Same as Figs. 33–35 except for Σ. The small circle in each halo diagram is the parhelic circle, which for the sun elevation here has a radius of only 10°.

Rear Hemisphere

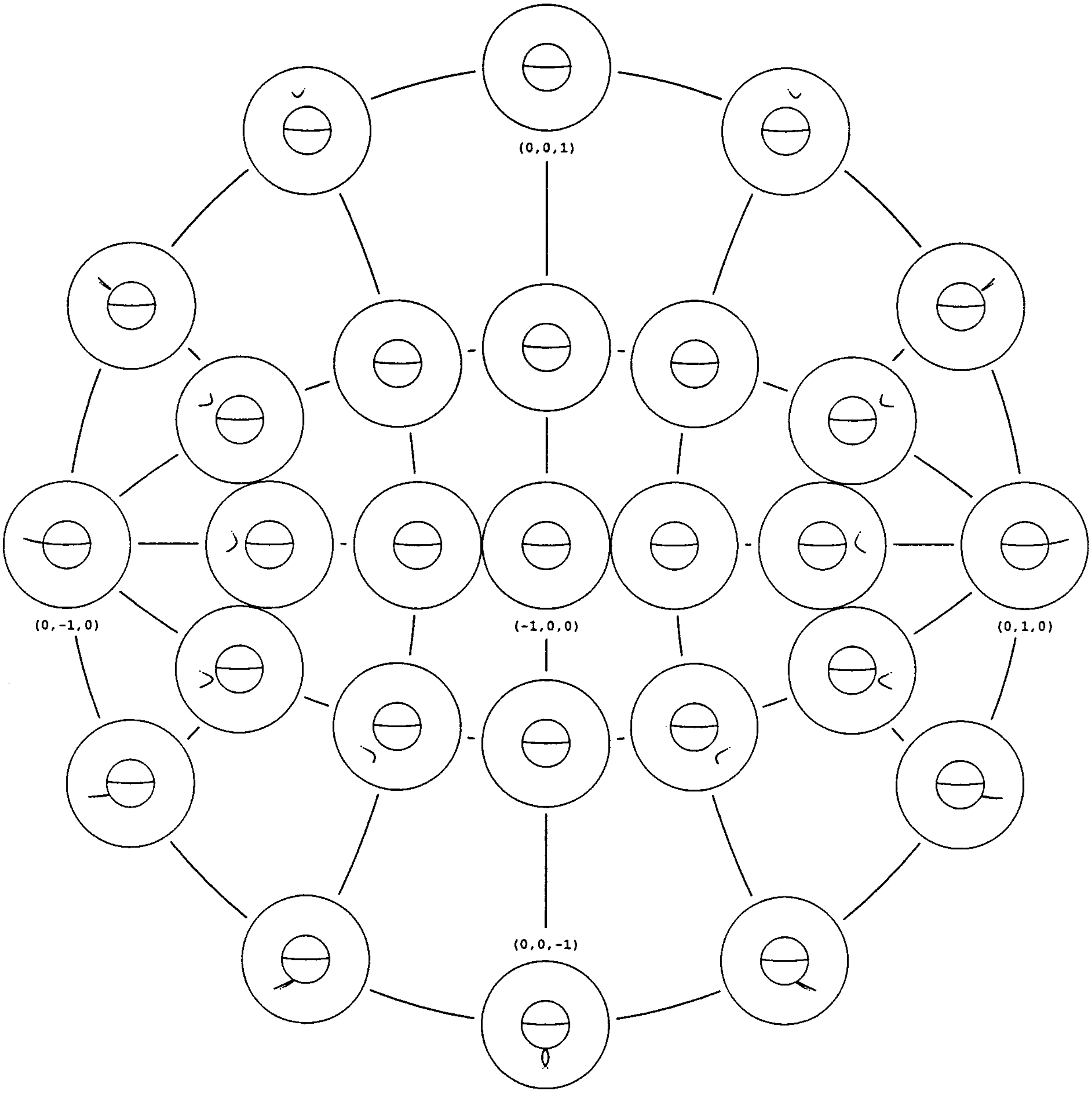

Fig. 37. Point halos with $\alpha = 60$ ($\Delta_m = 22$) and $\Sigma = 20$, and with poles $\mathbf{P}_u$ on the rear hemisphere ($x \leq 0$). Compare Fig. 34, which shows halos with poles on the front hemisphere ($x \geq 0$).

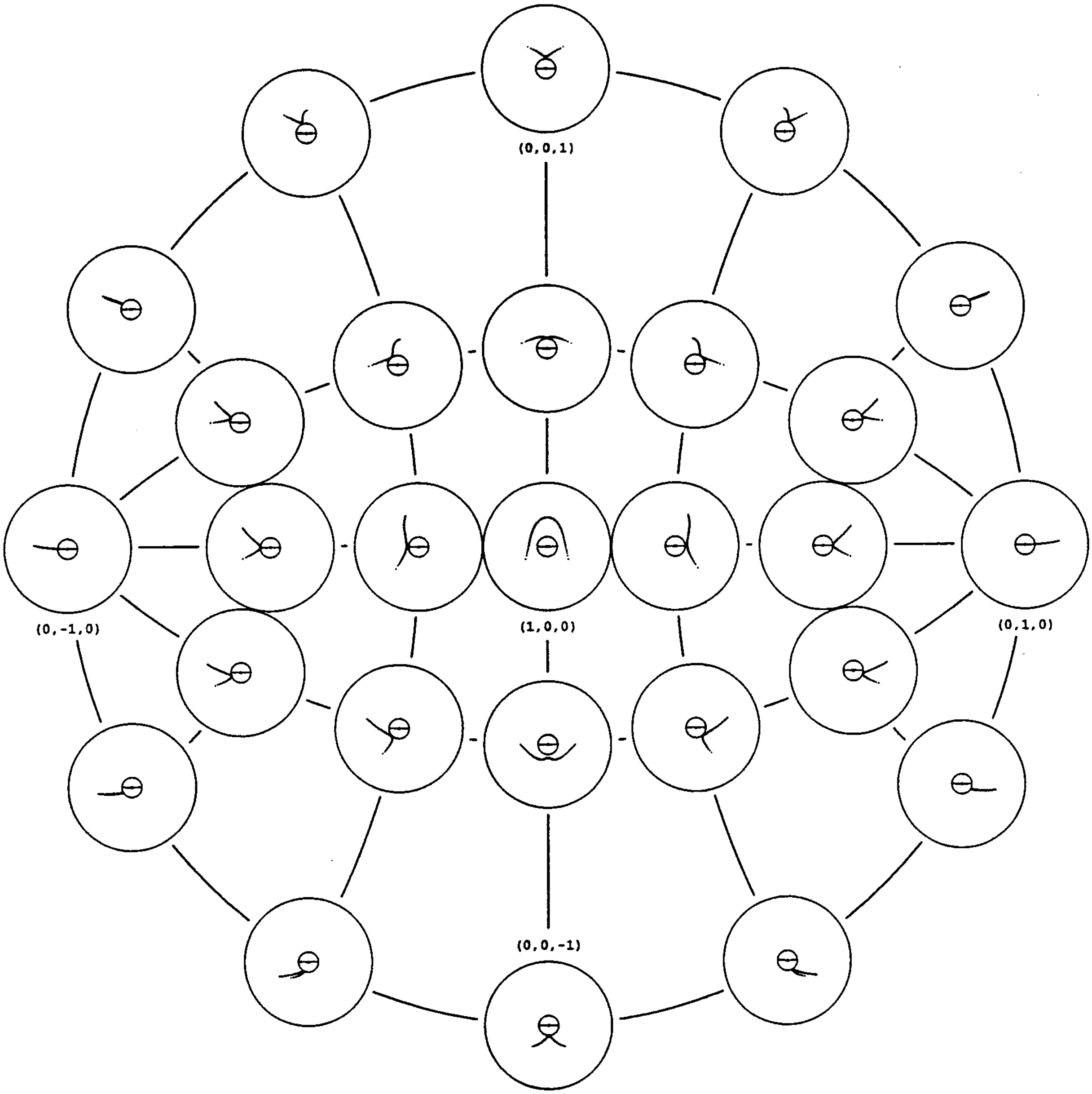

Fig. 38. Point halos with wedge angle α = 28 (Δ_m = 9) and sun elevation Σ = 20. Same as Fig. 34 except for α.

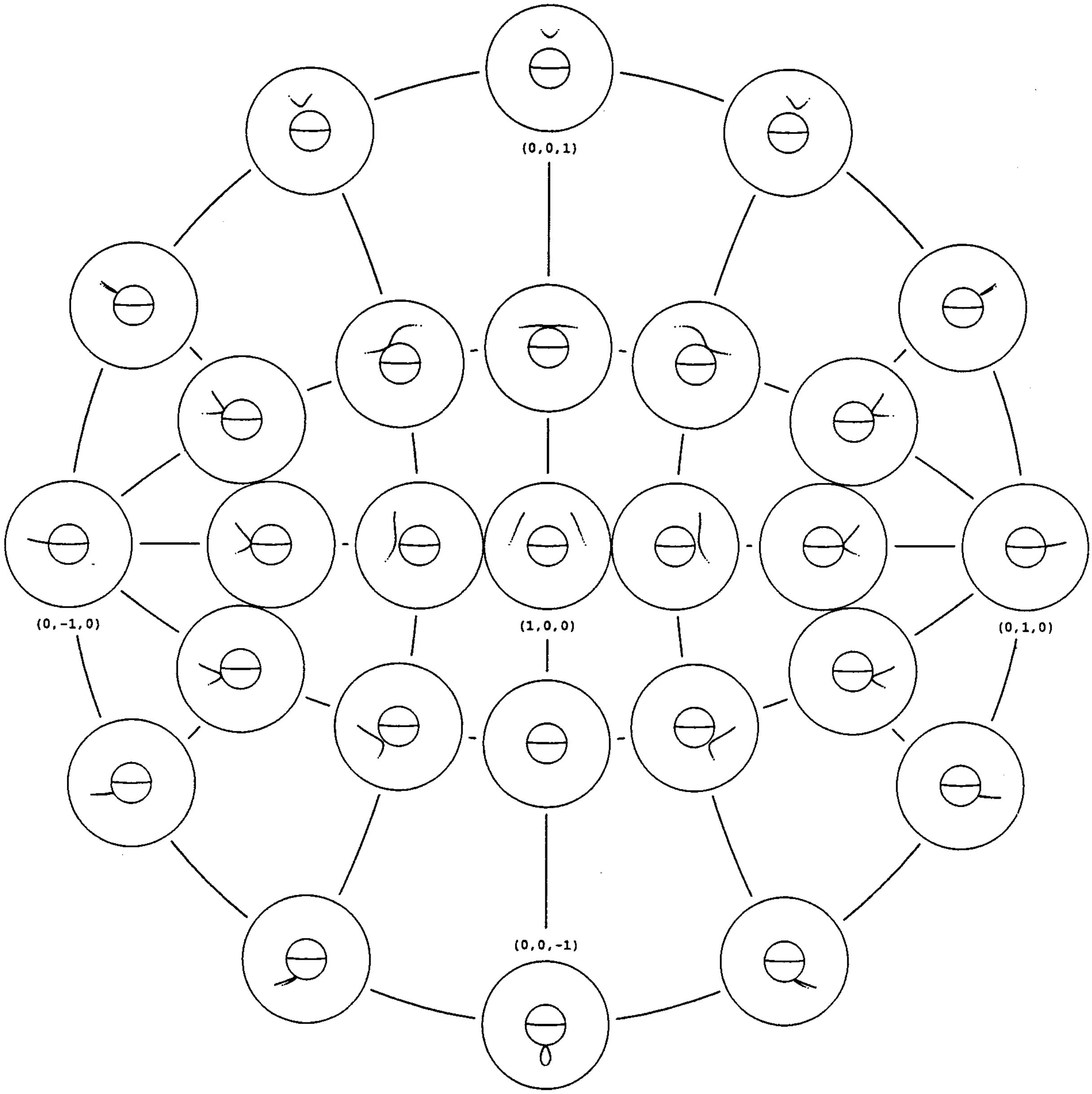

Fig. 39. Point halos with $\alpha = 52.4$ ($\Delta_m = 18$) and $\Sigma = 20$. Same as Figs. 34 and 38 except for α.

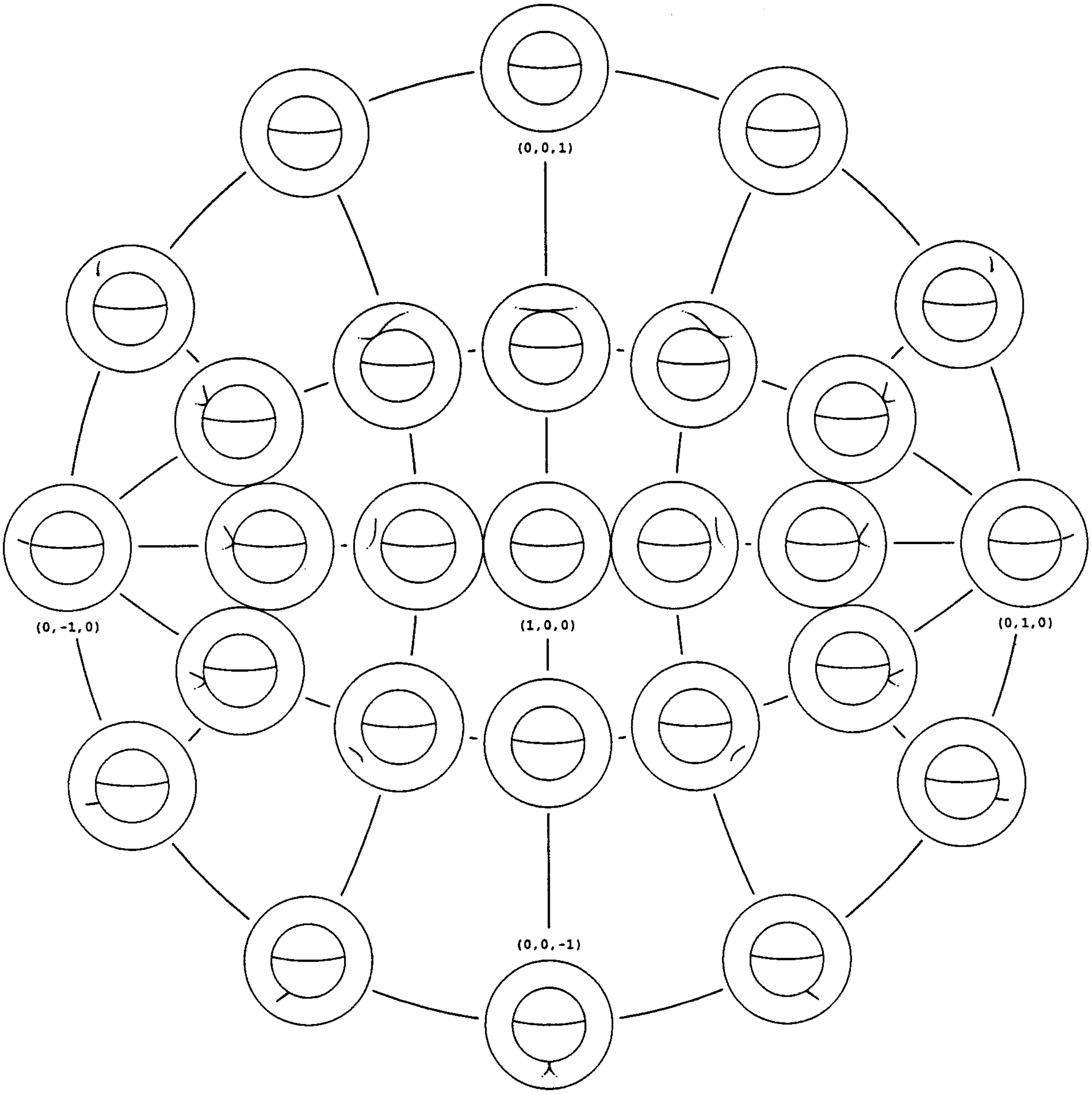

Fig. 40. Point halos with $\alpha = 80.2$ ($\Delta_m = 35$) and $\Sigma = 20$. Same as Figs. 34, 38, and 39 except for α.

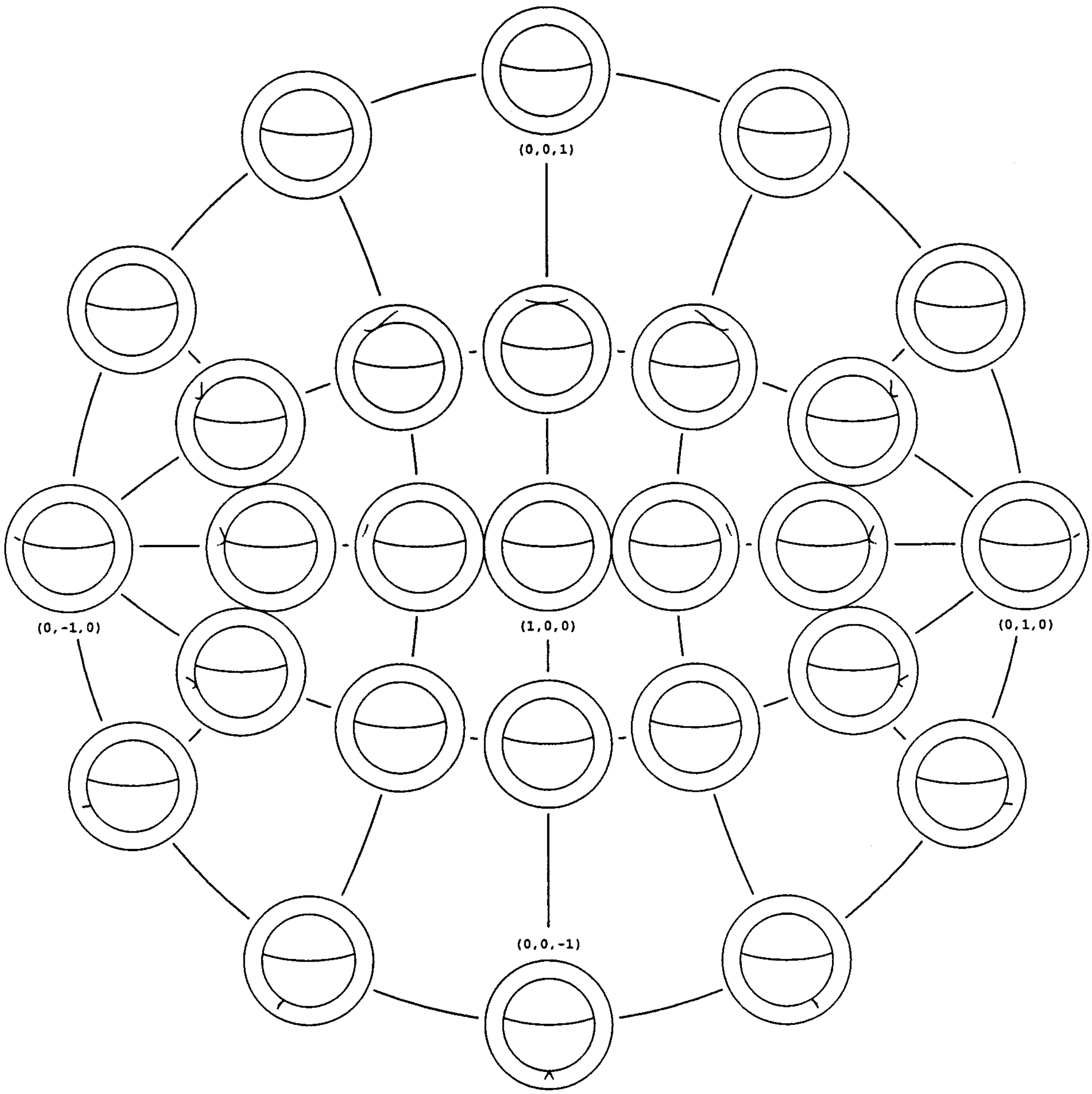

Fig. 41. Point halos with $\alpha = 90$ ($\Delta_m = 46$) and $\Sigma = 20$. Same as Figs. 34 and 38–40 except for α.

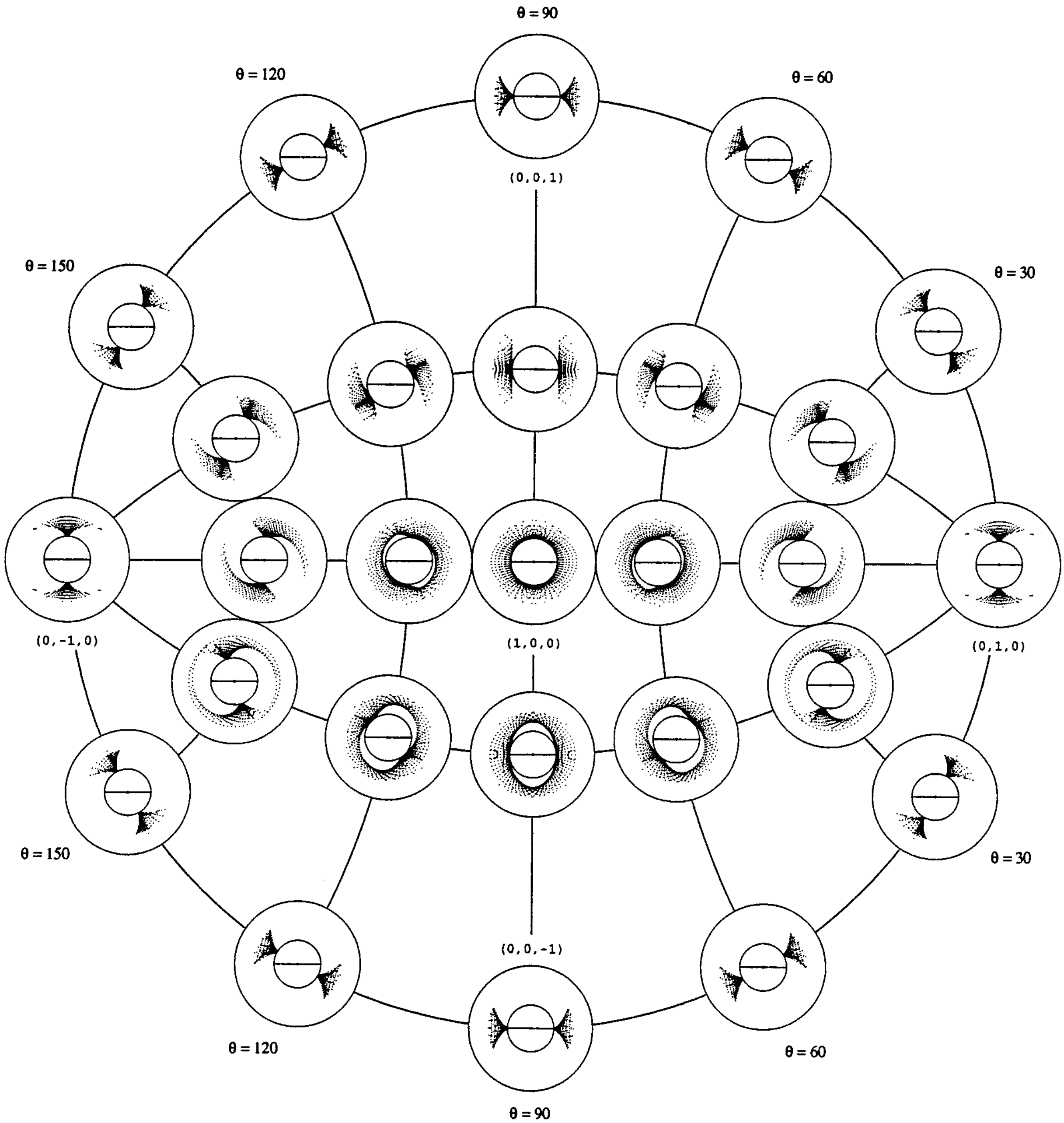

Fig. 42. Great circle halos ($\psi = 90$) with wedge angle $\alpha = 60$ (circular halo radius $\Delta_m = 22$) and sun elevation $\Sigma = 0$.

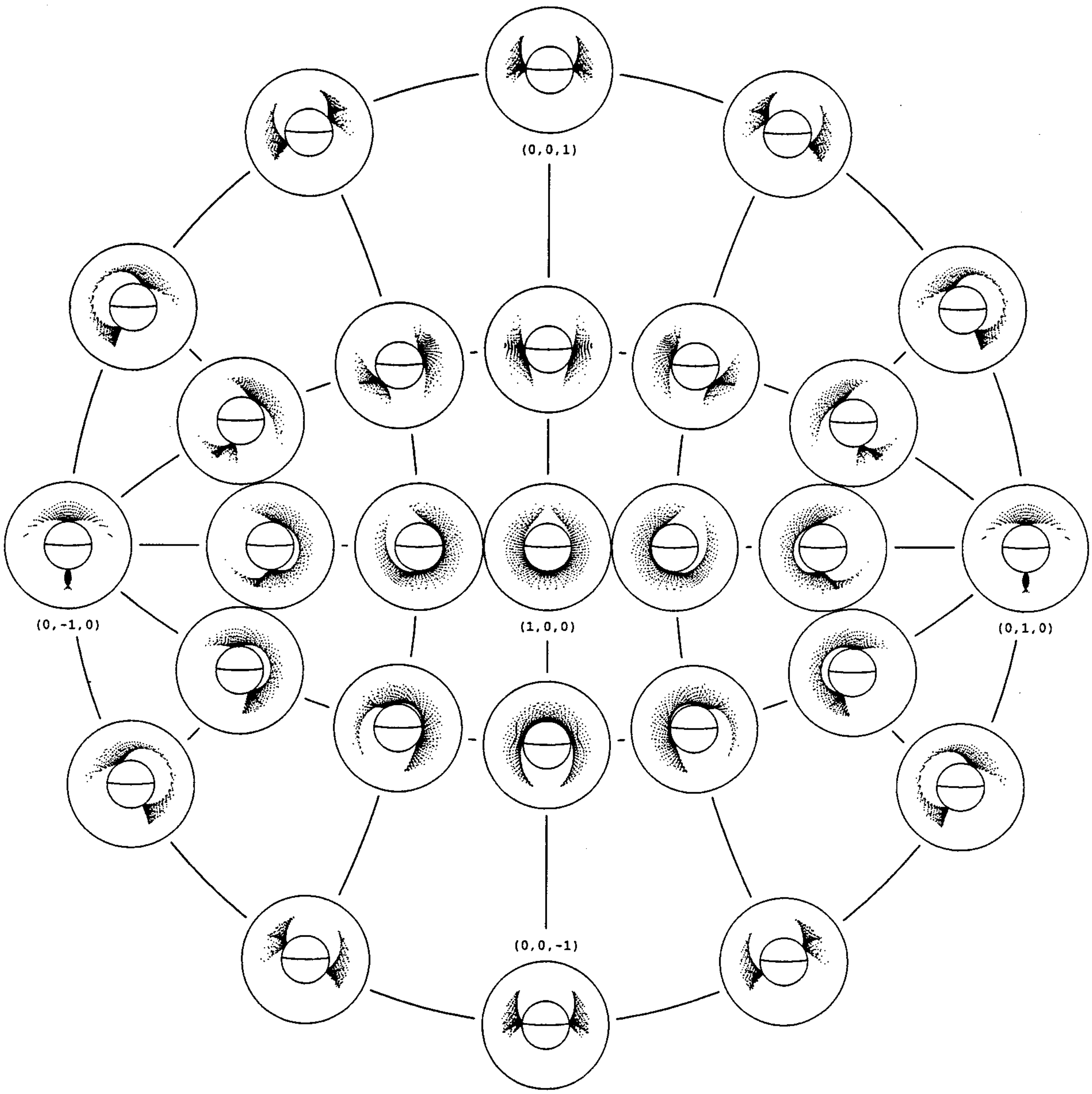

Fig. 43. Great circle halos with $\alpha = 60$ ($\Delta_m = 22$) and $\Sigma = 20$. Same as Fig. 42 except for Σ.

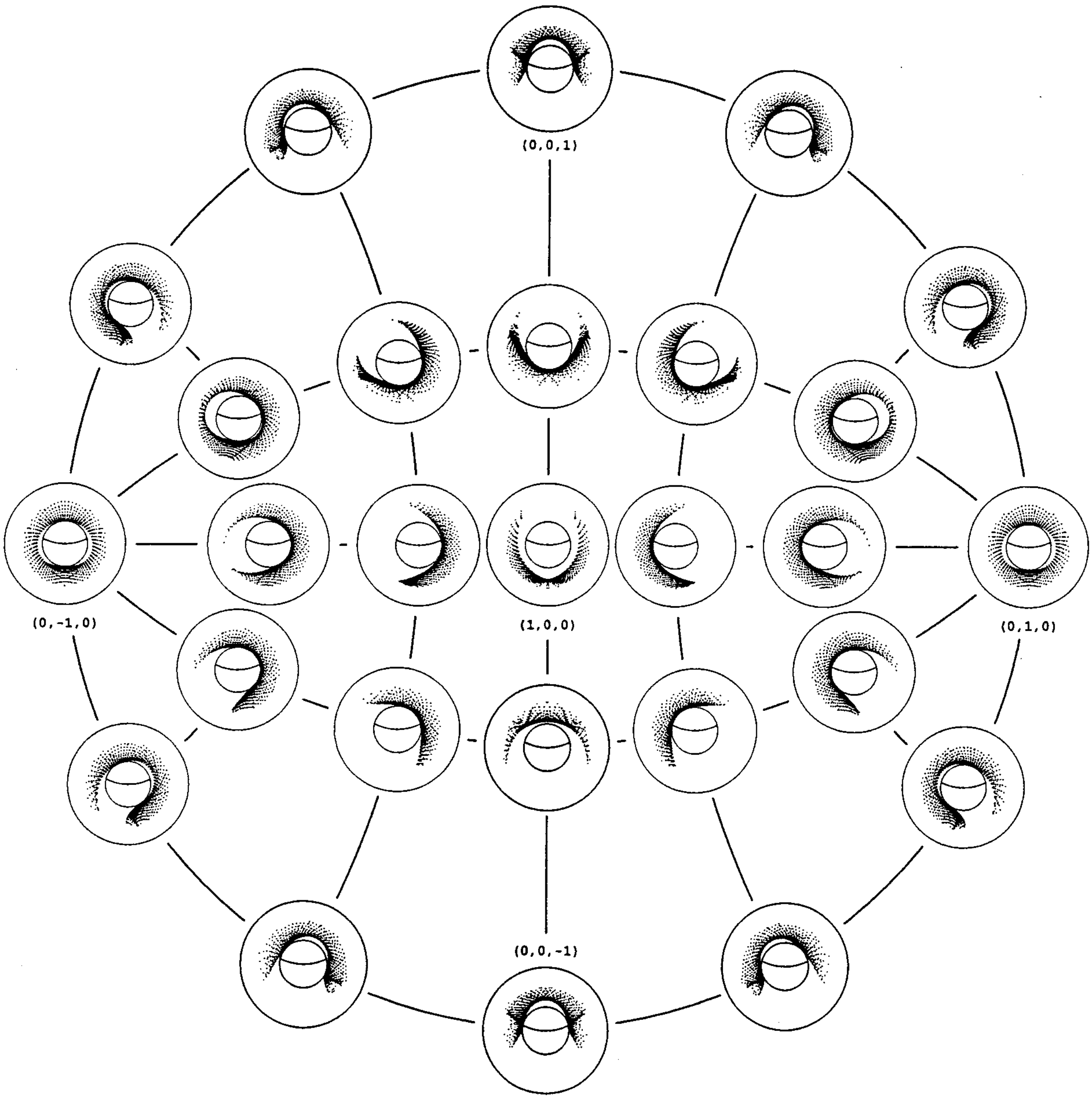

Fig. 44. Great circle halos with $\alpha = 60$ ($\Delta_m = 22$) and $\Sigma = 50$. Same as Figs. 42 and 43 except for Σ.

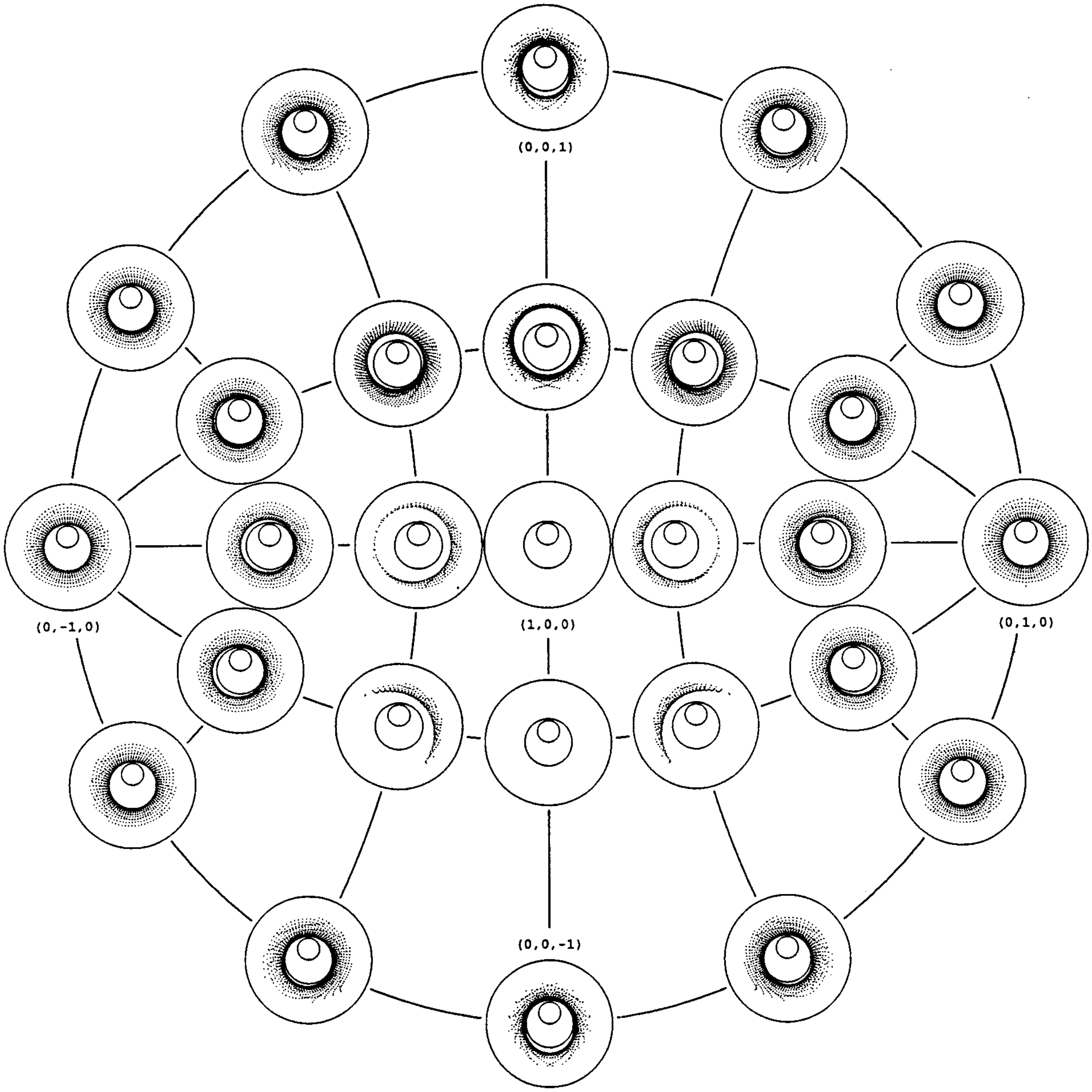

Fig. 45. Great circle halos with $\alpha = 60$ ($\Delta_m = 22$) and $\Sigma = 80$. Same as Figs. 42–44 except for Σ. The small circle in each halo diagram is the parhelic circle, which for the sun elevation here has a radius of only 10°.

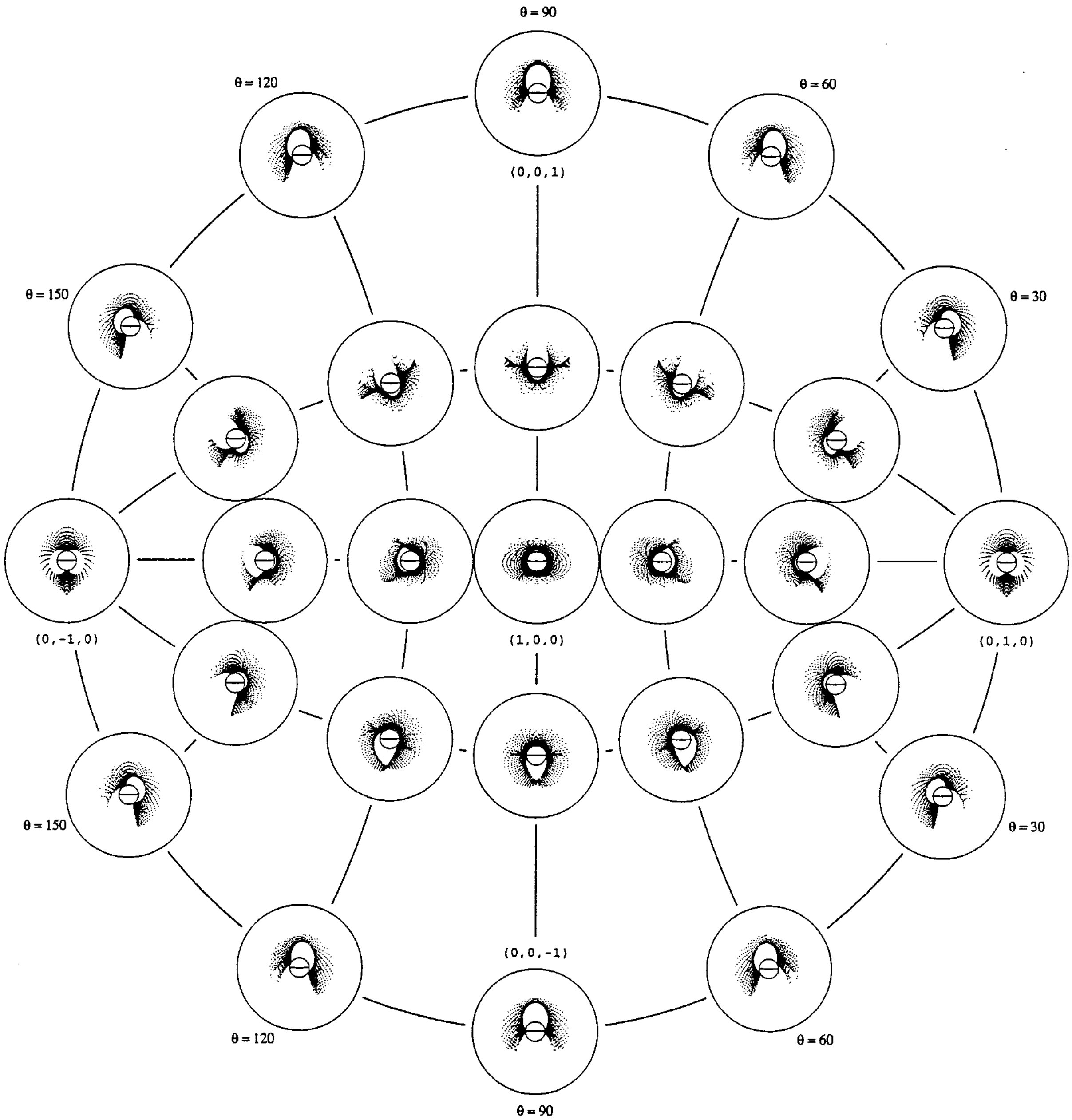

Fig. 46. Great circle halos with wedge angle $\alpha = 28$ ($\Delta_m = 9$) and sun elevation $\Sigma = 20$. Same as Fig. 43 except for α.

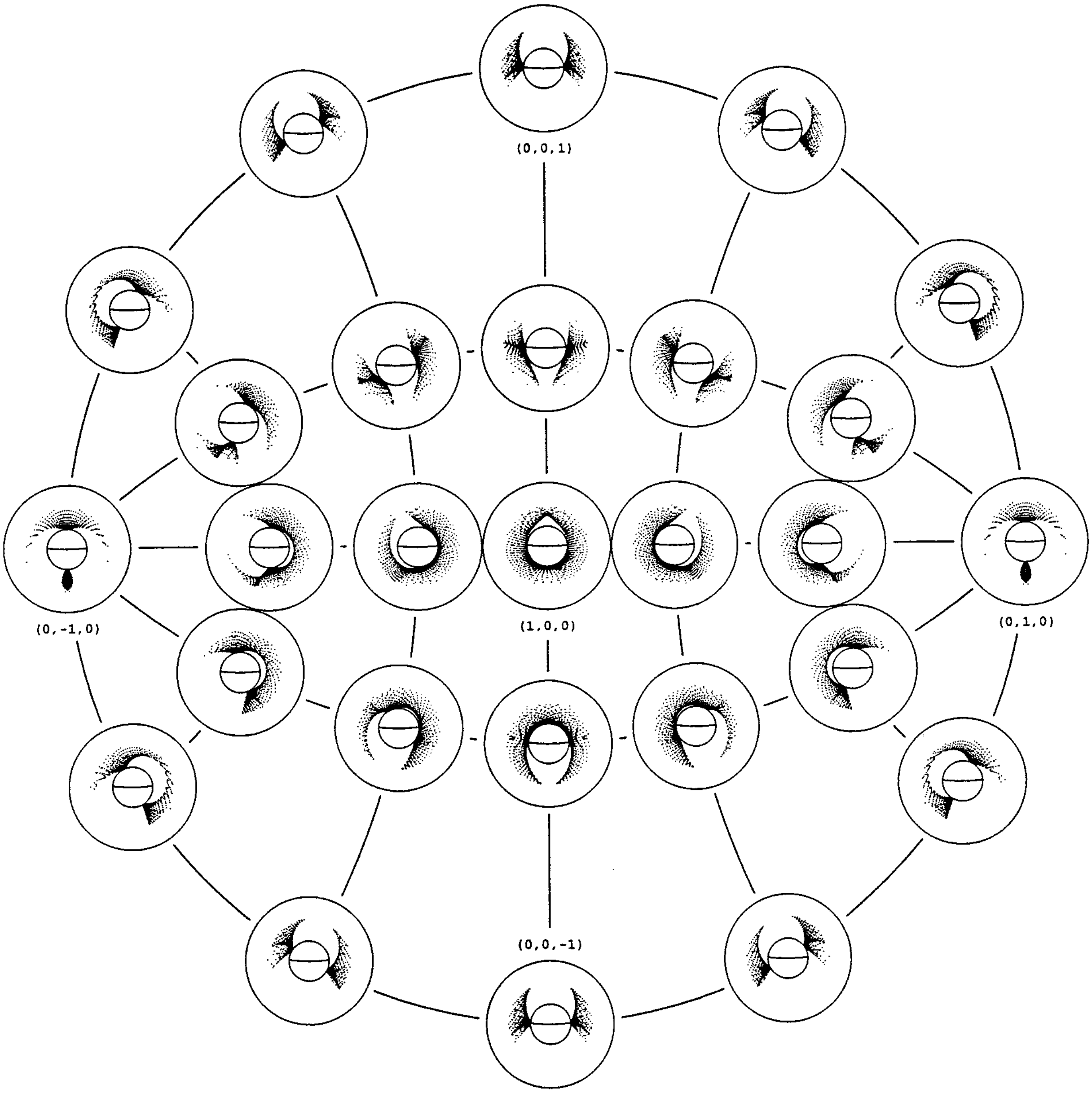

Fig. 47. Great circle halos with $\alpha = 52.4$ ($\Delta_m = 18$) and $\Sigma = 20$. Same as Figs. 43 and 46 except for α.

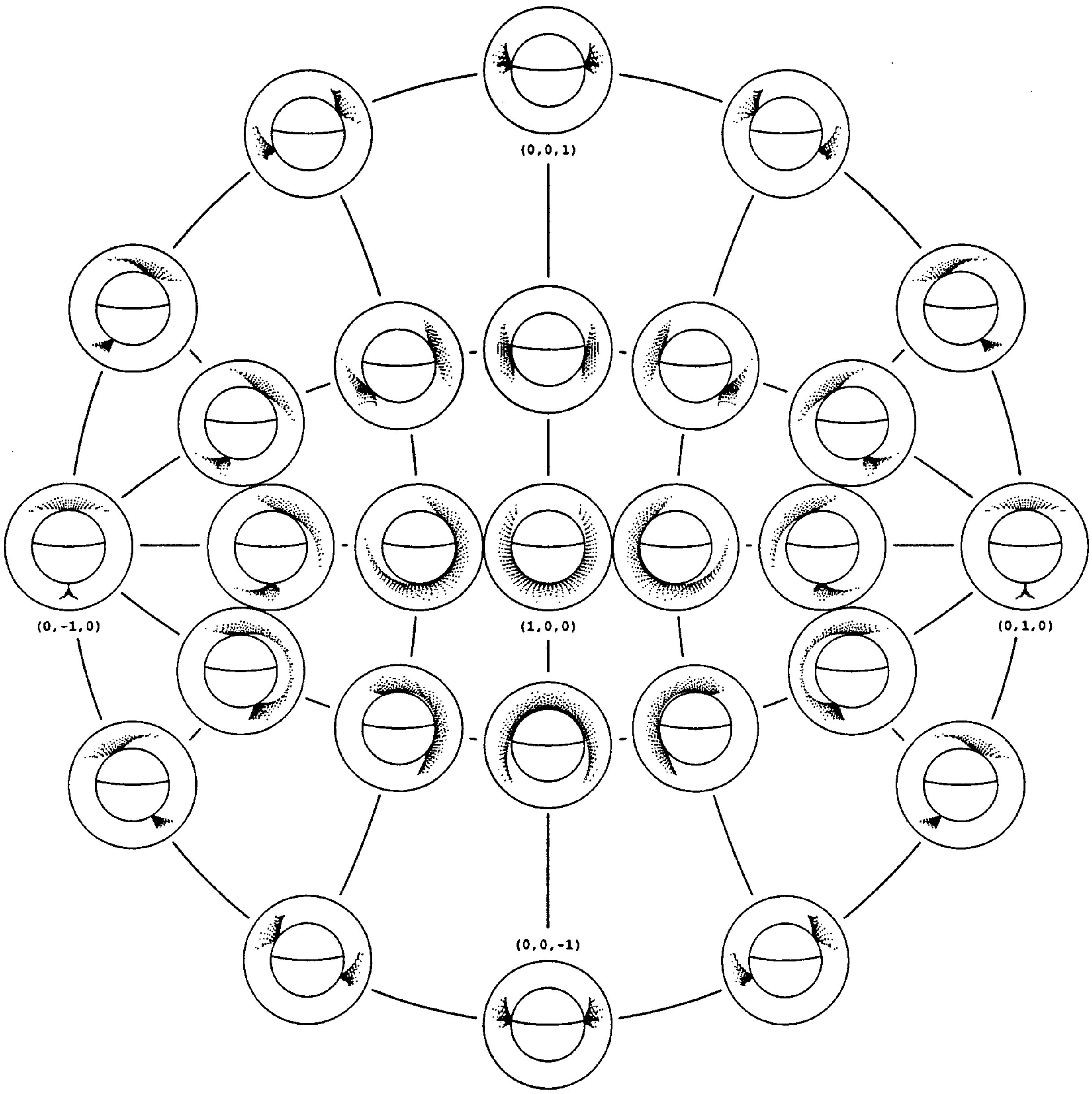

Fig. 48. Great circle halos with $\alpha = 80.2$ ($\Delta_m = 35$) and $\Sigma = 20$. Same as Figs. 43, 46, and 47 except for α.

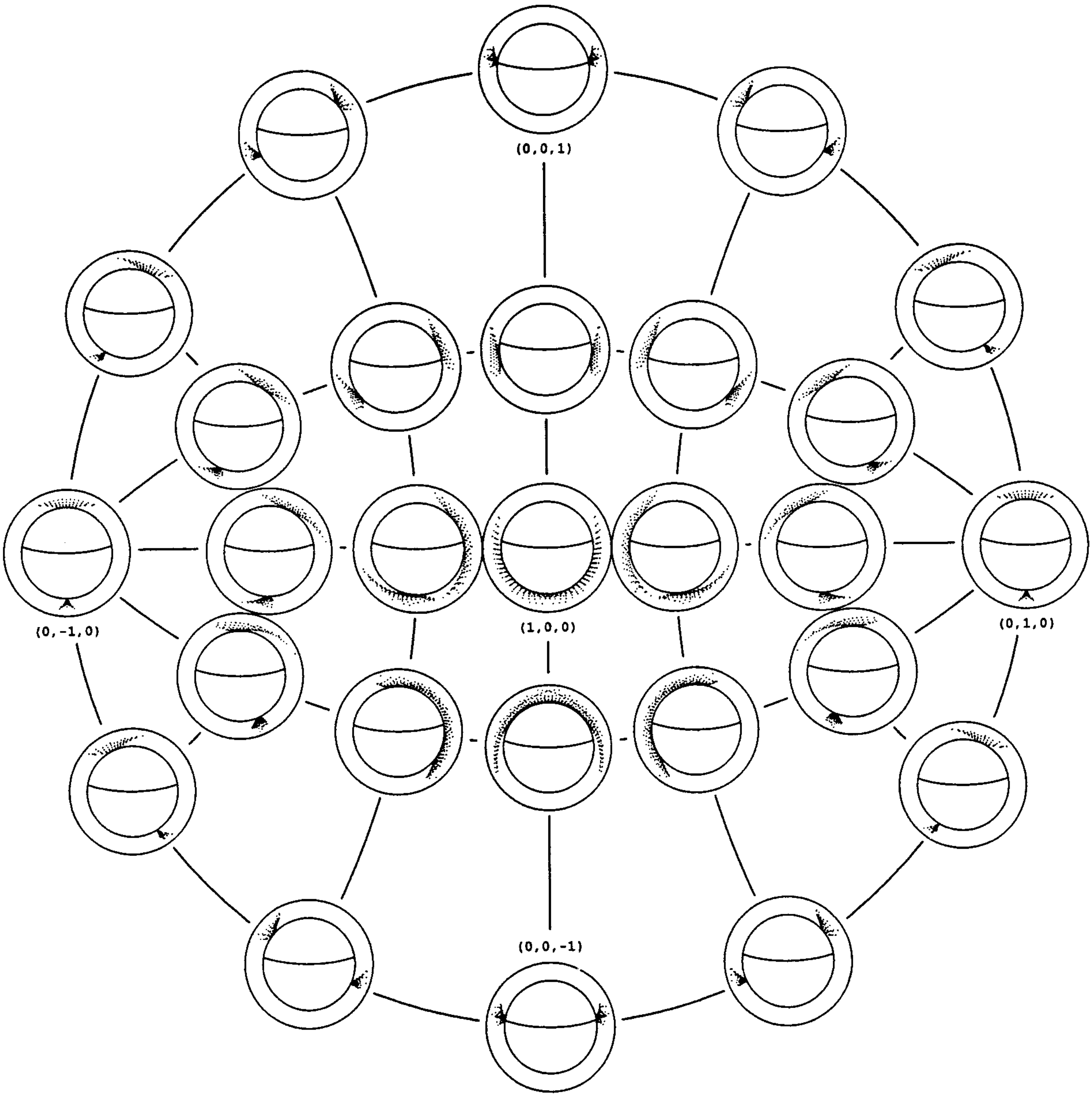

Fig. 49. Great circle halos with $\alpha = 90$ ($\Delta_m = 46$) and $\Sigma = 20$. Same as Figs. 43 and 46–48 except for α.

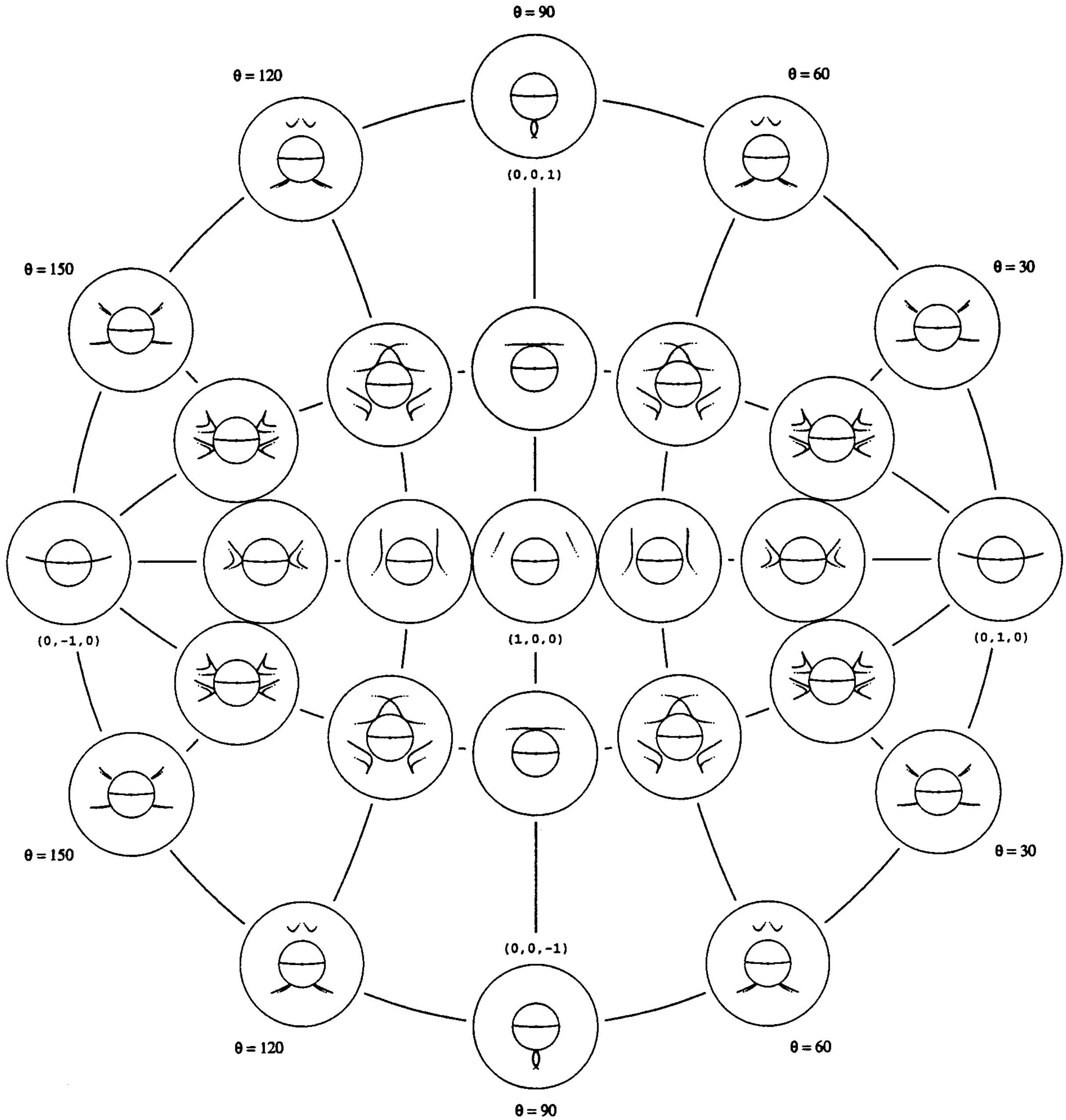

Fig. 50. Point halos with $\alpha = 60$ ($\Delta_m = 22$) and $\Sigma = 20$. Same as Fig. 34 except that here each simulation, located at $\mathbf{P}_u$, is the *mmm*-symmetric composite consisting of the halos with poles $\pm\mathbf{P}_u$, $\pm$yref $\mathbf{P}_{u'}$, $\pm$zref $\mathbf{P}_u$, and $\pm$xrot $\mathbf{P}_u$. For each halo in the simulation, the *x*-rotation, the *y*-reflection, the *z*-reflection, and the face interchange are also present, although not necessarily nonempty at the given sun elevation. It is the composite, rather than any of the components separately, that would be seen in most real halo displays.

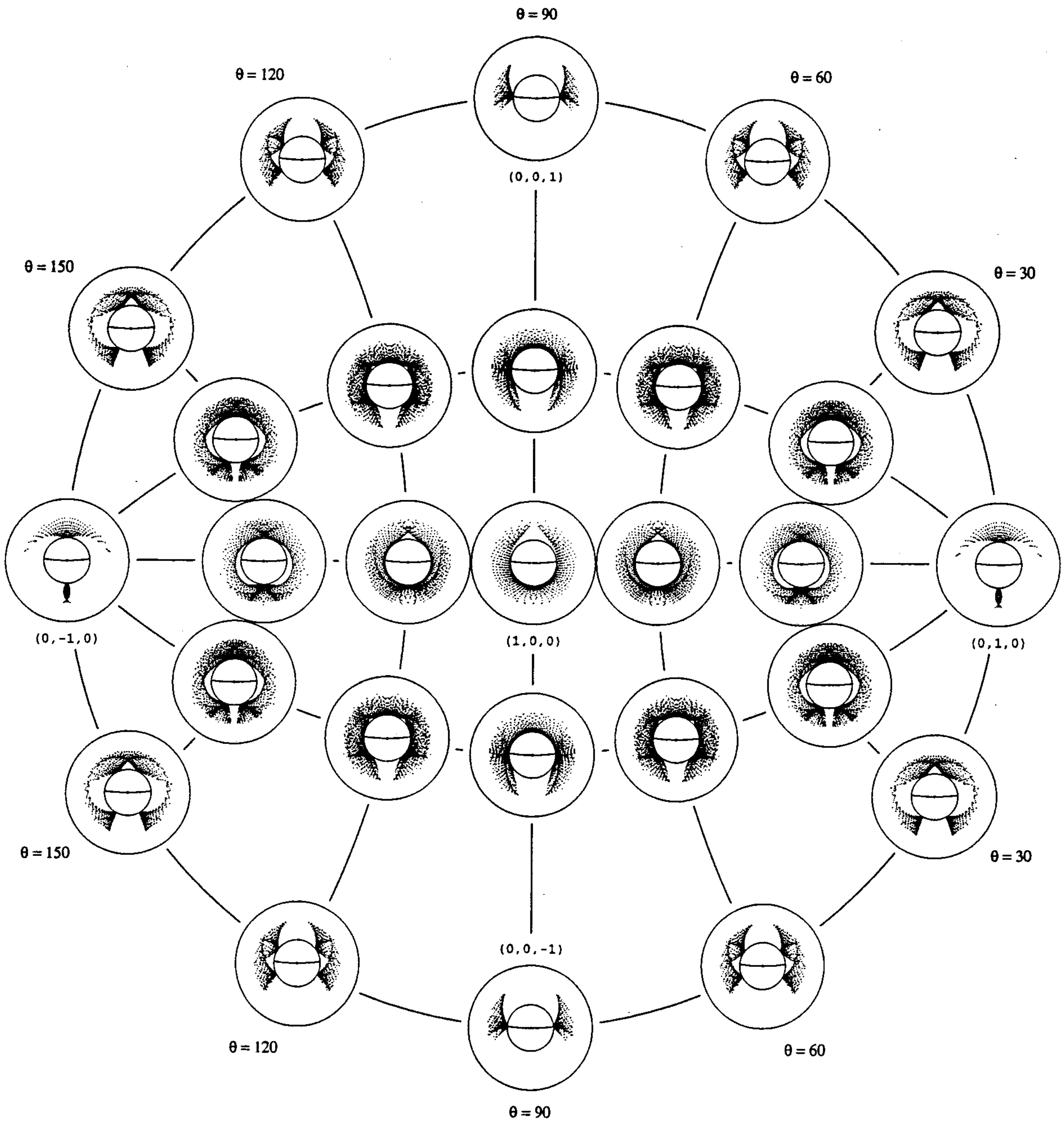

Fig. 51. Great circle halos with $\alpha = 60$ ($\Delta_m = 22$) and $\Sigma = 20$. Same as Fig. 43 except that here each simulation, located at $\mathbf{P}_u$, is the *mmm*-symmetric composite consisting of the halos with poles $\mathbf{P}_u$, yref $\mathbf{P}_u$, zref $\mathbf{P}_u$, and xrot $\mathbf{P}_u$. For each halo in the simulation, the x-rotation, the y-reflection, the z-reflection, and the face interchange are also present, although not necessarily nonempty at the given sun elevation. The x-rotation of a great circle halo, however, is the halo itself, and the z-reflection is the same as the y-reflection. It is the composite, rather than any of the components separately, that would be seen in most real halo displays.

Appendix B: The Pole Diagrams

In this appendix we give Parry, alternate Parry, and plate poles for all relevant wedges of the pyramidal crystal of Fig. 28. The poles are the coordinate vectors of the Parry, alternate Parry, and plate spin vectors $\mathbf{N}_3$, $\mathbf{N}_1 \times \mathbf{N}_3$, $\mathbf{N}_1$ (the crystal frame vectors) with respect to the various wedges. Each pole, together with the zenith angle ψ of the spin vector and the wedge angle α, determines a halo. Parry poles and $\psi = 0$ ($\psi = 90$) determine halos from Parry (alternate Lowitz) orientations. Alternate Parry poles and $\psi = 0$ ($\psi = 90$) determine halos from alternate Parry (Lowitz) orientations. Plate poles and $\psi = 0$ ($\psi = 90$) determine halos from plate (column) orientations. The alternate Parry poles are given explicitly only in Figs. 55 and 59, but they are easily inferred from the plate and Parry poles.

Each figure shows the poles for wedges having a fixed wedge angle α. Each pole is shown as a solid or open dot on the sphere and is labeled with its spin vector, either plate or Parry, and with its wedge $i\,j$. For each spin vector and hence for each crystal orientation class, a table lists the wedges and poles, with the poles given in Bravais coordinates (θ, δ). Wedges with the same pole and hence that make the same point halo are grouped together within each table. In addition, wedges with antipodal poles are located on the same line in the table. Their halos are x-rotations of each other, and if the halos are great circle halos, they are the same halo. Each group of wedges making the same great circle halo therefore consists of two groups of wedges for point halos, one group from the left column of the table, the other from the right column and facing the first. The tables also give s_1 and s_2, used in the Nonempty Halos Theorem, Subsection 2.F, to find the range of sun elevations for which a halo is nonempty, and they give s and t, used in the Contact Point Theorem, Subsection 2.G, to find contact points with the circular halo.

The front hemisphere poles in each table are arranged in order of decreasing θ and then increasing δ. Reading the left column from top to bottom therefore corresponds to scanning each Bravais circle from top to bottom (increasing δ) but scanning the front hemisphere as a whole from left to right (decreasing θ). Reading the right column from top to bottom corresponds to scanning each Bravais circle from bottom to top but scanning the rear hemisphere as a whole from right to left.

The Bravais coordinate grid shown in each diagram is the same as in Fig. 7, with Bravais circles $\theta = 0, 30, 60, \ldots, 180$, and Bravais meridians $\delta = -135, -90, -45, \ldots, 180$. The heavy curve on the front hemisphere is the boundary of the entry region, and the "$\times$" is the minimum deviation vector $\mathbf{D}_u$.

Most of the figures were made with MATHEMATICA. This research was supported in part by National Science Foundation grant OPP-9419235.

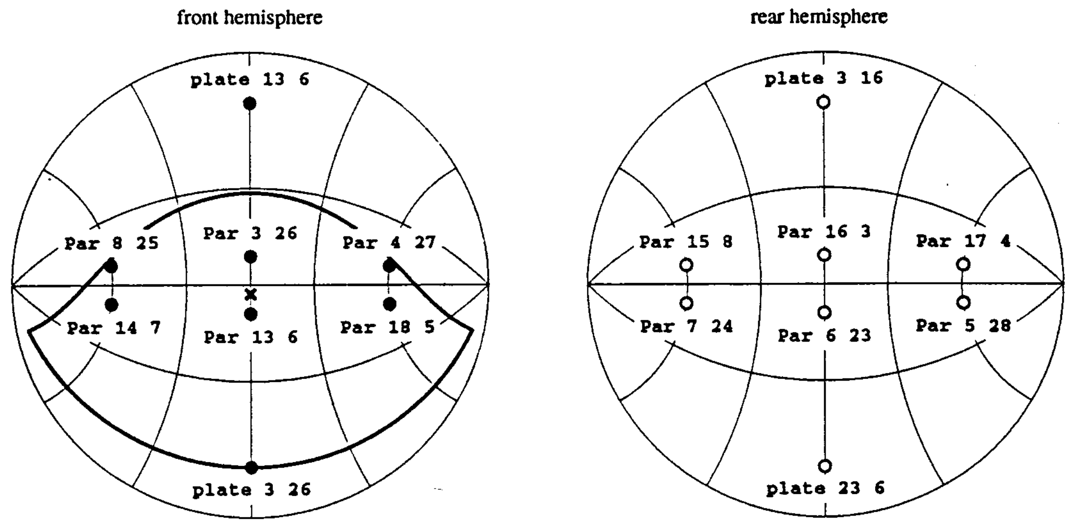

Wedges *i j* and poles *plate i j* = *B*(θ, δ); for plate and column orientations. (α = 28)

front hemisphere							rear hemisphere						
wedge	θ	δ	s_1	s_2	s	t	wedge	θ	δ	s_1	s_2	s	t
13 6	90	-76	33	152	80	0	*23 6*	90	104	28	147	100	180
14 7	90	-76					*24 7*	90	104				
15 8	90	-76					*25 8*	90	104				
16 3	90	-76					*26 3*	90	104				
17 4	90	-76					*27 4*	90	104				
18 5	90	-76					*28 5*	90	104				
3 26	90	76	0	119	72	180	*3 16*	90	-104	61	180	108	0
4 27	90	76					*4 17*	90	-104				
5 28	90	76					*5 18*	90	-104				
6 23	90	76					*6 13*	90	-104				
7 24	90	76					*7 14*	90	-104				
8 25	90	76					*8 15*	90	-104				

Wedges *i j* and poles *Par i j* = *B*(θ, δ); for Parry and alternate Lowitz orientations. (α = 28)

front hemisphere							rear hemisphere						
wedge	θ	δ	s_1	s_2	s	t	wedge	θ	δ	s_1	s_2	s	t
4 17	150	-14	0	148	62	280	*5 28*	30	166	32	180	118	100
8 25	150	-14					*7 14*	30	166				
14 7	150	14	0	143	60	265	*17 4*	30	-166	37	180	120	85
28 5	150	14					*25 8*	30	-166				
3 16	90	-14	0	90	18	0	*6 13*	90	166	90	180	162	180
3 26	90	-14					*6 23*	90	166				
13 6	90	14	0	84	10	180	*16 3*	90	-166	96	180	170	0
23 6	90	14					*26 3*	90	-166				
4 27	30	-14	0	148	62	80	*5 18*	150	166	32	180	118	260
8 15	30	-14					*7 24*	150	166				
18 5	30	14	0	143	60	95	*15 8*	150	-166	37	180	120	275
24 7	30	14					*27 4*	150	-166				

Fig. 52. Poles of 9° arcs (α = 28). There are four arcs from plate orientations and hence two from column orientations. There are twelve arcs from Parry orientations and hence six from alternate Lowitz orientations. For Σ = 20 the appearance of each 9° arc having a pole on the front hemisphere can be estimated from Figs. 38 and 46.

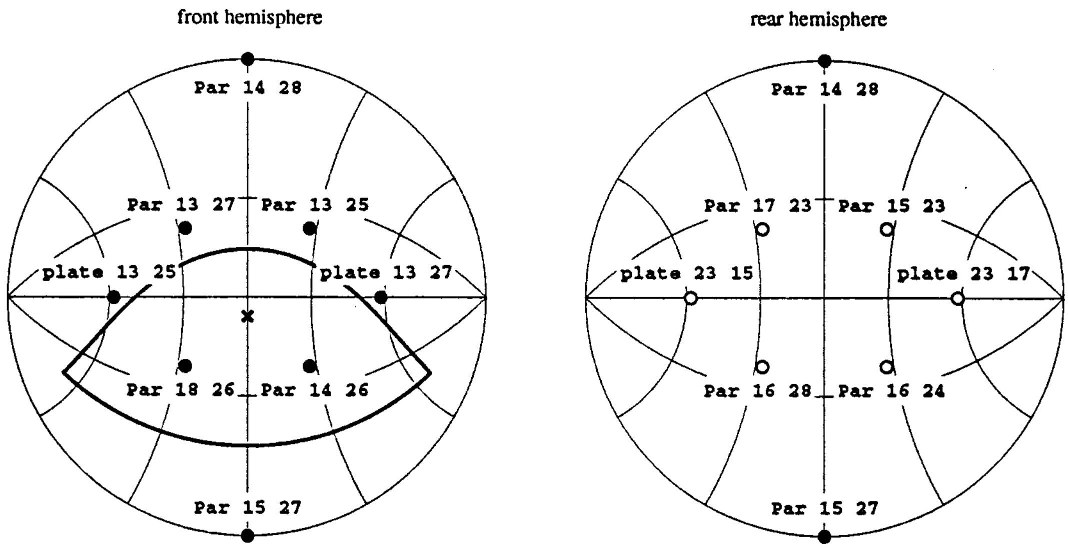

Wedges *i j* and poles *plate i j* = *B*(θ, δ); for plate and column orientations. (α = 52.4)

front hemisphere							rear hemisphere						
wedge	θ	δ	s_1	s_2	s	t	wedge	θ	δ	s_1	s_2	s	t
13 25	148	0	5	133	59	276	*23 17*	32	-180	47	175	121	96
14 26	148	0					*24 18*	32	-180				
15 27	148	0					*25 13*	32	-180				
16 28	148	0					*26 14*	32	-180				
17 23	148	0					*27 15*	32	-180				
18 24	148	0					*28 16*	32	-180				
13 27	32	0	5	133	59	84	*23 15*	148	-180	47	175	121	264
14 28	32	0					*24 16*	148	-180				
15 23	32	0					*25 17*	148	-180				
16 24	32	0					*26 18*	148	-180				
17 25	32	0					*27 13*	148	-180				
18 26	32	0					*28 14*	148	-180				

Wedges *i j* and poles *Par i j* = *B*(θ, δ); for Parry and alternate Lowitz orientations. (α = 52.4)

front hemisphere							rear hemisphere						
wedge	θ	δ	s_1	s_2	s	t	wedge	θ	δ	s_1	s_2	s	t
13 27	117	-34	14	118	50	323	*16 24*	63	146	62	166	130	143
23 15	117	-34					*26 18*	63	146				
18 26	117	34	0	95	36	230	*15 23*	63	-146	85	180	144	50
24 16	117	34					*27 13*	63	-146				
14 28	90	-90	67	154	99	0	*15 27*	90	90	26	113	81	180
18 24	90	-90					*17 25*	90	90				
24 18	90	-90					*25 17*	90	90				
28 14	90	-90					*27 15*	90	90				
13 25	63	-34	14	118	50	37	*16 28*	117	146	62	166	130	217
23 17	63	-34					*26 14*	117	146				
14 26	63	34	0	95	36	130	*17 23*	117	-146	85	180	144	310
28 16	63	34					*25 13*	117	-146				

Fig. 53. Poles of 18° arcs (α = 52.4). For Σ = 20 the appearance of each 18° arc having a pole on the front hemisphere can be estimated from Figs. 39 and 47.

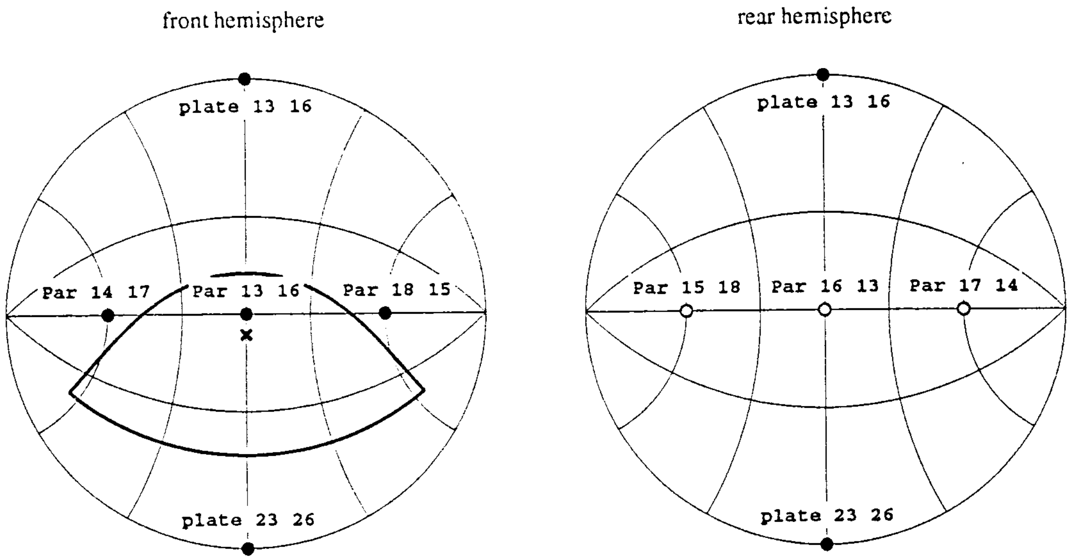

Wedges *i j* and poles *plate i j* = $B(\theta, \delta)$; for plate and column orientations. (α = 56)

wedge	θ	δ	s_1	s_2	s	t	wedge	θ	δ	s_1	s_2	s	t
13 16	90	-90	70	152	100	0	*23 26*	90	90	28	110	80	180
14 17	90	-90					*24 27*	90	90				
15 18	90	-90					*25 28*	90	90				
16 13	90	-90					*26 23*	90	90				
17 14	90	-90					*27 24*	90	90				
18 15	90	-90					*28 25*	90	90				

Wedges *i j* and poles *Par i j* = $B(\theta, \delta)$; for Parry and alternate Lowitz orientations. (α = 56)

front hemisphere							rear hemisphere						
wedge	θ	δ	s_1	s_2	s	t	wedge	θ	δ	s_1	s_2	s	t
14 17	150	0	9	132	60	276	*17 14*	30	-180	48	171	120	96
28 25	150	0					*25 28*	30	-180				
13 16	90	0	0	78	10	0	*16 13*	90	-180	102	180	170	180
23 26	90	0					*26 23*	90	-180				
18 15	30	0	9	132	60	84	*15 18*	150	-180	48	171	120	264
24 27	30	0					*27 24*	150	-180				

Fig. 54. Poles of 20° arcs (α = 56). For Σ = 0, 20, 50, and 80, the appearance of each 20° arc having a pole on the front hemisphere can be estimated from Figs. 33–36 and 42–45, which all have $\alpha = 60 \approx 56$.

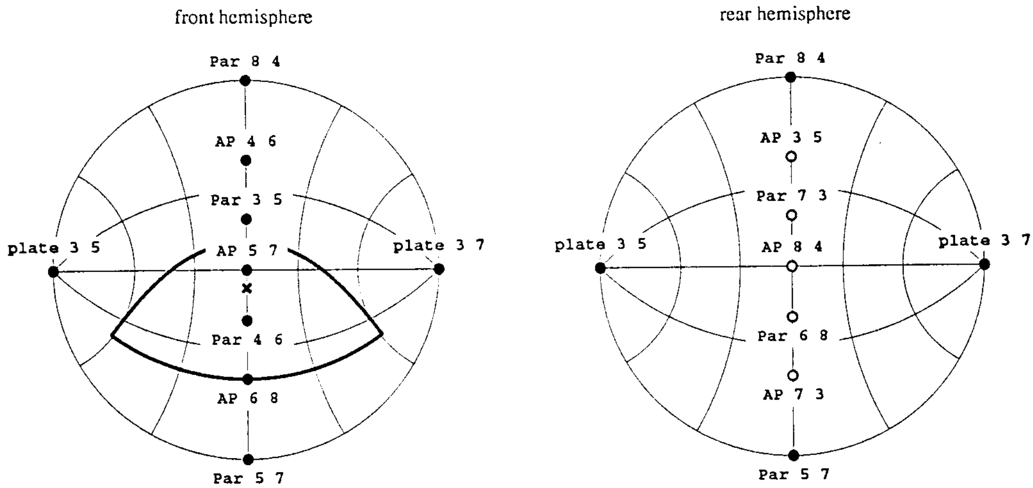

Wedges $i\,j$ and poles *plate* $i\,j = B(\theta, \delta)$; for plate and column orientations. ($\alpha = 60$)

	wedge	θ	δ	s_1	s_2	s	t	wedge	θ	δ	s_1	s_2	s	t	
left 22° parhelion (upper and lower tangent arcs)	*3 5*	180	0	29	151	90	270	*3 7*	0	0	29	151	90	90	right 22° parhelion (upper and lower tangent arcs)
	4 6	180	0					*4 8*	0	0					
	5 7	180	0					*5 3*	0	0					
	6 8	180	0					*6 4*	0	0					
	7 3	180	0					*7 5*	0	0					
	8 4	180	0					*8 6*	0	0					

Wedges $i\,j$ and poles *Par* $i\,j = B(\theta, \delta)$; for Parry and alternate Lowitz orientations. ($\alpha = 60$)

	front hemisphere							rear hemisphere							
	wedge	θ	δ	s_1	s_2	s	t	wedge	θ	δ	s_1	s_2	s	t	
upper sunvex Parry arc	*4 8*	90	-90	73	150	101	0	*5 7*	90	90	30	107	79	180	lower sunvex Parry arc
	8 4	90	-90					*7 5*	90	90					
upper suncave Parry arc	*3 5*	90	-30	13	90	41	0	*6 4*	90	150	90	167	139	180	
	3 7	90	-30					*6 8*	90	150					
lower suncave Parry arc	*4 6*	90	30	0	65	19	180	*5 3*	90	-150	115	180	161	0	
	8 6	90	30					*7 3*	90	-150					

Wedges $i\,j$ and poles *AP* $i\,j = B(\theta, \delta)$; for alternate Parry and for Lowitz orientations. ($\alpha = 60$)

	front hemisphere							rear hemisphere							
	wedge	θ	δ	s_1	s_2	s	t	wedge	θ	δ	s_1	s_2	s	t	
(lower Lowitz arcs)	*4 6*	90	-60	43	120	71	0	*7 3*	90	120	60	137	109	180	(lower Lowitz arcs)
	5 3	90	-60					*8 6*	90	120					
(unnamed Lowitz arcs)	*4 8*	90	0	0	76	11	0	*7 5*	90	-180	104	180	169	180	(unnamed Lowitz arcs)
	5 7	90	0					*8 4*	90	-180					
(upper Lowitz arcs)	*3 7*	90	60	0	77	49	180	*3 5*	90	-120	103	180	131	0	(upper Lowitz arcs)
	6 8	90	60					*6 4*	90	-120					

Fig. 55. Poles of 22° arcs ($\alpha = 60$). Halo names are given when they exist, with names in parentheses referring to great circle halos and the remaining names referring to point halos. For $\Sigma = 0$, 20, 50, and 80, the appearance of each 22° arc having a pole on the front hemisphere can be estimated from Figs. 33–36 and 42–45.

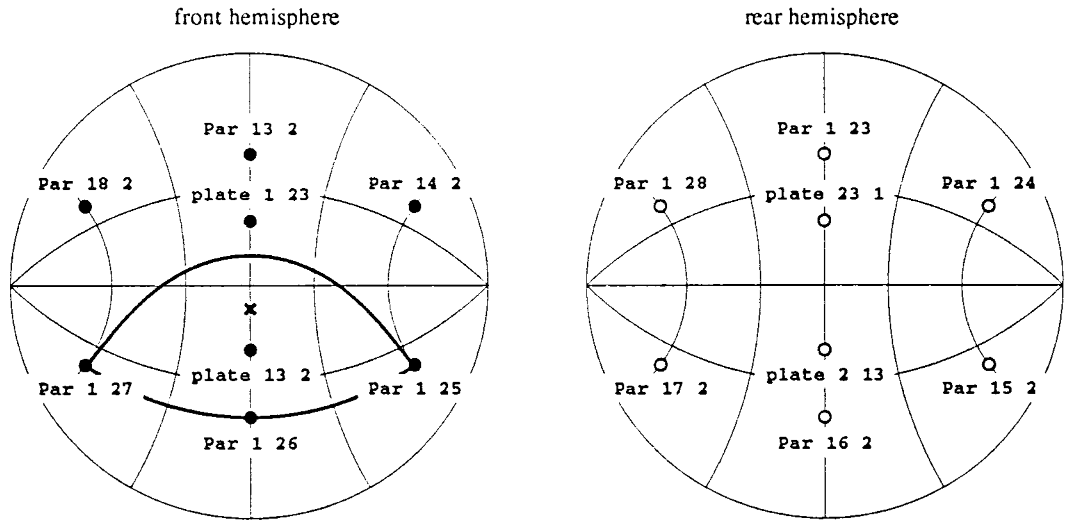

Wedges *i j* and poles *plate i j* = $B(\theta, \delta)$; for plate and column orientations. ($\alpha = 62$)

front hemisphere							rear hemisphere						
wedge	θ	δ	s_1	s_2	s	t	wedge	θ	δ	s_1	s_2	s	t
1 23	90	-31	16	90	42	0	*2 13*	90	149	90	164	138	180
1 24	90	-31					*2 14*	90	149				
1 25	90	-31					*2 15*	90	149				
1 26	90	-31					*2 16*	90	149				
1 27	90	-31					*2 17*	90	149				
1 28	90	-31					*2 18*	90	149				
13 2	90	31	0	63	20	180	*23 1*	90	-149	117	180	160	0
14 2	90	31					*24 1*	90	-149				
15 2	90	31					*25 1*	90	-149				
16 2	90	31					*26 1*	90	-149				
17 2	90	31					*27 1*	90	-149				
18 2	90	31					*28 1*	90	-149				

Wedges *i j* and poles *Par i j* = $B(\theta, \delta)$; for Parry and alternate Lowitz orientations. ($\alpha = 62$)

front hemisphere							rear hemisphere						
wedge	θ	δ	s_1	s_2	s	t	wedge	θ	δ	s_1	s_2	s	t
18 2	150	-59	40	150	80	299	*15 2*	30	121	30	140	100	119
24 1	150	-59					*27 1*	30	121				
1 27	150	59	1	119	70	247	*1 24*	30	-121	61	179	110	67
2 15	150	59					*2 18*	30	-121				
13 2	90	-59	44	118	70	0	*16 2*	90	121	62	136	110	180
23 1	90	-59					*26 1*	90	121				
1 26	90	59	0	74	48	180	*1 23*	90	-121	106	180	132	0
2 16	90	59					*2 13*	90	-121				
14 2	30	-59	40	150	80	61	*17 2*	150	121	30	140	100	241
28 1	30	-59					*25 1*	150	121				
1 25	30	59	1	119	70	113	*1 28*	150	-121	61	179	110	293
2 17	30	59					*2 14*	150	-121				

Fig. 56. Poles of 23° arcs ($\alpha = 62$). For $\Sigma = 0$, 20, 50, and 80, the appearance of each 23° arc having a pole on the front hemisphere can be estimated from Figs. 33–36 and 42–45, which all have $\alpha = 60 \approx 62$.

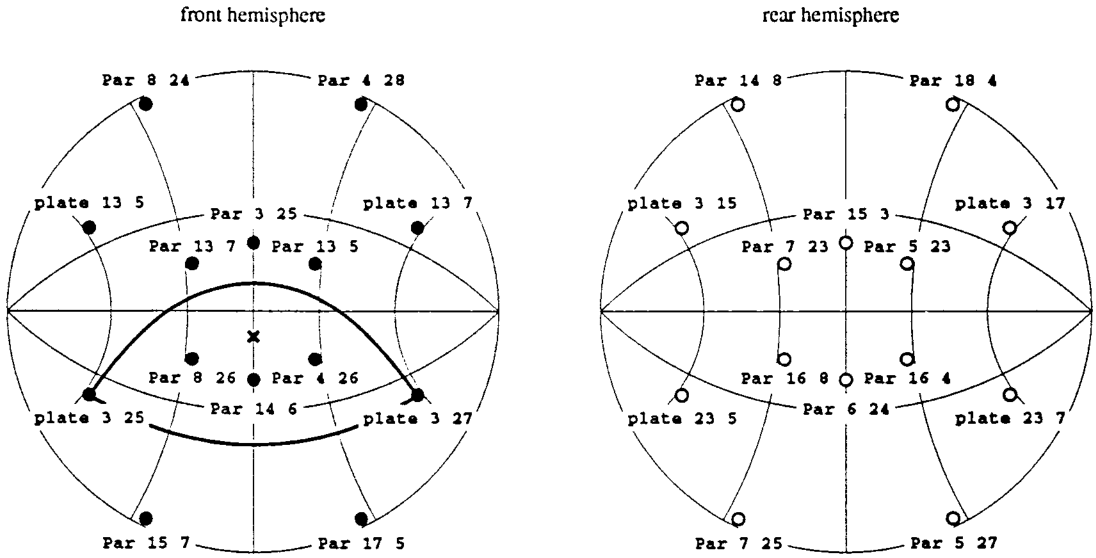

Wedges *i j* and poles *plate i j* = $B(\theta, \delta)$; for plate and column orientations. ($\alpha = 63.8$)

front hemisphere							rear hemisphere						
wedge	θ	δ	s_1	s_2	s	t	wedge	θ	δ	s_1	s_2	s	t
13 5	148	-58	41	148	80	300	*23 7*	32	122	32	139	100	120
14 6	148	-58					*24 8*	32	122				
15 7	148	-58					*25 3*	32	122				
16 8	148	-58					*26 4*	32	122				
17 3	148	-58					*27 5*	32	122				
18 4	148	-58					*28 6*	32	122				
3 25	148	58	0	117	69	246	*3 17*	32	-122	63	180	111	66
4 26	148	58					*4 18*	32	-122				
5 27	148	58					*5 13*	32	-122				
6 28	148	58					*6 14*	32	-122				
7 23	148	58					*7 15*	32	-122				
8 24	148	58					*8 16*	32	-122				
13 7	32	-58	41	148	80	60	*23 5*	148	122	32	139	100	240
14 8	32	-58					*24 6*	148	122				
15 3	32	-58					*25 7*	148	122				
16 4	32	-58					*26 8*	148	122				
17 5	32	-58					*27 3*	148	122				
18 6	32	-58					*28 4*	148	122				
3 27	32	58	0	117	69	114	*3 15*	148	-122	63	180	111	294
4 28	32	58					*4 16*	148	-122				
5 23	32	58					*5 17*	148	-122				
6 24	32	58					*6 18*	148	-122				
7 25	32	58					*7 13*	148	-122				
8 26	32	58					*8 14*	148	-122				

Fig. 57. Poles of 24° arcs ($\alpha = 63.8$). For $\Sigma = 0$, 20, 50, and 80, the appearance of each 24° arc having a pole on the front hemisphere can be estimated from Figs. 33–36 and 42–45, which have $\alpha = 60 \approx 63.8$. The tables are continued on the following page.

Wedges *i j* and poles *Par i j* = $B(\theta, \delta)$; for Parry and alternate Lowitz orientations. (α = 63.8)

front hemisphere							rear hemisphere						
wedge	θ	δ	s_1	s_2	s	t	wedge	θ	δ	s_1	s_2	s	t
4 18	117	-88	70	150	99	333	*5 27*	63	92	30	110	81	153
8 24	117	-88					*7 15*	63	92				
13 7	117	-24	14	109	44	319	*16 4*	63	156	71	166	136	139
23 5	117	-24					*26 8*	63	156				
4 16	117	24	0	90	29	248	*5 23*	63	-156	90	180	151	68
8 26	117	24					*7 13*	63	-156				
15 7	117	88	26	106	77	208	*18 4*	63	-92	74	154	103	28
27 5	117	88					*24 8*	63	-92				
3 15	90	-32	19	90	44	0	*6 14*	90	148	90	161	136	180
3 17	90	-32					*6 18*	90	148				
3 25	90	-32					*6 24*	90	148				
3 27	90	-32					*6 28*	90	148				
14 6	90	32	0	62	20	180	*15 3*	90	-148	118	180	160	0
18 6	90	32					*17 3*	90	-148				
24 6	90	32					*25 3*	90	-148				
28 6	90	32					*27 3*	90	-148				
4 28	63	-88	70	150	99	27	*5 17*	117	92	30	110	81	207
8 14	63	-88					*7 25*	117	92				
13 5	63	-24	14	109	44	41	*16 8*	117	156	71	166	136	221
23 7	63	-24					*26 4*	117	156				
4 26	63	24	0	90	29	112	*5 13*	117	-156	90	180	151	292
8 16	63	24					*7 23*	117	-156				
17 5	63	88	26	106	77	152	*14 8*	117	-92	74	154	103	332
25 7	63	88					*28 4*	117	-92				

Fig. 57. Continued from the preceding page.

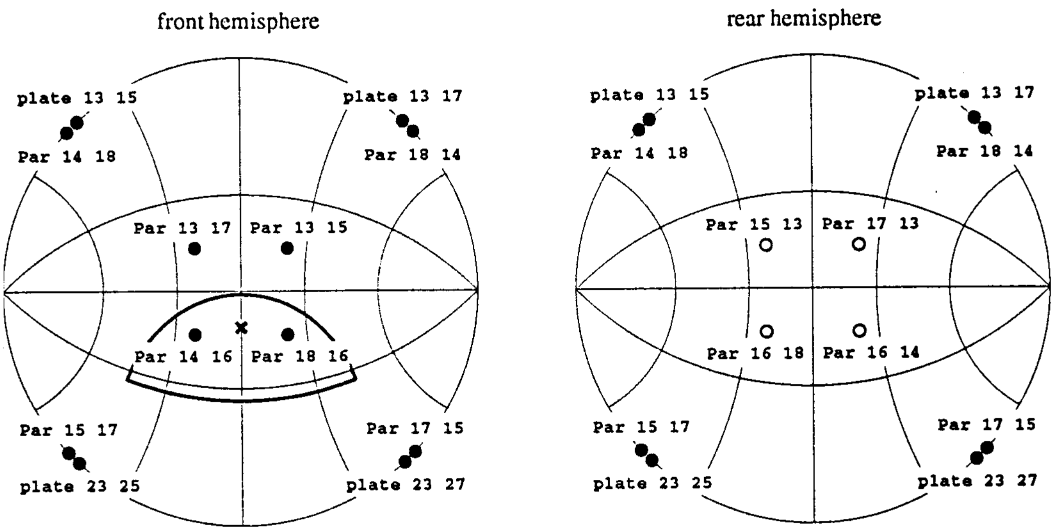

Wedges *i j* and poles *plate i j* = *B*(θ, δ); for plate and column orientations. (α = 80.2)

wedge	θ	δ	s_1	s_2	s	t	wedge	θ	δ	s_1	s_2	s	t
13 15	133	-90	78	151	103	315	*23 27*	47	90	29	102	77	135
14 16	133	-90					*24 28*	47	90				
15 17	133	-90					*25 23*	47	90				
16 18	133	-90					*26 24*	47	90				
17 13	133	-90					*27 25*	47	90				
18 14	133	-90					*28 26*	47	90				
23 25	133	90	29	102	77	225	*13 17*	47	-90	78	151	103	45
24 26	133	90					*14 18*	47	-90				
25 27	133	90					*15 13*	47	-90				
26 28	133	90					*16 14*	47	-90				
27 23	133	90					*17 15*	47	-90				
28 24	133	90					*18 16*	47	-90				

Wedges *i j* and poles *Par i j* = *B*(θ, δ); for Parry and alternate Lowitz orientations. (α = 80.2)

front hemisphere							rear hemisphere						
wedge	θ	δ	s_1	s_2	s	t	wedge	θ	δ	s_1	s_2	s	t
14 18	137	-90	76	152	102	312	*17 15*	43	90	28	104	78	132
28 24	137	-90					*25 27*	43	90				
15 17	137	90	28	104	78	228	*18 14*	43	-90	76	152	102	48
27 25	137	90					*24 28*	43	-90				
13 17	111	-22	25	93	44	328	*16 14*	69	158	87	155	136	148
23 25	111	-22					*26 28*	69	158				
14 16	111	22	0	71	22	260	*17 13*	69	-158	109	180	158	80
28 26	111	22					*25 23*	69	-158				
13 15	69	-22	25	93	44	32	*16 18*	111	158	87	155	136	212
23 27	69	-22					*26 24*	111	158				
18 16	69	22	0	71	22	100	*15 13*	111	-158	109	180	158	280
24 26	69	22					*27 23*	111	-158				

Fig. 58. Poles of 35° arcs (α = 80.2). For Σ = 20 the appearance of each 35° arc having a pole on the front hemisphere can be estimated from Figs. 40 and 48.

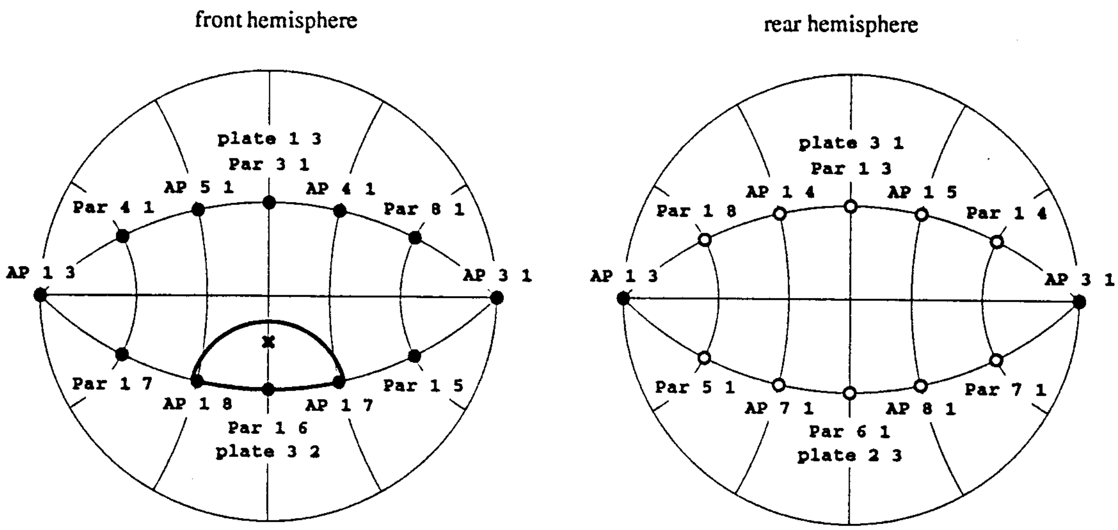

Wedges *i j* and poles *plate i j* = *B*(θ, δ); for plate and column orientations. (α = 90)

	front hemisphere								rear hemisphere								
	wedge		θ	δ	s_1	s_2	s	t	wedge		θ	δ	s_1	s_2	s	t	
circumzenith arc	*1*	*3*	90	-45	58	90	68	0	*2*	*3*	90	135	90	122	112	180	(infralateral arcs)
(infralateral arcs)	*1*	*4*	90	-45					*2*	*4*	90	135					
	1	*5*	90	-45					*2*	*5*	90	135					
	1	*6*	90	-45					*2*	*6*	90	135					
	1	*7*	90	-45					*2*	*7*	90	135					
	1	*8*	90	-45					*2*	*8*	90	135					
circumhorizon arc	*3*	*2*	90	45	0	32	22	180	*3*	*1*	90	-135	148	180	158	0	(supralateral arc)
(supralateral arc)	*4*	*2*	90	45					*4*	*1*	90	-135					
	5	*2*	90	45					*5*	*1*	90	-135					
	6	*2*	90	45					*6*	*1*	90	-135					
	7	*2*	90	45					*7*	*1*	90	-135					
	8	*2*	90	45					*8*	*1*	90	-135					

Fig. 59. Poles of 46° arcs (α = 90). Here halo names are given when they exist, with names in parentheses referring to great circle halos and the remaining names to point halos. For Σ = 20 the appearance of each 46° arc having a pole on the front hemisphere can be found from Figs. 41 and 49. The tables are continued on the following page.

Wedges $i\,j$ and poles $Par\,i\,j = B(\theta, \delta)$; for Parry and alternate Lowitz orientations. ($\alpha = 90$)

	front hemisphere							rear hemisphere						
	wedge	θ	δ	s_1	s_2	s	t	wedge	θ	δ	s_1	s_2	s	t
left Parry supralateral arc	*4 1*	150	-45	58	117	79	298	*5 2*	30	135	63	122	101	118
	8 2	150	-45					*7 1*	30	135				
left Parry infralateral arc	*1 7*	150	45	28	92	62	258	*1 4*	30	-135	88	152	118	78
	2 5	150	45					*2 8*	30	-135				
circumzenith arc	*3 1*	90	-45	58	90	68	0	*6 1*	90	135	90	122	112	180
	3 2	90	-45					*6 2*	90	135				
circumhorizon arc	*1 6*	90	45	0	32	22	180	*1 3*	90	-135	148	180	158	0
	2 6	90	45					*2 3*	90	-135				
right Parry supralateral arc	*4 2*	30	-45	58	117	79	62	*5 1*	150	135	63	122	101	242
	8 1	30	-45					*7 2*	150	135				
right Parry infralateral arc	*1 5*	30	45	28	92	62	102	*1 8*	150	-135	88	152	118	282
	2 7	30	45					*2 4*	150	-135				

Wedges $i\,j$ and poles $AP\,i\,j = B(\theta, \delta)$; for alternate Parry and for Lowitz orientations. ($\alpha = 90$)

	front hemisphere							rear hemisphere							
	wedge	θ	δ	s_1	s_2	s	t	wedge	θ	δ	s_1	s_2	s	t	
left 46° parhelion (upper and lower tangent arcs to the 46° halo)	*1 3*	180	0	58	122	90	270	*1 6*	0	0	58	122	90	90	right 46° parhelion (upper and lower tangent arcs to the 46° halo)
	2 6	180	0					*2 3*	0	0					
	3 2	180	0					*3 1*	0	0					
	6 1	180	0					*6 2*	0	0					
	4 2	120	-45	58	105	71	328	*7 2*	60	135	75	122	109	148	
	5 1	120	-45					*8 1*	60	135					
	1 8	120	45	0	62	37	237	*1 5*	60	-135	118	180	143	57	
	2 7	120	45					*2 4*	60	-135					
	4 1	60	-45	58	105	71	32	*7 1*	120	135	75	122	109	212	
	5 2	60	-45					*8 2*	120	135					
	1 7	60	45	0	62	37	123	*1 4*	120	-135	118	180	143	303	
	2 8	60	45					*2 5*	120	-135					

Fig. 59. Continued from the previous page.

Appendix C: Glossary of Notation

A, $\mathbf{A}_u$,
B, $\mathbf{B}_u$,
C, $\mathbf{C}_u$ Wedge frame vectors. Eqs. (8), (21), and Fig. 4.

D, $\mathbf{D}_u$ Minimum deviation entry vector. Eqs. (42), (43), (21), and Fig. 9.

E, $\mathbf{E}_u$ Minimum deviation exit vector. Eqs. (44), (21), and Fig. 9.

H, $\mathbf{H}_u$ Halo point. Eqs. (11), (21), and Figs. 3 and 9.

k, $\mathbf{k}_u$ Zenith vector, $\mathbf{k} = (0, 0, 1)$. Eq. (21).

N, $\mathbf{N}_u$ Outward unit normal to entry face of wedge. Figs. 4 and 5.

$\mathbf{N}_0$ Outward unit normal to entry face of wedge in standard orientation. $\mathbf{N}_u = \mathbf{N}_0$. Eq. (10) and Fig. 5.

$\mathbf{N}_1, \mathbf{N}_2, \mathbf{N}_3, \ldots$ Outward unit normals to crystal faces 1, 2, . . . Eqs. (78) and (79).

P, $\mathbf{P}_u$ Spin vector. Eqs. (1), (21), and Fig. 1. The point $\mathbf{P}_u$ is the pole.

pr Projection. Eq. (2).

S, $\mathbf{S}_u$ Sun vector. Also see Eq. (21).

$\mathbf{Sn}(\theta)$ Point of lower boundary of entry region. Gives grazing entry. Eq. (50).

$\mathbf{Sx}(\theta)$ Point of upper boundary of entry region. Gives grazing exit. Eq. (49).

T Light point for ray within the wedge. Eq. (6) and Figs. 2 and 3.

$\mathbf{V}_u$ Coordinate vector of a vector $\mathbf{V}$ with respect to the frame u. Eqs. (21), (23), and Fig. 6.

$\mathbf{X}$, $\mathbf{X}_u$ Inward unit normal to exit face of wedge. Figs. 4 and 5.

$\mathbf{X}_0$ Inward unit normal to exit face of wedge in standard orientation. $\mathbf{X}_u = \mathbf{X}_0$. Eq. (10) and Fig 5.

AL Alternate Lowitz orientations. Subsection 3.A.

AP Alternate Parry orientations. Subsection 3.A.

$B(\theta, \delta)$ Point with Bravais (B-centered) coordinates (θ, δ). Eq. (26),

C Contact circle. Fig. 18.

$D(s, t)$ Point with D-centered coordinates (s, t). Fig. 16.

d Deviation projected onto the normal plane. Fig. 9.

e Identity matrix.

H Halo point locus. Subsection 2.C and Fig. 11.

K Zenith locus. Subsection 2.A and Fig. 14.

$K(\psi, \mathbf{P}_u)$ Circle with angular radius ψ and center $\mathbf{P}_u$. Subsection 2.A.

n Index of refraction for ice. Eq. (6). We take $n = 1.31$.

$\mathrm{rot}(\phi, \mathbf{Y})$ Rotation through angle ϕ about the point $\mathbf{Y}$. Subsection 2.G.

S Sun locus. Subsection 2.C and Fig. 11.

S^2 Unit sphere

$S(\Delta, \tau)$ Point with S-centered (sun-centered) coordinates (Δ, τ). Fig. 16.

$SO(3)$ Group of all orientations (rotations)—orthogonal matrices with determinant 1. Subsection 2.A.

(s, t) D-centered coordinates. Fig. 16.

s_1 and s_2 Angular distances from $\mathbf{P}_u$ to the nearest and farthest points of the entry region. Subsection 2.F.

$U(K)$ Halo-making set with zenith locus K. Subsection 2.A.

wedge $i\,j$ Wedge with entry face i and exit face j. Face numbers are as in Figs. 26 and 28.

$w'(v)$ Frame of the wedge whose entry and exit normals are $w(\mathbf{N})$ and $w(\mathbf{X})$, where $\mathbf{N}$ and $\mathbf{X}$ are the entry and exit normals of a wedge with frame v. Eqs. (14) and (15).

w^* Pole symmetry induced by the crystal symmetry w and spin vector $\mathbf{P}$. Eq. (82).

xref Reflection in the plane $x = 0$; yref and zref are analogous.

xrot Rotation through 180° about the x-axis; yrot and zrot are analogous.

$\mathrm{xrot}(\phi)$ Rotation through angle ϕ about the x-axis; $\mathrm{yrot}(\phi)$ and $\mathrm{zrot}(\phi)$ are analogous.

x-rotation Eq. (69) with $w = \mathrm{xrot}$.

y-reflection Eq. (69) with $w = \mathrm{yref}$.

z-reflection Eq. (69) with $w = \mathrm{zref}$.

Z Group of rotations about the z-axis. Subsection 2.A.

Zu Coset containing u. Eq. (31).

α Wedge angle, the angle between the entry and exit faces of the wedge. Fig. 5.

$\alpha_{\max}$ Largest wedge angle that will allow light to pass through a wedge. Subsection 2.B.

Δ Deviation between $\mathbf{S}$ and $\mathbf{H}$. Eq. (40) and Fig. 9.

Δ_m Minimum value of Δ. Eq. (41) and Fig. 17.

(Δ, τ) S-centered coordinates. Fig. 16.

$\Delta\tau$ Half-spread of contact points. Eq. (66) and Fig. 20.

η Zenith angle of halo point $\mathbf{H}$. Fig. 11.

(θ, δ) Bravais (B-centered) coordinates. Eq. (26).

λ See Eq. (3).

Σ Sun elevation.

σ Zenith angle of sun $\mathbf{S}$. Hence $\sigma = 90 - \Sigma$. Fig. 11.

τ Bearing of the halo point from the sun. Fig. 11.

τ_{var} Variation in the bearing τ for a given halo and a given Σ.

ψ Zenith angle of spin vector. Eq. (1) and Fig. 1.

References and Notes

1. F. Pattloch and E. Tränkle, “Monte Carlo simulation and analysis of halo phenomena,” J. Opt. Soc. Am. A **1,** 520–526 (1984).
2. R. A. R. Tricker, “Arcs associated with halos of unusual radii,” J. Opt. Soc. Am. **69,** 1093–1100 and 1195 (1979).
3. Half of $SO(3)$ and the partition can be visualized as follows. The orientations in $SO(3)$ whose (one-point) zenith loci are on the upper hemisphere are pictured as the upper hemisphere with a line segment $0 \le \phi < 360$ attached at each point and pointing radially outward—a boy's head with a brush haircut. The segment—strand of hair—attached to the sphere at $\mathbf{Y}$ is the coset $Zu = \{\mathrm{zrot}(\phi) \cdot u\}$, where u, corresponding to $\phi = 0$ and thought of as a point on the sphere, is the rotation that takes $\mathbf{Y}$ to $\mathbf{k}$ and that has horizontal rotation axis. The halo-making sets are the sets consisting of entire segments—no hairs are split. The zenith locus of a halo-making set is the portion of scalp from which its hair is growing. (The brush cut picture can be extended to most of $SO(3)$ by extending the hemisphere downward toward the South Pole $-\mathbf{k}$. But the South Pole cannot be added to complete the picture, since there the above description of u is not enough.)
4. S. W. Visser, “Die Halo-Erscheinungen,” in *Handbuch der Geophysik*, F. Linke and F. Möller, eds. (Gebrüder Borntraeger, Berlin-Nikolassee, 1942–1961), Vol. 8, pp. 1027–1081.
5. The group W of orthogonal transformations w satisfying $w\mathbf{k} = \pm\mathbf{k}$ is a subgroup of the group $O(3)$ of all orthogonal transformations, and Z is a normal subgroup of W. The quotient group W/Z consists of the four cosets $Z \cdot e$, $Z \cdot \mathrm{xrot}$, $Z \cdot \mathrm{yref}$, and $Z \cdot \mathrm{zref}$, which correspond to the four lines of Table 1. The homomorphism of W onto $\{e, -e, \mathrm{yref}, -\mathrm{yref}\}$ that is implicit in the theorem can be expressed as $w = \mathrm{zrot}(\phi) \cdot \mathrm{yref}^i \cdot \mathrm{zref}^j \to Z \cdot \mathrm{yref}^i \cdot \mathrm{zref}^j \to (-1)^j \mathrm{yref}^{i+j}$, the first mapping being the quotient map onto W/Z. The quotient group formally captures our intuition that we often do not worry about $\mathrm{zrot}(\phi)$.

6. A subtle and logically important point that can nevertheless be ignored on a first reading is that whether a given rotation u is a plate (Parry, alternate Parry, etc.,) orientation depends on the wedge under consideration. Technically, this is because the vector $\mathbf{N}_1(u)$ depends on the wedge as well as on u, since u starts with the crystal oriented so that the specified wedge is in standard orientation. For example, the plate orientations for wedge 1 6 have the form $u = \text{zrot}(\phi)\text{yrot}(-45)$, whereas the plate orientations for wedge 3 1 have the form $u = \text{zrot}(\phi)\text{yrot}(45)$. They are not the same.
7. J. Moilanen, M. Pekkola, and M. Riikonen, Finnish Halo Observers Network, URSA, Raatimiehenkatu 3 A 2, 00140, Helsinki, Finland (personal communication, 1994).
8. Thus Par $i\,j = \mathbf{P}_u$, where $\mathbf{P} = \mathbf{N}_3$ and where the matrix u gives the orientation, or frame, of wedge $i\,j$. In Section 1 we said that since the spin vector $\mathbf{P}$ is a wedge vector, then $\mathbf{P}_u$ is independent of u. That, however, assumed there was only one wedge under consideration (and one spin vector). Now $\mathbf{P}_u$ depends on u. The technical explanation is that $\mathbf{P}(u)$ [e.g., Eq. (24)] depends not only on u but on the wedge under consideration. But it is probably best to think less technically: At any moment there is the vector $\mathbf{P}$, and there are the wedge frame vectors $\mathbf{A}$, $\mathbf{B}$, $\mathbf{C}$ for the wedge under consideration. Then $\mathbf{P}_u$ is given by Eq. (21) as always. Equation (23) is also correct, with $\mathbf{A}$, $\mathbf{B}$, $\mathbf{C}$ being the columns of the matrix u. Of course $\mathbf{P}_u$ depends on the choice of spin vector as well as on the frame.
9. G. P. Können, "Identification of odd-radius halo arcs and of 44°/46° parhelia by their inner edge polarization," Appl. Opt. **37,** 1450–1456 (1998).
10. G. P. Können, "Polarization and intensity distributions of refraction halos," J. Opt. Soc. Am. **73,** 1629–1640 (1983).
11. W. Tape, *Atmospheric Halos* (American Geophysical Union, Washington, D.C., 1994).
12. R. Greenler, *Rainbows, Halos, and Glories* (Cambridge U. Press, New York, 1980).
13. F. Schaaf, "A field guide to atmospheric optics," Sky Telesc. **77**(3), 254–259 (1989).
14. M. Pekkola, "Viimeisten halojen ensimmäiset valokuvat," Tähdet ja Avaruus **20**(1), 31–36 (1990).
15. M. Pekkola, "Harrastajan palstat—Kustavin halonäytelmä," Tähdet ja Avaruus **22**(2), 36–37 (1992).
16. M. Pekkola, "Harrastajan palstat—Kolme komeaa halonäytelmää," Tähdet ja Avaruus **23**(6), 40–41 (1993).
17. O. R. Norton, Science Graphics, Bend, Oregon 97708 (personal communication, 1996).
18. T. Kobayashi, "Vapour growth of ice crystals between −40 and −90 C," J. Meteorol. Soc. Jpn. **43,** 359–367 (1965).
19. T. Kobayashi and K. Higuchi, "On the pyramidal faces of ice crystals," Contrib. Inst. Low Temp. Sci. Hokkaido Univ. Ser. A, No. 12, 43–54 and 13 plates (1957).
20. If there are at least three linearly independent vectors among $\mathbf{P}_{v_1}, \ldots, \mathbf{P}_{v_k}$, then there is at most one induced pole symmetry w^* for the given w, $\mathbf{P}$, and V. Otherwise there may be more than one w^*.